DIPARTIMENTO DI INGEGNERIA
CIVILE EDILE E AMBIENTALE

SAPIENZA
UNIVERSITÀ DI ROMA

DOTTORATO DI RICERCA IN INGEGNERIA IDRAULICA
CICLO XXII

Lagrangian study of hydrocarbons transport and dispersion in marine environment

Michela De Dominicis

RELATORI:
DOTT. GIOVANNI LEUZZI
DOTT. PAOLO MONTI

CORRELATORE:
PROF.SSA NADIA PINARDI

COORDINATORE
DOTTORATO:
PROF. ANTONIO CENEDESE

Contents

Chapter 1

1 Introduction

"La costruzione d'un modello era dunque per lui un miracolo d'equilibrio tra i principi (lasciati nell'ombra) e l'esperienza (inafferrabile), ma il risultato doveva avere una consistenza molto più solida degli uni e dell'altra. In un modello ben costruito, infatti, ogni dettaglio dev'essere condizionato dagli altri, per cui tutto si tiene con assoluta coerenza, come in un meccanismo dove se si blocca un ingranaggio tutto si blocca. […] la realtà vediamo bene che non funziona e che si spappola da tutte le parti; dunque non resta che costringerla a prendere la forma del modello, con le buone o con le cattive" (Palomar, Italo Calvino)[1].

In the study of natural processes, the use of models stems from the need to answer the questions "Why will it happen?", "How will it happen?", "Where will it happen?" and "When will it happen?" Unfortunately, predicting how, when and where is always very challenging. The reason why it is difficult to predict a natural phenomenon is because the forecasts depend on the precise knowledge of a number of parameters and boundary conditions that are known very roughly. The construction of a model must be based

[1] "*The construction of a model, therefore, was for him a miracle of equilibrium between principles (left in shadow) and experience (elusive), but the result should be more substantial than either. In a well-made model, in fact, every detail must be conditioned by the others, so that everything holds together in absolute coherence, as in a mechanism where if one gear jams, everything jams.[…]*"

primarily on the objective that you want to pursue and in finding all the “ingredients” necessary for its operation.

At the beginning of the XXI century, what drives the desire to understand the reality and to represent it into a model? **“***Need driven versus curiosity driven**. Basic science is question driven; in contrast, the new applications science is guided more by societal needs than scientific curiosity. Rather than seeking answers to questions, it focuses on creating the ability to seek courses of action and determine their consequences”(Dozier & Gail, “The Emerging Science of Environmental Applications, The Fourth Paradigm, 2009).* In the past, science and research were mainly addressed to look to the reality with analytical eye, breaking the real phenomena in order to analyze them, searching for a theory that allows to study the disorder of nature. Although, far from achieving a complete knowledge of reality, science is slowly veering towards operational science or science applications: *“knowledge developed primarily for the purpose of scientific understanding is being complemented by knowledge created to target practical decisions and action. This new knowledge endeavor can be referred to as the science of environmental applications.” (Dozier & Gail, “The Emerging Science of Environmental Applications, The Fourth Paradigm, 2009).*

The work of the present thesis stems from the need to manage the problems of marine pollution. Ships can pollute waterways and oceans in many ways. An oil spill is a release of a liquid petroleum hydrocarbon into the environment due to human activity, and is a form of pollution. The term often refers to marine oil spills, where oil is released into the open ocean or coastal waters. Oil spills include releases of crude oil from tankers, offshore platforms, drilling rigs and wells, as well as spills of refined petroleum products (such as gasoline, diesel) and their by-products, and heavier fuels used by large ships such as bunker fuel, or the spill of any oily refuse or waste oil. ("Hindsight and Foresight, 20 Years After the Exxon Valdez Spill". NOAA. 2010-03-16). Oil spills can have devastating effects. While being toxic to marine life, the hydrocarbons are very difficult to clean up, and last for years in the sediment and marine environment. Discharge of cargo residues from bulk carries can pollute ports, waterways and oceans. In many instances vessels intentionally discharge illegal wastes despite foreign and domestic regulation prohibiting such actions. Illegal discharges of oil from ships are often limited in size and scattered, but,

surprisingly, their sum is higher than that from oil spills, and they may create a chronic impact of oil in certain areas. For instance littoral sediments affected by low or moderated but continuous oil spills, like the coasts of the Bay of Algeciras (near the Strait of Gibraltar) are more polluted than those affected by accidental oil spills such as the Prestige accident (2002) (Morales-Caselles, 2007). Oil discharges may be accidental. In all cases, the spills have both immediate and longer-term effects, including contamination of farmed fish and shellfish for human consumption.

The list of the past oil spills all over the world oceans is extremely long. There have been a number of large oil spills from tankers in the European Seas area over the last few decades, with examples including:

-The Torrey Canyon off England in 1967 (93000 tons);

- The Amoco Cadiz off Brittany in 1978 (260000 tons);

-The Haven off Genoa, Italy, in 1991 (114000 tons of crude oil, most of which burned);

- The Aegean Sea off northwest Spain in 1992 (80000 tons);

- The Braer off Shetland in 1993 (85000 tons of crude oil);

- The Sea Empress off Wales in 1996 (72000 tons of crude oil);

- The Erika off Brittany in 1999 (of the 30000 tons of heavy fuel oil on board, more than 10000 tons got into the marine environment);

- The Prestige off northwest Spain in late 2002 (more than 25000 tons of heavy fuel oil, with 50000 tons remaining in the wreck).

Finally, we have to remember the largest accidental marine oil spill in the history of the petroleum industry: the Deepwater Horizon oil spill in the Gulf of Mexico, which flowed for three months in 2010. The spill stemmed from a sea-floor oil gusher that resulted from the April 20, 2010 Deepwater Horizon drilling rig explosion. On July 15, 2010, the leak was stopped after the release of nearly 7.0×10^5 m^3 of crude oil, as scientists report in *Science* (Crone & Tolstoy, 2010). It is the most serious environmental disaster in the United States, ten times bigger of the oil spill from the tanker Exxon Valdez in1989.

Such accidents may become more frequent with increasing oil extraction in hazardous location, like the Arctic, or politically unstable areas: *"The Deep Horizon explosion was the inevitable result of a relentless effort to extract oil from ever deeper and more*

hazardous locations. In fact, as long as the industry continues its relentless, reckless pursuit of "extreme energy" -- oil, natural gas, coal, and uranium obtained from geologically, environmentally, and politically unsafe areas -- more such calamities are destined to occur." (Michael Klare, TomDispatch, 2010, United States)

In addition, we must remember that in some areas of the world oil spill occurs, of which we often do not even know, such the case of the Niger delta: "*The Deepwater Horizon disaster caused headlines around the world, yet the people who live in the Niger delta have had to live with environmental catastrophes for decades […] One report, compiled by WWF UK, the World Conservation Union and representatives from the Nigerian federal government and the Nigerian Conservation Foundation, calculated in 2006 that up to 1.5m tons of oil – 50 times the pollution unleashed in the Exxon Valdez tanker disaster in Alaska – has been spilled in the delta over the past half century."* (John Vidal, The Observer, 30 May 2010, Great Britain)

Science can assist the society during environmental emergencies. The success in the management of an oil spill depends on several factors including the ability to detect the spills and the capabilities to forecast the drift and transformations of oil over time. In recent years there has been a growth of interest for the prediction of particle trajectories in the sea. One of the most important applications is the forecast of oil spills in the open ocean and coastal seas. Transport and dispersion processes can be simulated using a Lagrangian particle tracking model coupled with Eulerian circulation models. Forecasting of the Lagrangian trajectories relies on the accuracy of ocean currents. The advent of operational oceanography and accurate operational models of the circulation make possible the knowledge of the ocean currents fields, which can be provided by the analyses and forecasts available hourly or daily by a forecasting Ocean General Circulation Model (OGCM), such as the Mediterranean ocean Forecasting System, MFS, (Pinardi et al. 2003).

The purpose of this thesis are: the improvement of the Lagrangian model of transport and transformation of hydrocarbons MEDSLIK (Lardner et al., 2006) in the deterministic and stochastic components of the equations of particle trajectories; the calibration and validation of the model by collecting Lagrangian data (drifting surface buoys), in situ data

of oil slick detected by satellite; the study of the stochastic component of transport using the data of drifter trajectories.

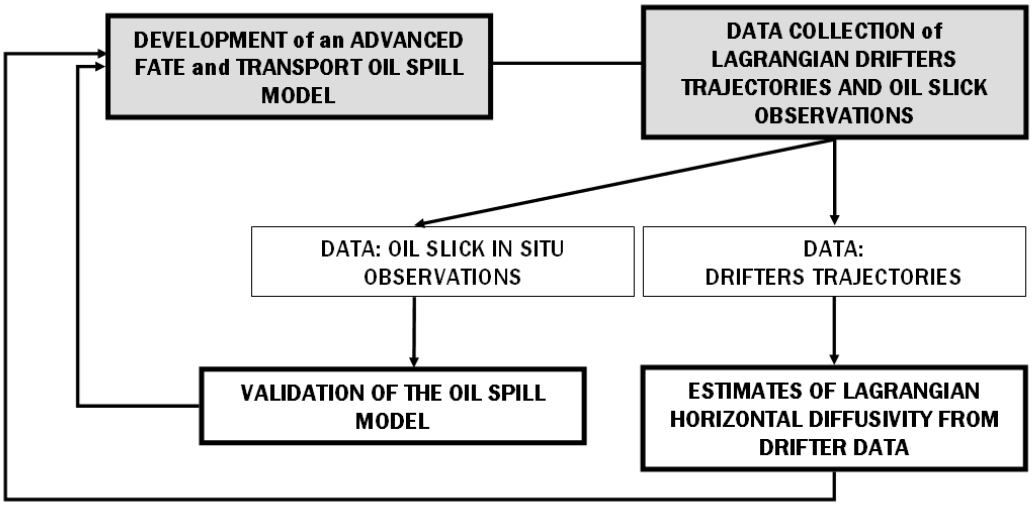

Figure 1.1. Logical structure of thesis.

This thesis is organized into 3 chapters. Each chapter consists of the content of a manuscript which will be submitted for publication in a refereed academic journal.

"Nella vita del signor Palomar c'è stata un'epoca in cui la sua regola era questa: primo, costruire nella sua mente un modello, il più perfetto, logico, geometrico possibile; secondo, verificare se il modello s'adatta ai casi pratici osservabili nell'esperienza; terzo, apportare le correzioni necessarie perché modello e realtà coincidano" (Palomar, Italo Calvino)[2]. This sentence perfectly sums up the structure of my thesis: the attempt to represent reality using a model, next the model validation using data and finally the aim to improving it.

[2] "*In Mr. Palomar's life there was a period when his rule was this: first, to construct in his mind a model, the most perfect, logical, geometrical model possible; second, to see if the model is adapted to the practical situations observed in experience; third, to make the corrections necessary for model and reality to coincide*"**.**

"…primo, costruire nella sua mente un modello, il più perfetto, logico, geometrico possibile..."[3]

First, a model designed to predict the transport and weathering of an oil spill has been developed.

In chapter 2, the upgrade of the MEDSLIK model, so-called MEDSLIK-II is presented. The model predicts the evolution in time of the geographic position and chemical changes of an oil slick and uses a Lagrangian representation of the oil slick. MEDSLIK-II simulates the transport of the surface slick governed by the water currents and by the wind. It uses the current velocity fields provided by MFS and by other higher resolution operational hydrodynamic models: the Adriatic Forecasting System (AFS) (Oddo et al. 2006), the Sicily Channel Regional Model (SCRM) (Gaberšek et al. 2007) and the Thyrrenian regional model (Napolitano, in preparation). MEDSLIK-II includes a proper representation of high frequency currents and wind fields in the advective components of the Lagrangian trajectory model, the introduction of the Stokes drift velocity and the coupling with the remote-sensing data to be used as initial conditions. Oil parcels are also dispersed by turbulent fluctuation components that are parameterized with a random walk scheme. In addition to advective and diffusive displacements, the oil spill parcels characteristics change due to various physical and chemical processes that transform the oil (evaporation, emulsification, dispersion in water column, adhesion to coast).

"…secondo, verificare se il modello s'adatta ai casi pratici osservabili nell'esperienza…"[4]

Second, the oil spill model has been validated with surface drifter data, with satellite data and with in situ data in different Mediterranean regions.

Verification of the oil spill forecasting is both a crucial issue and a difficult task to perform. The reason for this is the lack of information. The main objective of the oceanographic cruise presented in chapter 3, organized in the framework of the PRIMI project (PRogetto pilota Inquinamento Marino da Idrocarburi), was to visit oil slicks detected by satellite and whose displacement was predicted by the MEDSLIK-II model,

[3] "*…: first, to construct in his mind a model, the most perfect, logical, geometrical model possible…*"
[4] "*…second, to see if the model is adapted to the practical situations observed in experience…*"

coupled with the oceanographic operational models available in the Mediterranean Sea. The area selected for the cruise was the central Mediterranean (southern Tyrrhenian Sea, Sardinia Channel, Sicily Channel, western Ionian Sea). During the cruise the in situ data on the oil-spill characteristics and composition have been acquired. The data collected have been used for the validation of the dispersion and transformation model.

"…terzo, apportare le correzioni necessarie perché modello e realtà coincidano."[5]
Third, using the drifter observations our understanding of the turbulent processes has been improved, in order to arrive at a better representation of the stochastic component of transport.
The drifters are oceanographic instruments used to study the surface circulation and oceanographic dynamics, are designed to be transported by ocean currents. In chapter 4 the data collected during the MREA07/08 (Marine Rapid Environmental Experiment) will be presented, during this experiment the drifters were deployed in the Ligurian Sea. Next, drifter trajectories collected during the DOLCEVITA (Dynamics Of Localized Currents and Eddy Variability In The Adriatic) drifter program are presented. During the DOLCEVITA project several drifters were deployed in different areas of the Adriatic Sea.
Chapter 4 presents the study of the Lagrangian diffusivity K and the time scales T, to be used as input parameters for dispersion in oil spill models. To this end the first step has been to compute K and T using the drifters deployed during the Marine Rapid Environmental Assessment 2007-2008 (MREA) exercise in the Ligurian Sea. The second step is the analysis of the relation between the horizontal diffusivity and the wind and current field, which can be provided by Eulerian models. This last analysis has been performed using the drifters, deployed in the Adriatic Sea as part of DOLCEVITA drifter program.

[5] *"…third, to make the corrections necessary for model and reality to coincide."*

Chapter 2

2 Development and sensitivity studies of an advanced fate and transport oil spill model

2.1 Introduction

Representing the transport and fate of an oil slick at sea is a formidable task. Many factors affect the motion and transformation of the oil slick and some of the most relevant are: the meteo-marine conditions at the air-sea interface (wind, waves, air and water temperature), the initial volume and chemical characteristics of the oil and finally the marine currents at different space and time scales. All these factors are interrelated and must be considered together to arrive at an accurate estimate of the oil evolution and movement.

According to the state-of the-art reviews on oil spill numerical (ASCE, 1996; Reed et al. 1999), a large number of oil-spill models are available today that can represent oil transport and fate processes in the sea water. Over the years, models have developed complex representation of the relevant processes: starting with two-dimensional particle-tracking models such as GNOME (NOAA, 2002) and PICHI (Castanedo et al. 2010) we arrive to complex oil slick polygon representations and advanced physical and chemical advection-diffusion three-dimensional models (Wang et al., 2008; Wang & Shen, 2010). Some of the most sophisticated operational models are also: MEDSLIK (Lardner et al. 2006), MOTHY (Daniel et al. 2003), POSEIDON Oil Spill Model (Nittis et al. 2006) and TESEO (Sotillo et al. 2008), SINTEF OSCAR 2000 (Reed et al. 1995), OD3D (Hackett et al. 2006), Seatrack Web SMHI model (Ambj\örn 2007) and OILMAP (ASA, 1997).

In this chapter we present an upgrade of the MEDSLIK model, so-called MEDSLIK-II. The latter is designed to predict the geographic position and chemical changes of an oil slick using a Lagrangian formalism, i.e., the oil slick is represented by a large number of component particles which move following particle trajectory equations and are transformed by physical and chemical processes. In other words, the model considers particle advective and diffusive displacements due to mean and turbulent water movements

and in addition the oil spill parcels change their buoyancy and volume due to evaporation, emulsification, dispersion in water column, adhesion to the coast. The novel characteristics of MEDSLIK-II are a proper representation of high frequency currents and wind fields in the advective components of the particle trajectory equations derived from the generalized Langevin equation and the initialization of the oil slick position, age and volume with realistic shape functions from remote sensing data. In addition the model uses the recently available operational oceanographic analyses and forecasts (Pinardi et al., 2002, 2003) as part of the deterministic components of the particle trajectory equations and it discusses the corrections needed to account for missing or not well resolved transport processes by the analyses and forecasts available.

In the past, only climatological currents calculated from the observed temperature and salinity measurements were available and sometimes the deterministic advective component of the particle trajectory was estimated directly from the wind, using the well known Ekman spiral wind driven current solution (Apel, 1987). The advent of operational ocean forecasting makes it possible to have almost continuous estimates of the sea currents due to the combination of wind and geostrophic effects. In this chapter we will formulate in a very general way the equations for transport and transformation of oil spill at the surface and we will analyze the sensitivity of the oil spill hindcasts model to several parameterizations.

The organization of the chapter is as follows. Section 2.2 gives an overview of the theoretical approach used to write the transport and fate equations for the oil spill active tracer. Section 2.3 illustrates the basic equations describing the oil transport processes. Section 2.4 presents the equations describing the chemical-physical processes affecting the oil. Section 2.5 illustrates the coupling with the operational oceanographic products and with remote sensing data. Section 2.6 presents an application of the MEDSLIK-II model to several test cases.

2.2 The model equations and state variables

The movement of oil in the marine environment is usually regarded as due to advection by the large scale flow field and the dispersion caused by the turbulent flow components. In an Eulerian framework, while the oil moves, its concentration changes due to several

physical processes, called the weathering processes. The generalized active tracer equation for a substance, C, released in a flow with an Eulerian formalism, is written as:

$$\frac{\partial C}{\partial t} + \mathbf{U} \cdot \nabla C = \nabla \cdot (\mathbf{K} \nabla C) + \sum_{j=1}^{N} r_j(C) \qquad (2.1)$$

where C(x,y,z,t) is the concentration of the tracer field as a function of space and time coordinates, normally with units of mass of substance over volume, $\frac{\partial}{\partial t}$ is the local time rate of change operator, **U** is the mean flow field with components (U,V,W) and **K** is the diffusivity tensor which parameterize the turbulent effects, $r_j(C)$ are the transformation rates that modify the tracer concentration by diabatic and chemical reactions.

Solving numerically equations (2.1) is a well known problem in oceanographic (Noye 1987), meteorological (Boughton et al. 1987) and ecosystem (Sibert et al. 1999) modelling and a number of well documented approximations and implementations have been used over the past thirty years for both passive and active tracers (Haidvogel & Beckmann, 1999). Recent understanding (Woods 2002) has changed the approach substantially and the tracer equations (2.1) has been substituted by a number of equations for properties of the 'constituent particles', i.e. the concentration is transformed into a discrete set of particles, which are characterized by some properties. The concentration at a certain point and time is then found assembling the particle together.

In order to model the oil concentration with particle constituents some basic assumptions are needed. One of the most important one is the consideration that the constituent particles do not influence the water hydrodynamics and processes. This assumption has limitations for example at the surface of the ocean because floating oil modifies the air-sea interactions and the surface wind drag, but it is considered to be valid here. In addition the oil volume is modified by physical and chemical processes and here we assume that the transport processes are separated from the transformation processes. In other words, we hypothesize that the position changes are small and during these movements the particles behave as passive tracer constituents. In summary the constituent particles move through infinitesimal displacements without inertia (as water parcels) and without interactions between themselves. After such infinitesimal displacements, the volume associated to the particle is transformed by physical and chemical processes.

If we apply such an hypothesis to equation 2.1 we effectively split the equation into two basic processes, advection, diffusion, and tracer trasformation. This can be done by writing:

$$\frac{\partial C}{\partial t} = \frac{\partial C_1}{\partial t} + \frac{\partial C_2}{\partial t} \tag{2.2a}$$

$$\frac{\partial C_1}{\partial t} = -\mathbf{U} \cdot \nabla C_1 + \nabla \cdot (\mathbf{K} \nabla C_1) \tag{2.2b}$$

$$\frac{\partial C_2}{\partial t} = \sum_{j=1}^{N} r_j(C) \tag{2.2c}$$

We now solve 2.2b with a Lagrangian particle formalism and express C_1 as a function of the particle volume of oil and number of particles in a new Eulerian grid, so called oil tracer grid, defined in the coordinates system (x_T, y_T, z_T) with a spatial resolution (δx_T, δy_T, δz_T).

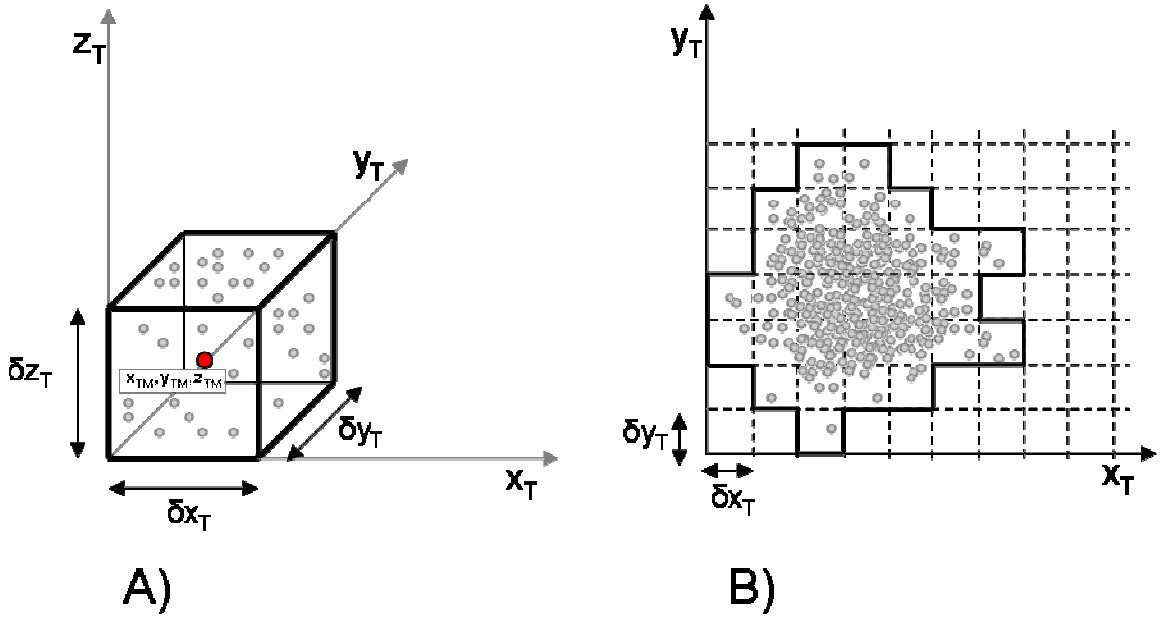

Figure 2.1. Schematic view of the oil tracer grid (the grey spheres represent the oil particles): A) 3D view of one cell of the oil tracer grid; B) 2D view of the oil tracer grid.

First, the particles move (2.2b), then the "active" part of the equation is solved (2.2c). Next the number of particles inside each tracer grid box, $N(x_{TM}.t)$, is counted together (see equation 2.3) and finally the concentration in the grid cell, $C(x_{TM},t)$, is reconstructed using

the number of particles in each grid point (see equation 2.4). Then we start again with the active part of the tracer.

The particle position vector, $\mathbf{x_K}(t)$, is defined as $\mathbf{x_K}(t) = (x_K(t), y_K(t), z_K(t))$, with $k = 1, n$. The number of particles in the oil tracer grid unit volume $\delta V = \delta x_T \delta y_T \delta z_T$ around the position (x_{TM}, y_{TM}, z_{TM}) is

$$N(\mathbf{x}_{TM}, t) = \dim\left\{ \mathbf{n_K}; \begin{array}{c} x_{TM} - \frac{\delta x_T}{2} \le x_K(t) \le x_{TM} + \frac{\delta x_T}{2} \\ y_{TM} - \frac{\delta y_T}{2} \le y_K(t) \le y_{TM} + \frac{\delta y_T}{2} \\ z_{TM} - \frac{\delta z_T}{2} \le z_K(t) \le z_{TM} + \frac{\delta z_T}{2} \end{array} \right\} \quad (2.3)$$

where $\mathbf{n_K}$ is the vector of number of particles.

The concentration at a certain time t at the position

$$C(\mathbf{x}_{TM}, t) = \frac{N(\mathbf{x}_{TM}, t)\upsilon(t)}{\delta x_T \delta y_T \delta z_T}\rho \quad (2.4)$$

where $\upsilon(t)$ is the volume of oil of each particle and ρ is the oil density. The oil density must provided as input to the model and remains constant over time. The oil density depends on the oil type. The different types of oil are commonly classified using the API number: American Petroleum Institute gravity, or API gravity, is a measure of how heavy or light a petroleum liquid is compared to water. From the API, it is possible to calculate the oil density. The conversion from API to density first requires conversion to specific gravity:

$$SG = \frac{141.4}{(API + 131.5)} \quad (2.5)$$

Then the specific gravity can subsequently be converted to density

$$\rho = SG\rho_W \quad (2.6)$$

The $\upsilon(t)$ changes only due to the transformation processes (equation 2.2c), while $N(x_{TM},t)$ changes to both the transformation (equation 2.2c) and the advection-diffusion processes (equation 2.2b). The number of particles in the oil tracer grid unit volume changes due to the particle advection and diffusion, to the dispersion of particle in water column, to the spreading and to the absorption or release of particles by the coast.

The initial particle oil volume $\upsilon(t_0)$ is calculated as

$$\upsilon(t_0) = \frac{V}{n} \tag{2.7}$$

where V is the total oil volume released and n is the total number of particles released.

The particle oil volume is considered to be divided in two components: the evaporative and non-evaporative particle oil volume. The initial components are defined as

$$\begin{aligned} \upsilon_E(t_0) &= \left(1 - \frac{\varphi_{NE}}{100}\right) \cdot \upsilon(t_0) \\ \upsilon_{NE}(t_0) &= \frac{\varphi_{NE}}{100} \cdot \upsilon(t_0) \end{aligned} \tag{2.8}$$

where φ_{NE} is the residual percentage, i.e. the percentage of the non-evaporative component of the oil, which has to be known.

The volume of the evaporative component of the oil left in the particle decreases due to the evaporation and the diagnostic relationship is

$$\upsilon_E(t) = \left[\left(1 - \frac{\varphi_{NE}}{100}\right) - f^E(t)\right] \cdot \upsilon(t_0) \tag{2.9}$$

where $f^E(t)$ is the fraction of oil evaporated (described in section 2.4.1). The volume of the non-evaporative component of the oil left in the particle change due to the absorption onto the coast and is given by:

$$\upsilon_{NE}(t) = \upsilon_{NE}(t)\left(1 - f^C(t)\right) \tag{2.10}$$

where $f^C(t)$ is the fraction of oil absorbed onto the coast (see section 2.4.1).

The transformation and movement of the slick with a constituent particle formalism is then characterized by two sets of variables: the slick state variables and the particle state variables. The particle state variables are the three dimensional particle position, $\mathbf{x}(t) = (x(t), y(t), z(t))$, the non-evaporative volume of the oil for each particle, $\upsilon_{NE}(t)$ and the evaporative volume of the oil for each particle, $\upsilon_E(t)$. The slick state variables are the oil volume of the thick part of the slick, $V^{TK}(t)$, the oil volume of the thin part of the slick,

$V^{TN}(t)$, the fraction of water in the oil-water mousse, $f^{W}(t)$, the oil viscosity, $\eta(t)$ and the viscosity of the oil-water mousse, $\eta_{EM}(t)$.

The total number of equations to be written are ten and six of them are predictive while four are only diagnostics. Prognostic equations are written for the thin and thick oil slick volume variables, for the fraction of water in the oil-water-mousse and for the particle positions. The latter are a specific form of the generalized Langevin equations and they will be described in the Section 2.3. The diagnostic equations for $\upsilon_{NE}(t)$ and $\upsilon_{E}(t)$ have been already described (equations 2.9 and 2.10). The time rate of change of $V^{TK}(t)$, $V^{TN}(t)$, $f^{W}(t)$ and the diagnostic equations for $\eta(t)$ and $\eta_{EM}(t)$ are given by empirical formulas. They are related to five processes: evaporation, dispersion, emulsification, spreading and beaching. Both the diagnostic ad prognostic equations for the slick state variables are given in Section 2.4.

2.3 Time rate of change of particle positions

The time rate of change of particle position state variables are given by a set of uncoupled Langevin equations:

$$\frac{d\mathbf{x}(t)}{dt} = \mathbf{A}(\mathbf{x},t) + \mathbf{B}(\mathbf{x},t)\xi(t) \qquad (2.11)$$

where the vector $\mathbf{A}(\mathbf{x},t)$ represents the so-called deterministic part of the flow field, corresponding to the mean field **U** in (2.1), while the second term is a stochastic or diffusion term. The stochastic term is composed by the tensor $\mathbf{B}(\mathbf{x},t)$ that characterizes the random motion and $\xi(t)$, a random factor taking values between 0 and 1. If we define $W(t) = \int_0^t \xi(s)ds$ and apply the Itō assumption (Tompson & Gelhar 1990), the equation (2.11) becomes equivalent to the Itō stochastic differential equation:

$$d\mathbf{x}(t) = \mathbf{A}(\mathbf{x},t)dt + \mathbf{B}(\mathbf{x},t)d\mathbf{W}(t) \qquad (2.12)$$

where dt is the Lagrangian time step and $d\mathbf{W}(t)$ is a random increment of the "Wiener process" $\mathbf{W}(t)$. The Wiener process describes the path of a particle due to Brownian

motion modelled by independent random increments $d\mathbf{W}(t)$ sampled from a normal distribution with zero mean, $\langle dW(t) \rangle = 0$, and second order moment with $\langle dW \cdot dW \rangle = dt$. Thus we can replace $d\mathbf{W}(t)$ in (2.12) with a vector $\mathbf{Z}$ of independent random numbers, normally distributed, i.e. $\mathbf{Z} \in N(0,1)$, and multiplied by $\sqrt{dt}$:

$$d\mathbf{x}(t) = \mathbf{A}(\mathbf{x},t)dt + \mathbf{B}(\mathbf{x},t)\mathbf{Z}\sqrt{dt} \tag{2.13}$$

The unknown tensors $\mathbf{A}(\mathbf{x},t)$ and $\mathbf{B}(\mathbf{x},t)$ in (2.13) are most commonly written as (Risken 1989):

$$d\mathbf{x}(t) = \begin{pmatrix} U(\mathbf{x},t) \\ V(\mathbf{x},t) \\ W(\mathbf{x},t) \end{pmatrix} dt + \begin{bmatrix} \sqrt{2K_x} & 0 & 0 \\ 0 & \sqrt{2K_y} & 0 \\ 0 & 0 & \sqrt{2K_z} \end{bmatrix} \begin{pmatrix} Z_1 \\ Z_2 \\ Z_3 \end{pmatrix} \sqrt{dt} \tag{2.14}$$

where **A** is diagonal and equal to the eulerian field velocity components, **B** is diagonal and equal to K_x, K_y, K_z turbulent diffusivity coefficients in the three directions and Z_1, Z_2, Z_3 are random vector amplitudes. Physically, equation (2.14) describes the displacement of a particle resulting from the advection due to the mean flow (deterministic) and turbulent flow component (stochastic).

In MEDSLIK-II, equation (2.14) takes the following form:

$$d\mathbf{x}(t) = \begin{pmatrix} U(\mathbf{x},t) \\ V(\mathbf{x},t) \\ 0 \end{pmatrix} dt + d\mathbf{x}'(t) \tag{2.15}$$

where for simplicity we have indicated with $d\mathbf{x}'(t)$ the particle displacement due to the turbulent motion. The first term in (2.14) is called the deterministic transport while the second is the turbulent transport term. The fluid vertical velocity has been neglected since it is normally small, of the order of 10^{-2} times the horizontal current velocity magnitude. The vertical particle positions are then changed only by vertical turbulent displacements.

We expand the deterministic transport term in three different components:

$$d\mathbf{x}(t) = \left[\mathbf{U}_c(\mathbf{x},t) + \mathbf{U}_w(\mathbf{x},t) + \mathbf{U}_s(\mathbf{x},t)\right]dt + d\mathbf{x}'(t) \tag{2.16}$$

where $\mathbf{U}_c(\mathbf{x},t)$, hereafter called the current velocity term, is the water current velocity due to a combination of non-local wind and buoyancy forcing, $\mathbf{U}_w(\mathbf{x},t)$, hereafter called local wind velocity term, is the velocity due to the local wind effects (Ekman currents), $\mathbf{U}_s(\mathbf{x},t)$, hereafter called the wave current term, is the velocity due to wave-induced currents or Stokes drift.

The Lagrangian horizontal particle motion is resolved applying an Euler forward scheme to the ordinary differential equations (2.16). The particle position at time step $t+\Delta t$, is calculated as follows:

$$\mathbf{x}(t+\Delta t) = \mathbf{x}(t) + \mathbf{U}(t,\mathbf{x}(t))\Delta t + \Delta \mathbf{x}'(t) \qquad (2.17)$$

where $\mathbf{x}(t)$ represents the particle position at the current time step and $\mathbf{U}(t,\mathbf{x}(t))$ is the Eulerian ocean current velocity for the current time step at the particle position.

2.3.1 The current and local wind velocity term

Ocean currents near the ocean surface are due to the effects of atmospheric forcing which can be subdivided into two main categories, buoyancy fluxes and wind stresses. Wind stress forcing is by far the most important one in terms of kinetic energy of the induced motion, accounting for 70% or more of the currents amplitude over the oceans (Wunsch 1998).

One part of the wind induced currents are due to non-local winds, i.e. local currents are induced by remotely located winds, and they are dominated by geostrophic or quasigeostrophic dynamical balances (Pedlosky 1986). By definition, geostrophic and quasigeostrophic motion has a time scale of several days and it considers mesoscale motion in the ocean, a very important component of the large scale flow field represented in (2.14). It is customary to indicate that geostrophic or quasigeostrophic currents dominate below the mixed layer even if sometime they can emerge and be dominant also in this layer (few tens of meters in the equatorial area up to hundred meters at high latitudes). The mixed layer dynamics is typically considered to be ageostrophic and one of the most common time dependent, wind induced motion occurring at the surface is composed of inertial oscillations (Pollard 1970). Additional ageostrophic components of surface currents

due to local winds are dominated by rotational effects and vertical diffusivities, the so-called Ekman currents (Price et al. 1987)(Lenn & Chereskin 2009). All these components should be adequately considered in the deterministic eulerian velocity field of (2.15).

Depending on the model used to compute this velocity field, it could be necessary to make distinction between the current components. In the past years, oil spill models used the current velocity field, $\mathbf{U}_c(\mathbf{x},t)$, from climatological and geostrophic computations(A.H. Al-Rabeh 1994)(A. H. Al-Rabeh et al. 2000) and then the ageostrophic Ekman current components were added by the term $\mathbf{U}_w(\mathbf{x},t)$. It is well known that Ekman currents at the surface can be parametrized as a function of wind intensity and angle, i.e.:

$$\begin{aligned} U_w &= \alpha(W_x\cos\beta + W_y\sin\beta) \\ V_w &= \alpha(-W_x\sin\beta + W_y\cos\beta) \end{aligned} \qquad (2.18)$$

where W_x and W_y are the wind zonal and meridional components at 10 m respectively and α and β are two parameters called drift factor and drift angle. There has been considerable dispute among modellers on the choice of the best values of the drift factor and angle, most models using a value of around 3% for the former and a value between 0° and 25° for the latter (A.H. Al-Rabeh 1994).

With the advent of operational oceanography and accurate operational models of the circulation (Pinardi & Coppini 2010, Coppini et al. 2010), the geostrophic and ageostrophic current velocity fields can be provided by the analyses and forecasts, available hourly or daily, of a forecasting Ocean General Circulation Model (OGCM). In our paper the advecting velocities for MEDSLIK-II are taken from the Mediterranean ocean Forecasting System, MFS, (Pinardi et al. 2003) and the surface water current velocities are derived from the high resolution analyses and forecasts of MFS (Tonani et al., 2008). Thus the term $\mathbf{U}_c(\mathbf{x},t)$ contains a rather satisfactory representation of the surface ageostrophic currents and the $\mathbf{U}_w(\mathbf{x},t)$ term could be neglected. However we argue that we can consider the terms (2.18) as correction terms accounting for model errors. In a recent paper, Coppini et al. (2010) showed that using (2.16) best results were achieved with $\mathbf{U}_c(\mathbf{x},t)$ at 30 meters depth from the MFS OGCM with the addition of $\mathbf{U}_w(\mathbf{x},t)$ as in (2.10), instead of using surface currents directly. The choice of 30 m corresponds

approximately to the Ekman layer e-folding depth for the Mediterranean Sea, i.e., the depth at which Ekman currents go to zero.

In conclusion if an OGCM model is sufficiently capable to resolve the Ekman dynamics, the correct choice should be to set the wind-induced current velocity, $\mathbf{U}_w(\mathbf{x},t)$, to zero and use only the water surface flow from the OGCM which already contains the local wind effects.

2.3.2 The wave current term

Waves give rise to transport of pollutants by wave-induced velocity, the so-called Stokes drift velocity. This current component is represented by the last term of equation (2.8), $\mathbf{U}_s(\mathbf{x},\mathrm{t})$, that should be definitely added to the Eulerian current velocity field since normally OGCM are not coupled with wave models.

The Stokes drift is the net displacement of a particle in a fluid due to wave motion, resulting essentially from the fact that the particle moves faster forward when the particle is at the top of the wave induced circular orbit than backward, when it is at the bottom of its orbit. The Stokes drift is the difference between the start and end positions, divided by a predefined amount of time (usually one wave period). The Stokes drift has been introduced in MEDSLIK-II using an analytical formulation that depends from the wind amplitude but in general the model could use the Stokes drift from the output of a complete numerical wave model.

More generally, the Stokes drift velocity is the difference between the average Lagrangian flow velocity of a fluid particles and the average Eulerian flow velocity of the fluid at a fixed position (the average is usually done over one wave period) and can be written as (Craik 1985):

$$\overline{\mathbf{u}_s}^{\mathrm{t}} = \overline{\mathbf{u}_L}^{\mathrm{t}} - \overline{\mathbf{u}_E}^{\mathrm{t}} \qquad (2.19)$$

where the time average operator is indicated by $\overline{}^{\mathrm{t}}$ and the time average Eulerian velocity vector is $\overline{\mathbf{u}_E}^{\mathrm{t}} = \overline{\mathbf{u}(\mathbf{x},\mathrm{t})}^{\mathrm{t}}$ with $\mathbf{x} = (\mathrm{x},\mathrm{y},\mathrm{z})$ the space vector, while the Lagrangian

velocity vector is $\overline{\mathbf{u}_L}^t = \overline{\mathbf{u}(\xi,t)}^t$, where $\xi = (x,y,z)$ is the Lagrangian position vector of a fluid particle.

For simplicity, the case of infinite-deep water is considered, with linear wave propagation of a sinusoidal wave on the free surface of a fluid layer (Phillips 1977):

$$\eta = a\cos(kr - \omega t) \qquad (2.20)$$

where η is the free surface elevation, a is the wave amplitude, k is the wave number, $k = \frac{2\pi}{\lambda}$, ω is the angular frequency, $\omega = \frac{2\pi}{T} = 2\pi f$, r is the distance along the wave propagation direction, λ is the wave length, T is the wave period and f the wave frequency. The wavelength and the wave period satisfy the deep-water dispersion relation $\omega^2 = gk$ where g is the gravity acceleration.

The component of the Stokes drift velocity D_s in the wave propagation direction is estimated by Phillips (1977) using a Taylor expansion around **x** of the Eulerian horizontal-velocity component, along the wave propagation direction, called $u_r = \frac{\partial \xi_r}{\partial t}$, at the position ξ:

$$D_s = \overline{u_r(\xi,t)} - \overline{u_r(\mathbf{x},t)} = \omega k a^2 e^{2kz}\left[\sin^2(kr-\omega t) + \cos^2(kr-\omega t)\right] \qquad (2.21)$$

Performing the time averaging, the horizontal component of the Stokes drift velocity for deep-water waves is approximately (Phillips 1977):

$$D_s(\omega, z) \approx \omega k a^2 e^{2kz} \qquad (2.22)$$

As it can be seen, the Stokes drift velocity is a nonlinear quantity in terms of the wave amplitude and it decays exponentially with depth.

We now have to find an expression of the wave amplitude, a, as a function of wind amplitude and then integrate on the wind wave spectra.

Let's introduce the significant wave height, that is the height of the highest 1/3 of the waves. If the sea contains a narrow range of wave frequencies, H_s is related to the standard deviation of sea-surface displacement and is defined as $H_s = 4\langle \eta^2 \rangle^{1/2}$, where $\langle \eta^2 \rangle^{1/2}$ is the standard deviation of surface displacement.

The wave energy is related to the variance of sea-surface displacement by:

$$E = \rho_w g\left\langle \eta^2 \right\rangle = \frac{1}{2}\rho_w g a^2 = \frac{1}{16}\rho_w g H_s^2 \tag{2.23}$$

where ρ_w is water density, g is gravity, $\left\langle \eta^2 \right\rangle^{1/2}$ is the variance of the surface displacement. In MEDSLIK-II the calculation of significant wave height and Stokes drift is based on a discrete wave spectrum approach, because the average of the wave spectrum, S, is equal to the variance of the surface displacement:

$$\left\langle \eta^2 \right\rangle = \int_0^\infty S(\omega)d\omega \tag{2.24}$$

As a consequence the wave amplitude is

$$a^2 = 2\left\langle \eta^2 \right\rangle = 2\int_0^\infty S(\omega)d\omega \tag{2.25}$$

Knowing now the wave spectra we can compute the amplitude and then the Stokes drift. Over the years, multiple equations have been formulated to describe the wave spectrum as a function of wind speed. We have chosen to use the Joint North Sea Wave Project (JONSWAP) spectrum parameterization (K. Hasselmann et al. 1973) taking the wind and the fetch into account:

$$S(\omega) = \frac{\alpha g^2}{\omega^5}\exp\left[-\frac{5}{4}\left(\frac{\omega_p}{\omega}\right)^4\right]\gamma^r \tag{2.26}$$

The parameters $r, \alpha, \omega_p, \gamma, \sigma$ were determined during the JONSWAP experiment and are expressed by the following formulas

$$r = \exp\left[-\frac{(\omega-\omega_p)^2}{2\sigma^2\omega_p^2}\right]\ ; \alpha = 0.076\left(\frac{W^2}{Fg}\right)^{0.22};$$

$$\omega_p = 22\left(\frac{g^2}{FW}\right)^{1/3}; \gamma = 3.3; \sigma = \begin{cases} 0.07 & \omega \le \omega_p \\ 0.09 & \omega \ge \omega_p \end{cases} \tag{2.27}$$

where F is the fetch, which is the distance over the wind blows with constant velocity, and W is the wind velocity intensity at 10 meters over the sea surface. Practically, the fetch is

calculated as the minimum distance between the oil slick centre and the coast in the opposite direction of the wind direction. Expressing the amplitude as function of the wave spectrum, and taking the integral on the wave frequency equation (2.22) becomes:

$$D_s(z) = 2\int_0^\infty \omega k(\omega) S(\omega) e^{2k(\omega)z} d\omega \tag{2.28}$$

Considering the surface, we obtain the Stokes drift velocity component in the direction of the wave propagation:

$$D_s(z=0) = 2\int_0^\infty \omega k(\omega) S(\omega) d\omega \tag{2.29}$$

Practical wave analysis use the frequency, f, instead of the angular frequency ω. Putting $k = \frac{\omega^2}{g}$ and $\omega = 2\pi f$, equation (2.29) can be rewritten as

$$D_s(z=0) = 2\int_0^\infty \omega(f) k(f) S(f) df = \int_0^\infty \frac{16(\pi f)^3}{g} S(f) df \tag{2.30}$$

Equation (2.29) has been implemented in the MEDSLIK-II, considering the direction of the wave propagation equal to the wind direction. The two components of the Stokes drift velocity, $\mathbf{U}_S$ (see equation (2.16)) are:

$$\begin{aligned} U_s(z=0) &= D_s \cos\vartheta \\ V_s(z=0) &= D_s \sin\vartheta \end{aligned} \tag{2.31}$$

where ϑ is the wind direction, $\vartheta = \text{arctg}\left(\frac{W_y}{W_x}\right)$ and W_x, W_y are the wind zonal and meridional components at 10 m respectively.

2.3.3 Turbulent transport term

The stochastic factor in equation (2.15) is parameterized as follows:

$$\begin{aligned} dx'(t) &= Z_1\sqrt{2K_x dt} = [2n-1]\sqrt{2K_h dt} \\ dy'(t) &= Z_2\sqrt{2K_y dt} = [2n-1]\sqrt{2K_h dt} \\ dz'(t) &= Z_3\sqrt{2K_z dt} = [2n-1]\sqrt{2K_v dt} \end{aligned} \tag{2.32}$$

where *n* is a random real number taking values between 0 and 1 from a uniform distribution and the other symbols have been already described. Equation (2.32) represents the pure random walk model with no memory, i.e., the simplest stochastic model of diffusive processes in the stochastic differential equation (2.13). Thus, the particle moving through the fluid receives at each time step a random impulse due to the action of the incoherent turbulent motions and it has no memory of its previous turbulent displacement.

2.4 Time rate of change of oil volume

In this section we will discuss the time rate of change of the slick state variables and the particle state variables related to the chemical characteristics of the oil slick.

The time rate of change of slick state variables are due to several processes, called weathering, schematically represented in Fig. 2.2. The lighter fractions of the oil disappear through evaporation, while the remaining fractions can be emulsified or dispersed below the water surface. In addition, for the first several hours, a given spill spreads mechanically over the water surface under the action of gravitational forces. Thus four processes contribute to the rate of change of slick state variables: spreading, emulsification, evaporation and dispersion.

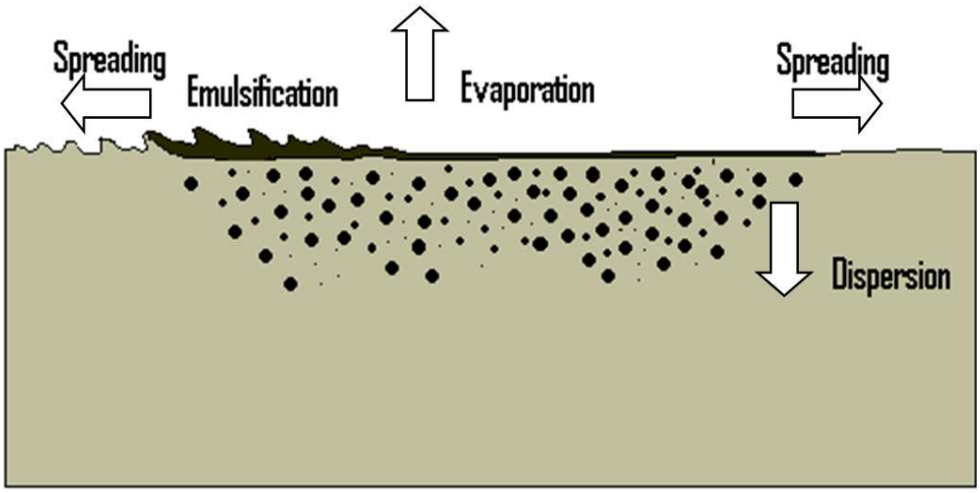

Figure 2.2. Weathering Processes.

The slick state variables rate of change is given in terms of modified Mackay's fate algorithms for evaporation, emulsification and dispersion. The basis of Mackay's model is

to divide the spill into a thick slick and a thin slick (or sheen). Evaporation and dispersion are considered separately for these two parts of the slick.

Let $V^{TK}(t)$ and $V^{TN}(t)$ be the volumes of oil respectively in the thick and the thin slicks, $A^{TK}(t)$ and $A^{TN}(t)$ their two surface areas and $T^{TK}(t)$ and $T^{TN}(t)$ their thicknesses. It is assumed that the thickness $T^{TN}(t)$ of the thin slick is constant and equal to 10 μm, which is a typical observed value for the final thickness of the sheen.

The time rate of change equations for the thick and the thin slick volumes are:

$$\begin{aligned}\frac{\partial V^{TK}}{\partial t} &= -\left.\frac{\partial V^{TK}}{\partial t}\right|_{(E)} - \left.\frac{\partial V^{TK}}{\partial t}\right|_{(D)} - \left.\frac{\partial V^{TN}}{\partial t}\right|_{(S)} \\ \frac{\partial V^{TN}}{\partial t} &= -\left.\frac{\partial V^{TN}}{\partial t}\right|_{(E)} - \left.\frac{\partial V^{TN}}{\partial t}\right|_{(D)} + \left.\frac{\partial V^{TN}}{\partial t}\right|_{(S)}\end{aligned} \qquad (2.33)$$

where $\left.\frac{\partial V^{TK}}{\partial t}\right|_{(E)}$ and $\left.\frac{\partial V^{TN}}{\partial t}\right|_{(E)}$ are the rate of volume lost by evaporation, $\left.\frac{\partial V^{TK}}{\partial t}\right|_{(D)}$ and $\left.\frac{\partial V^{TN}}{\partial t}\right|_{(D)}$ are the rate of volume lost by dispersion and $\left.\frac{\partial V^{TN}}{\partial t}\right|_{(S)}$ is the rate of volume of oil changing from the thick to the thin volume of the slick due to the spreading. In the next sections each term in (2.33) is described in details.

Evaporation brings to an increase in the viscosity of the oil, and the formula used for this is

$$\eta(t) = \eta_0 \exp(K^{(E)} f^{TK}(t)) \qquad (2.34)$$

where η_0 is the initial viscosity, $f^{TK}(t)$ is the fraction of oil evaporated from the thick slick, described in the section 2.4.2, and $K^{(E)}$ is a constant that determines the increase of viscosity with evaporation (with a default nondimensional value of 4).

Emulsification refers to the process by which water becomes mixed with the oil in the slick. Let $f^{w}(t)$ be the fraction of water in the oil-water mousse. Then Mackay's model for the time rate of change of this fraction is (Mackay et al., 1979):

$$\left.\frac{\partial f^{w}}{\partial t}\right|_{(M)} = C_2^{(M)}(W(t)+1)^2\left[1 - C_3^{(M)} f^{w}(t-\Delta t)\right] \qquad (2.35)$$

where $C_2^{(M)}$ is a constant which controls the rate of water absorption, $C_3^{(M)}$ is a constant which controls maximum water fraction in the mousse and W(t) is the wind speed. This model is based on assuming mousse formation is a first-order process with the water-in-oil fraction having an upper limit of $\left(C_2^{(M)}\right)^{-1}$ (default value taken as 75% for light oils but decreasing with API number for heavy oils).

The principal effect of emulsification is to create a mousse with greatly increased viscosity. It is supposed that the viscosity η_{EM} of the mousse is given by

$$\eta_{EM}(t) = \eta(t)\exp\left[\frac{2.5f^{w}(t)}{1 - C_1^{(M)} f^{w}(t)}\right] \qquad (2.36)$$

where $C_1^{(M)}$ is a constant which controls the effect of water fraction on mousse viscosity. Emulsification is assumed to continue until η_{EM} reaches a maximum value η_{MAX} when the state of the oil consists of floating tar balls.

2.4.1 The link between particle variables and slick variables

To link the slick variables to the particle variables we have to define the following quantities: the fraction of oil evaporated, $f^{(E)}(t)$, the fraction of oil dispersed, $f^{(D)}(t)$ and the fraction of oil absorbed onto the coast, $f^{(C)}(t)$.

The fraction of oil evaporated, $f^{(E)}(t)$, is defined as the ratio between the total volume of oil evaporated and the initial volume of oil

$$f^{(E)}(t) = \frac{V^{TK}(t)\big|_{(E)} + V^{TN}(t)\big|_{(E)}}{V^{TK}(t_0) + V^{TN}(t_0)} \qquad (2.37)$$

where $V^{TK}(t)\big|_{(E)}$ and $V^{TN}(t)\big|_{(E)}$ is the volume of oil evaporated from the thick and thin slick, respectively, calculated using equation (2.41) and (2.44).

The fraction of oil dispersed, $f^{(D)}(t)$, is defined as the ratio between the total volume of oil dispersed and the initial volume of oil and it is equal to

$$f^{(D)}(t) = \frac{V^{TK}(t)\big|_{(D)} + V^{TN}(t)\big|_{(D)}}{V^{TK}(t_0) + V^{TN}(t_0)} \qquad (2.38)$$

where $V^{TK}(t)\big|_{(D)}$ and $V^{TN}(t)\big|_{(D)}$ is the volume of oil dispersed beneath the thick and thin slick, respectively, calculated using equation (2.46) and (2.50).

During its transport the particle can arrive on the coast and a certain fraction of the oil can become permanently attached there, for example by seeping into the sand or forming a tar layer on the rock. It is assumed that the fraction of a beached parcel seeping is:

$$f^{(C)}(t) = 1 - 0.5^{\frac{dt}{T_S}} \qquad (2.39)$$

where Ts is a half-life for seepage or other mode of permanent attachment. The amount of oil remaining in any parcel that is on the beach is then reduced by this fraction while the volume of oil lost is counted as remaining permanently on the given coastal segment. The half-lives Ts are assigned to each coastal segment depending on coastal type.

2.4.2 Time rate of change of oil slick state variables due to evaporation

Evaporation changes the volume of the thick and thin part of the slick. The volume of oil lost by evaporation is computed using Mackay's algorithm for evaporation (Mackay et al., 1980).

For the thick oil slick, the time rate of change of the fraction of oil evaporated, f^{TK}, is the product of the vapour pressure, P_{oil} and the change in the evaporative exposure, $\frac{dE^{TK}}{dt}$, which units are $[bar^{-1}\ s^{-1}]$:

$$\left.\frac{df^{TK}}{dt}\right|_{(E)} = P_{oil}\frac{dE^{TK}}{dt} \qquad (2.40)$$

The time rate of change of the the volume lost by evaporation from the thick slick, $V^{TK}(t)\big|_{(E)}$, is expressed as the original total volume multiplied by the rate of change of the fraction (equation 2.40):

$$\left.\frac{\partial V^{TK}}{\partial t}\right|_{(E)} = \left.\frac{df^{TK}}{dt}\right|_{(E)} \left[V^{TK}(t_0) + V^{TN}(t_0)\right] \qquad (2.41)$$

where $V^{TK}(t_0)$, $V^{TN}(t_0)$ are the initial volume of the thick and thin slick respectively.

The oil vapour pressure is expressed in the form:

$$P_{oil} = P_0 e^{(-cf^{TK}t)} \qquad (2.42)$$

where P0 is the initial vapour pressure and c is a constant that measures the rate of decrease of vapour pressure with the fraction already evaporated. The change in evaporative exposure is expressed as:

$$\frac{dE^{TK}}{dt} = \frac{K_M V_{MOL} A^{TK}(t)(1 - f^{TK}(t))}{RT(t)V^{TK}(t)} \qquad (2.43)$$

where A^{TK} is the area of the thick part of the slick, T is the temperature (expressed in K) and K_M is the evaporative exposure to wind, R is the gas constant which is equal to $8.2 \cdot 10^{-5}\,\mathrm{bar\,m^3\,mol^{-1}\,°K}$ and V_{MOL} is the molar volume of the oil ($2 \cdot 10^{-4}\,\mathrm{mol\,m^{-3}}$). For K_M we assume $K_M = 0.0067 \cdot (3.6 \cdot W(t))^{0.78}$ where W is the 10 m wind modulus.

For the thin slick oil, it is supposed that the light component evaporates immediately. The time rate of change of the volume evaporated from the thin slick equals the total content of light component in the thin slick:

$$\left.\frac{\partial V^{TN}}{\partial t}\right|_{(E)} = V^{TN}(t)\frac{(f_{max} - f^{TN}(t))}{(1 - f^{TN}(t))} \qquad (2.44)$$

where f_{max} is the initial fraction of light component, which represents the maximum value that f^{TN} can attain.

The evaporative component in the thin slick has been assumed to disappear immediately, but the thin slick, trough the spreading process, is fed by oil from the thick slick that has not in general fully evaporated. The fraction $f^{TN}(t)$ of oil in the thin slick is then written as:

$$\frac{df^{TN}}{dt} = -\left.\frac{\partial V^{TN}}{\partial t}\right|_{(s)} \frac{(f_{max} - f^{TK}(t))}{V^{TN}(t)} \tag{2.45}$$

2.4.3 Time rate of change of oil slick state variables due to dispersion

The model of dispersion of oil into the water column (Buist 1979) and Mackay (Mackay et al., 1979). Wave action drives oil into the water, forming a cloud of droplets beneath the spill. The droplets are classified as either large droplets that rapidly rise and coalesce again with the spill, or small droplets that rise more slowly, and may be immersed long enough to diffuse into the lower layers of the water column. In the latter case they are lost from the surface spill and considered to be permanently dispersed. The criterion that distinguishes the small droplets is that their rising velocity under buoyancy forces is comparable to their diffusive velocity, while for large droplets the rising velocity is much larger.

Consider first the thick slick, on each time step, a fraction of the small droplets is assumed to be lost by dispersion to the lower layers of the water column, according to the following rate:

$$\left.\frac{\partial V^{TK}}{\partial t}\right|_{(D)} = \frac{1}{2}(C_1^{(D)} - v_S)c_S A^{TK}(t) + \frac{dX_S}{dt} \tag{2.46}$$

where $C_1^{(D)}$ is the upward diffusive velocity of the small droplets (constant value), v_S is the rising velocity of the small droplets (constant value), c_S is the fraction of the small droplets and X_S is the volume of small droplets beneath the thick slick. The amount of small droplets is equal:

$$X_S(t) = c_S u_m A^{TK}(t) \tag{2.47}$$

where um is the vertical thickness of the droplet cloud (constant value). The large droplets are not regarded as dispersed since they eventually re-coalesce with the slick. The fraction of the small droplets is calculated using the following expression:

$$c_s = \frac{2C_3^{(D)}(W(t)+1)^2 T^{TK}(t) f_{S-TK}}{v_s + C_1^{(D)}} \tag{2.48}$$

where $C_3^{(D)}$ is a constant which controls the rate of dispersion of all droplets by waves, W(t) is the wind speed and f_{S-TK} is the fraction of small droplets in the dispersed oil beneath the thick slick, equal to

$$f_{S-TK} = \left[1 + C_4^{(D)} \left(\frac{\eta_{EM}}{10}\right)^{1/2} \left(\frac{T^{TK}(t)}{0.001}\right)\left(\frac{\sigma}{24}\right)\right]^{-1} \tag{2.49}$$

where $C_4^{(D)}$ is a constant which controls the fraction of droplets below a critical size, η_{EM} is the emulsified oil viscosity (see equation 2.36) and σ is interfacial surface tension between oil and water (constant value).

The thin slick is treated much more simply. Only small droplets are assumed to be formed beneath it. It is assumed that these droplets are all lost to the surface spill, according to the following rate:

$$\left.\frac{\partial V^{TN}}{\partial t}\right|_{(D)} = C_3^{(D)} (W(t)+1)^2 T^{TN}(t) A^{TN}(t) f_{S-TN} \tag{2.50}$$

$$f_{S-TN} = \left(1 + C_5^{(D)} \frac{\sigma}{24}\right)^{-1} \tag{2.51}$$

where $C_5^{(D)}$ is a constant which controls the dispersion from the thin slick (sheen) and f_{S-TN} is the fraction of small droplets in the dispersed oil beneath the thin slick.

2.4.4 Time rate of change of oil slick state variables due to spreading

To complete the algorithms we need models for the changes in areas of the thick and thin slicks and the rate of flow of oil from the one into the other (Mackay et al., 1977 and 1980). For the thick slick, spreading consists of two parts, one a loss of area due to oil flowing from the thick to the thin slicks and a second corresponding to Fay's gravity-viscous phase of the spreading (Fay, 1971).

The rate of volume flowing from the thick to the thin slick is related to the increment in area of the thin slick:

$$\left.\frac{\partial V^{TK}}{\partial t}\right|_{(S)} = -\left.\frac{\partial V^{TN}}{\partial t}\right|_{(S)} = \left.\frac{\partial A^{TN}}{\partial t}\right|_{(S)} T^{TN}(t) \qquad (2.52)$$

Mackay approximates the increment in area of the thin slick by a formula similar to the Fay formula: proportional to the cube root of the area times the time step times an exponential function of the thickness of the thick slick that reflects the tendency of the slicks to stop spreading when they become very thin:

$$\left.\frac{\partial A^{TN}}{\partial t}\right|_{(S)} = C_1^{(S)}\left(A^{TN}(t)\right)^{1/3} \exp\left(\frac{-C_3^{(S)}}{T^{TK}(t)+0.00001}\right) \qquad (2.53)$$

The rate of change of the area of the thick slick per time step is

$$\left.\frac{\partial A^{TK}}{\partial t}\right|_{(S)} = \frac{1}{T^{TK}(t)}\left.\frac{\partial V^{TK}}{\partial t}\right|_{(S)} + C_2^{(S)}\left(A^{TK}(t)\right)^{1/3}\left(T^{TK}(t)\right)^{4/3} \qquad (2.54)$$

where $C_2^{(S)}$ is a constant.

Thus, once we have a value for $\left.\frac{\partial A^{TN}}{\partial t}\right|_{(S)}$, we can update the area, A^{TK}, of the thick slick.

Mechanical spreading is considered to occur for an initial period of 48 hours after the release of each sub-spill or until the thickness of the thick part of the slick becomes equal to that of the thin slick if this occurs first. If this occurs, the program terminates all further spreading, transfers all the remaining oil in the thick slick and in the droplet clouds beneath it to the thin slick and from that point on ignores evaporation and dispersion from the thick slick.

Thus, on each time step the area of the thick and thin part of the slick is updated using the empirical formulas of equations (2.53) and (2.54) and the new thickness of the slick can be computed as:

$$T^{TK}(t) = \frac{V^{TK}(t)}{A^{TK}(t)} \qquad (2.55)$$

2.5 MEDSLIK-II model implementation

2.5.1 MEDSLIK-II input data: the coupling with meteo-oceanographic fields

MEDSLIK-II requires as input the wind forcing, the sea surface temperature and the sea currents. The wind forcing, i.e. the wind velocity components at 10 m over the sea surface, is provided by atmospheric forecasting model, while the currents and temperature by oceanographic forecasting models.

The atmospheric wind and the oceanographic fields (i.e. currents, temperature) are given at a series of fixed-point grid and time instants. Particles composing tracers are normally given at intermediate grid points so that spatial and temporal interpolation is needed: the current velocities and the wind velocity have to be calculated at the location of a given particle. The wind velocity considered in the particle displacement is the wind velocity in the nearest grid point to the particle position. Instead, the current velocities in the particle position are computed applying a bilinear interpolation to the velocities surrounding the particle position, performing a linear interpolation first in one direction, and then again in the other direction. All positions and velocities are referenced in a system based on the indices of the grid cells and the local position within a given cell (see Figure 2.3). Transformation functions handle the conversions between geographical coordinates and the internal representation in MEDSLIK-II. Thus, in the following equation when talking about x,y it is the internal coordinate directions that are referred to. The current velocity components of the particle in the position (x,y) is determined from the equation:

$$q_{x,y} = \left(q_{m,n}(m+1-x) + q_{m+1,n}(x-m)\right)(n+1-y) + \left(q_{m+1,n+1}(m+1-x) + q_{m,n+1}(x-m)\right)(y-n) \quad (2.56)$$

where q is the zonal or meridional velocity component, (m,n),(m+1,n),(m+1,n+1),(m,n+1) are the 4 grid point nearest to the particle position, x,y is the particle position expressed in the internal coordinate reference system.

In the weathering calculation the wind velocity and the sea surface temperature are necessary: the values considered are those in the grid point nearest the slick centre position.

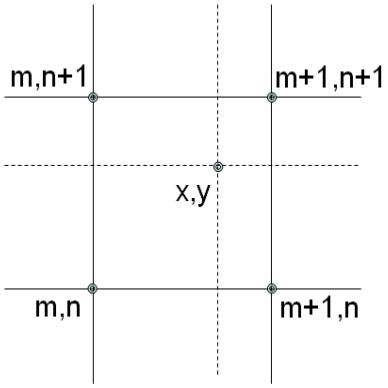

Figure 2.3. A 2-D schematic showing how internal positions are defined in the grid.

2.5.2 MEDSLIK-II input data: the initialization using remote sensing data

The oil spill data required to define a numerical oil spill initial condition are: location, time, oil type area and thickness of the oil slick, as well as the age of the oil spill from initial release in the sea. This information can be easily provided to MEDSLIK-II by satellite monitoring systems

MEDSLIK-II is particularly suitable to be used in order to predict the transport of a slick observed by satellite. In the original MEDSLIK model the initial spill could be only a point source, but in the case of a simulation of a slick observed by satellite, the initial spill must cover the entire slick area observed by the satellite. When a spill is detected by a satellite (Optical or SAR), the slick information, such as the position of the centre of the slick, the slick contour coordinates, the time of the observation and the area of the slick are usually computed by the satellite systems. The thickness of the slick and type of oil are required for an oil spill simulation, but frequently are not provided by the satellite monitoring systems, and need to be hypothesized.

MEDSLIK-II contains a dedicated subroutine that allows to read the slick polygonal coordinates and to distribute the spill parcels randomly into the slick area.

Let's call the slick polygonal coordinates (X_i, Y_i), where i is the number of edges of the slick polygonal. First MEDSLIK-II constructs a box circumscribing the slick contour. Next, we consider a particle with random coordinates contained inside the box, P=(P_x, P_y). Then, we have to check if that point is inside the slick contour.

The method implemented counts the number of times a vertical ray starting from the point P crosses the polygon boundary edge separating it's inside and outside. If this number is even, then the point is outside; otherwise, when the crossing number is odd, the point is inside. Looping trough all the polygon edges, we first have to check if there is any crossing of the vertical line starting from P with the polygonal. There are three conditions that must be verified.

First, we have to check, the following two conditions:

(1) if $X_i \le P_x < X_{i+1}$; (2) if $X_i > P_x$ and $X_{i+1} \le P_x$.

If one of these conditions is verified, then we have to compute the y coordinate of the actual intersection between the ray $x=P_x$ and the polygon, that is:

$$Y_{INT} = \frac{(P_x - X_i)(Y_{i+1} - Y_i) + Y_i (X_{i+1} - X_i)}{X_{i+1} - X_i}$$

The third condition to be verified is $Y_{INT} > P_y$, which means we have a valid crossing of $x=P_x$ (an upward crossing). This conditions have to be checked for all the polygon edges and we have to count how many time there is a valid crossing, if the number is odd the point is inside.

The procedure described above has to be repeated until the number of particles inside the polygon is equal to the number of particles representing the slick (usually 10000).

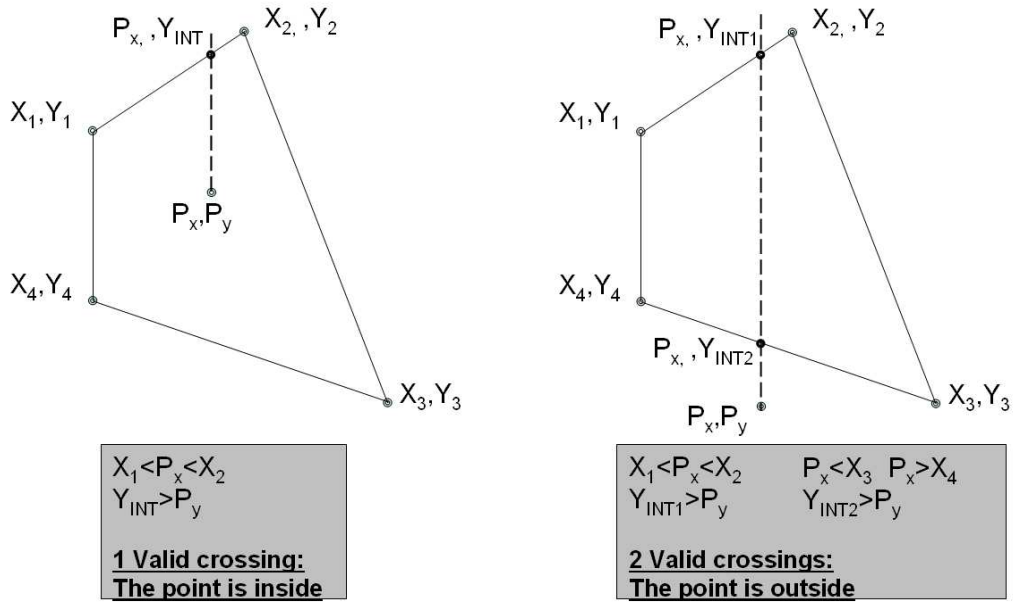

Figure 2.4. Schematic view of the method used to check if a point is inside a polygon.

A new feature of MEDSLIK-II is the possibility to initialize the slick variables: the oil viscosity $\eta(t_0)$, the oil volume of thick slick, $V^{TK}(t_0)$, the oil volume of thin slick, $V^{TN}(t_0)$ and the fraction of water in the oil-water mousse, $f^{w}(t_0)$. Usually, we are simulating the motion and weathering of an oil spill that has not just been released at sea. For example, this happens when we want to forecast the transport and weathering of an oil slick observed by satellite. So, the spill has already begun to undergo the transformation due to the weathering processes. Thus, the initial properties of the spill at time of the observation must be calculated.

In order to be realistic a new input data has been introduced in MEDSLIK-II: the age of the slick. This parameter should be provided by the satellite systems, otherwise it must be hypothesized.

The slick state variables at the time of the observation are calculated by running a simulation only considering the weathering processes (evaporation, dispersion, spreading and emulsification) for a time equal to the age of the slick, taking into account the wind and SST in the area where the spill is observed. After this initialization period, a simulation of the spill evolution considering the weathering processes calculation and advection calculation is performed.

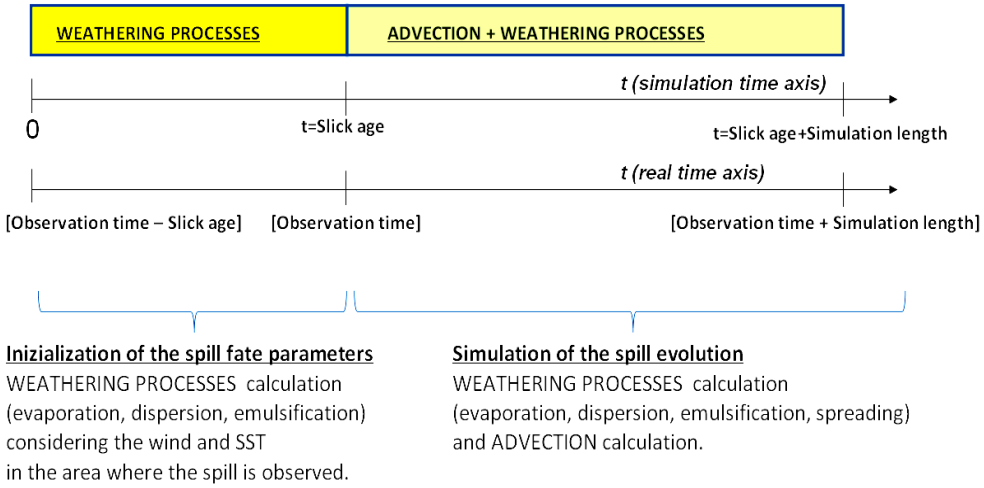

Figure 2.5. Scheme of the temporal axis of the simulation including the inizialization of the spill fate parameters.

2.5.3 MEDSLIK-II output data

MEDSLIK-II produces as output the horizontal spatial distribution of the oil on the water surface, $C_S(x_{TM}, t)$, of the oil dispersed in the water column, $C_D(x_{TM}, t)$, and of the oil on the coast, $C_C(L, t)$. In addition, MEDSLIK-II provides the total volume of oil on surface, $V_S(t)$, of oil dispersed, $V_D(t)$, of oil on the coast, $V_C(t)$, and the volume of oil water mousse, $V_W(t)$. The model classified the particles in three different classes: “on surface” (on the water surface), “dispersed” (in the water column) or “beached” (on the coast). The horizontal spatial distributions of oil ($C_S(x_{TM}, t)$, $CD(x_{TM}, t)$ $C_C(L, t)$) and the total volumes ($V_S(t)$, $V_D(t)$, $V_C(t)$) are found assembling together the particles within the same class.

As initial condition all the particles are considered to be on the water surface. Then, due to the transport and transformation processes, the particles can be moved in the water column or on the coast.

The probability of any particle to be dispersed into the water column, on a given time step is equal to

$$P^{(D)}(t) = \frac{f^{(D)}(t) - f^{(D)}(t - \Delta t)}{1 - f^{(D)}(t - \Delta t)} \qquad (2.57)$$

where $f^{(D)}(t)$ is the fraction of oil dispersed calculated using equation (2.38). For each particle and at each time step a random number, between 0 and 1, is called and a particle passed from the “on surface” status to “dispersed” status if the random number < $P^{(D)}(t)$.

At each time-step, the model checks whether the displacement of the parcel intersects any of the line segments that are used to approximate the coastal map. If it crosses more than one, the one nearest its starting point is taken, and the parcel is moved just to this point of intersection. Thus, the particle passes from the “on surface” status to the “beached” status. The beaching of a particle is not permanent and it is assumed that at subsequent time steps there is a probability that the parcel may wash back into the water. It is supposed (Torgrimson (1980); Shen et al. (1987)) that this probability of washing back on each time step is given in terms of a half-life. However, while on the beach, a fraction of the oil becomes permanently beached through seeping into the sand, becoming adsorbed onto rocks and so on. So oil on the beach consists of two categories, some that may later be washed back into the water column and some that may not. The rate of absorption as well as the probability of being washed off depends on the type of coastline and the model

allows classification of coasts into categories such as sandy beach, small or large pebbles, rocky coast, exposed headland, and so on. The probability of washing back is given by

$$P^{(C)}(t) = 1 - 0.5^{\frac{dt}{T_w}} \quad (2.58)$$

where T_w is the half-life for oil to remain on the beach before washing off again. A value of T_w is assigned to each coastal segment depending on the coastal type, for example sand beach, rocky coastline and so on.

At each time step, for each "beached" particle a random number generator is called and if the random number < $P^{(C)}(t)$ the parcel is released back into the water (its status becomes again "on surface").

The horizontal spatial distribution of the surface and dispersed oil, $C_S(x_{TM}, t)$ and $C_D(x_{TM},t)$, is calculated using the equation (2.4), simplified to two dimensions. Then, the $C_S(x_{TM},t)$ and $C_D(x_{TM},t)$ will be then expressed as volume of oil per unit area. They are calculated summing together the oil volume of each particle within each grid cell area and belonging to the same class:

$$C_S(\mathbf{x}_{TM}, t) = \frac{N_S(\mathbf{x}_{TM}, t)\upsilon(t)}{\delta x_T \delta y_T \delta z_T}\rho \quad (2.59)$$

$$C_D(\mathbf{x}_{TM}, t) = \frac{N_D(\mathbf{x}_{TM}, t)\upsilon(t)}{\delta x_T \delta y_T \delta z_T}\rho \quad (2.60)$$

where $N_S(x_{TM},t)$ is the number of particles "on surface" in the oil tracer grid unit area around the position (x_{TM}, y_{TM}) and $N_D(x_{TM},t)$ is the number of particles "dispersed" in the water column below the grid cell.

$N_S(x_{TM},t)$ and $N_D(x_{TM}, t)$ are calculated using equation (2.3) simplified to two dimensions. In MEDSLIK-II $\delta x_T, \delta y_T$ are usually set equal to 150 m.

The spatial distribution of oil on the coast, $C_C(L; t)$, is calculated using the equation (2.4), simplified to one dimension. $C_C(L,t)$ is expressed as volume of oil per linear km. The coastline is approximated by line segments and the volume of oil on each coastal segment is calculated by summing the oil volume of each particle stuck on the coastal segment and dividing the total volume by the length of the coastal segment:

$$C_c(L,t) = \frac{N_c(L,t)\upsilon(t)}{\delta l}\rho \quad (2.61)$$

where $N_C(L,t)$ is the number of particles "beached" in the coastal segment unit length, δl.
The total volumes of oil $V_S(t)$, $V_D(t)$, Vc(t) are calculated by summing together the oil volume of all the particles belonging to the same class.

$$\begin{aligned} V_S(t) &= N_S^{TOT}(t)\upsilon(t) \\ V_D(t) &= N_D^{TOT}(t)\upsilon(t) \\ V_C(t) &= N_C^{TOT}(t)\upsilon(t) \end{aligned} \tag{2.62}$$

where $N_S^{TOT}(t)$, $N_D^{TOT}(t)$, $N_C^{TOT}(t)$ are the total number of particle "on surface", "dispersed" and "beached", respectively.
The volume of oil water mousse is calculated as:

$$V_w(t) = \frac{V_S(t)}{1 - f_w(t)} \tag{2.63}$$

where $f_w(t)$ is the fraction of water in the oil-water mousse (see equation 2.35)

2.6 Case studies

In this section we illustrate three groups of sensitivity experiments in order to understand the sensitivity of the transformation and fate of oil at the surface as a function of different model assumptions. First we concentrate on the time rate of change of particle position sensitivity to the U_c, U_w and U_s terms of (2.16). Then we add the weathering processes and compare with satellite observations.
Several validation data sets will be used. The CODE drifters (Davis 1985) released during the MREA07 (Marine Rapid Environmental Experiment) in the Ligurian Sea (Poulain et al. 2010). The MREA drifters will be used here to study the U_c term resolution and the depth of U_c given by Eulerian model.
The SPHERE drifters were deployed south of Nice in the fall 2007, In the framework of the MERSEA project (Desaubies 2009), will be used to see the effects of U_w in (2.16). The SPHERE drifters are oil spill-following surface drifters specifically conceived for oil spill tracking, 39.5 cm diameter spheres designed on the basis of earlier experiments carried out in the late 1980s and early 1990s (Price et al. 2006). A new type of surface drifters, the Oil Spill Drifter (OSD), were used to study the Stokes' drift importance. The

OSD is a 32cm diameter cylinder and it has been designed with a reduced submergence in order to follow a surface oil spill (Archetti 2009). The OSDs were deployed in the coastal waters of the Northern Adriatic Sea in July 2009.

Finally, the satellite images of a slick observed on two consecutive days in the August 2008 near the Algerian coast, will be used to study the importance of the weathering processes.

2.6.1 Sensitivuty to the current and local wind transport terms.

To study the current and local wind transport terms, MEDSLIK-II has been used to simulate trajectory only without computing the oil transformation processes and the diffusion of the slick by turbulence. In the MREA drifters simulations, the oceanographic fields (hourly and daily currents) were provided to MEDSLIK-II by the operational oceanographic model MFS (Pinardi & Coppini 2010) and by a nested high resolution model (IRENOM). The winds are the ECMWF 6 hourly analyses.

The drifters employed were provided by NATO Undersea Research Centre (NURC) and by the Istituto Nazionale di Oceanografia e di Geofisica sperimentale (OGS). These drifters have been localized by Global Positioning System (GPS) at hourly intervals and their data telemetered via the Argos system. The time and deploy position of each drifter are listed in table 2.1. Several experiments were carried on varying the current horizontal resolution and depth, see table 2.2.

ID Drifter	Release Date (dd.mm.yy hh:mm)	Latitude (° ‘)	Longitude (° ‘)	Last signal (dd.mm.yy hh:mm)
74871	14.05.07 15:00	43° 49.218’	9° 8.772’	16.06.07 03:00
74872	14.05.07 14:00	43° 48.318’	9° 8.331’	26.09.07 18:00
74873	14.05.07 16:00	43° 49.896’	9° 9.696’	15.06.07 05:00
74874	14.05.07 15:00	43° 48.438’	9° 9.271’	30.06.07 05:00
74875	14.05.07 15:00	43° 48.936’	9° 9.324’	23.07.07 13:00

Table 2.1. Position and date of the deployment of the first cluster of drifters.

Experiment Name	MREA-EXP1	MREA-EXP 2	MREA-EXP 3	MREA-EXP 4
Model	MFS	MFS	IRENOM	MFS
Horizontal resolution	6.5 km	6.5 km	3 km	6.5 km
Temporal frequency	Daily fields	Hourly fields	Hourly fields	Hourly fields
Current depth	surface	Surface	Surface	30 m
Wind correction	0%	0%	0%	3%

Table 2.2. Table of the experiments designed to study the model sensitivity to the current resolution and frequency.

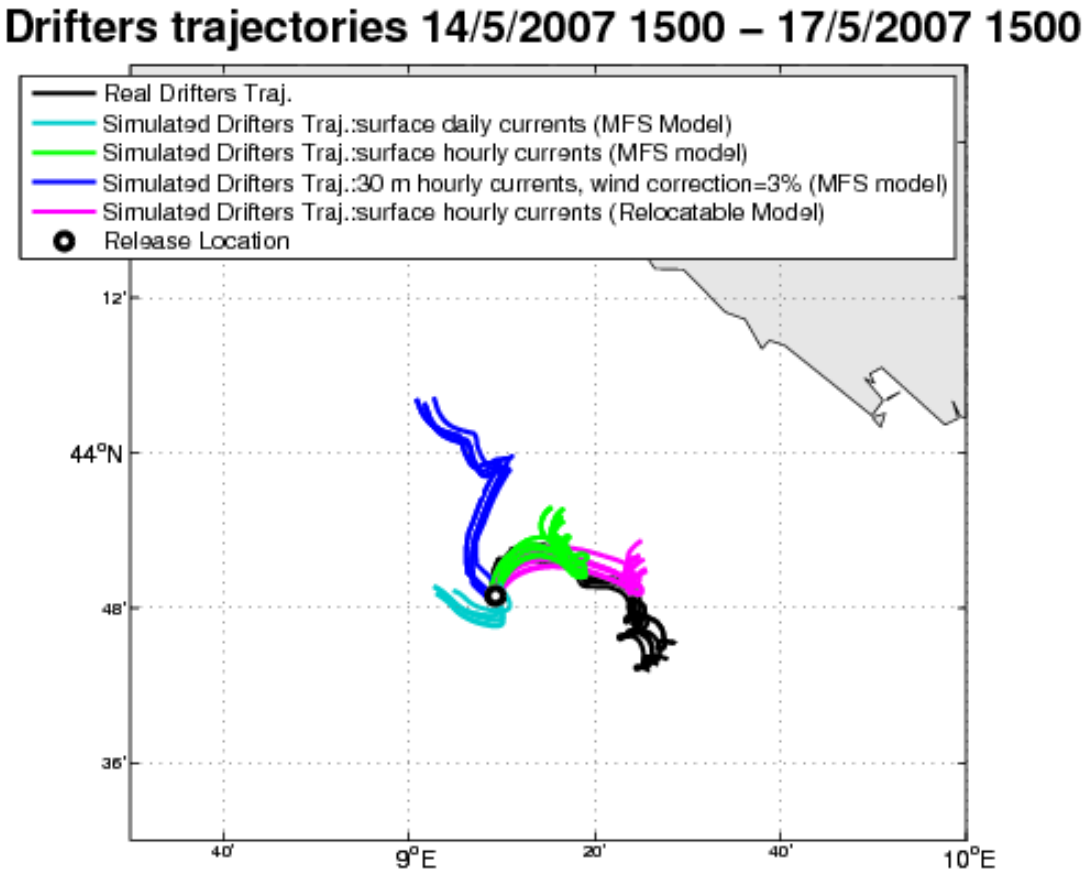

Figure 2.6. Observed drifter trajectories (black lines) and the Medslik-II trajectories from 14/05/2007 to 17/05/2007. The light blue lines are the trajectories obtained using the surface daily MFS currents (MREA-EXP1), the green lines are the trajectories obtained using the surface hourly MFS currents (MREA-EXP2) and the pink lines are the trajectories obtained using the surface hourly currents produced by the Relocatable model (horizontal resolution 3 km) (MREA-EXP3); the blue lines are the trajectories obtained using the 30 m hourly currents produced by the MFS and adding a 3% wind correction (MREA-EXP4).

Figure 2.6 shows the observed drifters tracks (black lines) and the MEDSLIK-II trajectories obtained using the MFS daily and hourly surface currents and the IRENOM currents. The IRENOM model provides higher horizontal resolution (3 km) current nested in MFS. The trajectories obtained using the daily MFS fields (light blue lines) are not capable to reproduce the correct drifter direction. When high frequency fields (MFS hourly currents) are used, the simulated drifters, at least for the first day, go in the correct direction (green lines). When higher resolution modeling (IRENOM hourly fields) is used for the Eulerian velocity field, the trajectories in the Ligurian Sea are better reconstructed (pink lines). When the Eulerian velocity field is not accurate enough, as the MREA07 case, there is a need for higher resolution currents, such as the one given by IRENOM.

Thus, increasing frequency and horizontal resolution of the current fields allows greater accuracy in the reproduction of the real trajectories.

As described in section 2.3.1 the advanced operational OGCMs can provide an accurate representation of the surface ageostrophic currents. In the past the oil spill models use the "drift factor approach", which was considered to be the most practical approach for adjusting the advection of oil slicks coming from rather low resolution circulation models which do not properly resolve the Ekman currents. With this method the drift velocity of the surface oil was considered to be the sum of a fraction of the wind velocity and the eulerian velocity field, supposed to represent the deeper (geostrophic) velocity field. In particular a 3% of the wind velocity was commonly added to geostrophic velocity (Mark Reed et al. 1994) (A.H. Al-Rabeh 1994). In the MREA-EXP2 and MREA-EXP4 simulations (see Table 2.2) we wanted to test the improvement of the simulations using the surface ageostrophic currents provided by an OGCM instead of using the 30 m currents (which are supposed to be the geostrophic currents), adding a 3% of the wind velocity and using a wind angle equal to 0° (see equation 2.18). In Figure 2.6 we can observe that when the surface MFS hourly currents are used, the simulated drifters, at least for the first day, go in the correct direction (green lines). Instead, following the common rule of the 30m current depth and 3% wind correction (blue lines) the simulated drifters don't reproduce the real trajectories. We can also observe that all the trajectories generated by the MEDSLIK-II model show a smaller displacement of the drifters than the actual displacement. The drifter location errors are the consequences of integrating wind and

ocean current fields that do not exactly represent the real-world conditions. Since the simulated trajectories are integrals of the input fields, their terminal locations bear an accumulation of the errors in those fields.

During the MERSEA project, seven drifters were deployed on the 10th of October 2007 in the Western Mediterranean south of Nice at varying distances from the coast. The drifters are oil monitoring buoys to emulate a surface oil spill (SPHERE). The MEDSLIK-II simulation has been done without computing the oil transformation processes or the spreading of the slick by turbulence. The currents were taken from MFS hourly analyses and winds are from ECMWF 6 hourly analyses. The simulations were carried out applying different "ageostrophic correction", 0%, 1%, 2% and 3%, that means adding a percentage of the wind velocity to the current velocity, this correction accounts for model errors in the representation of the ageostrophic current.

ID Drifter	Release Date (dd.mm.yy hh:mm)	Latitude (° ‘)	Longitude (° ‘)	Last signal (dd.mm.yy hh:mm)
75660	10.10.07 15:27	43° 36.80’	7° 24.30’	18.10.07 13:39
75661	10.10.07 14:15	43° 31.92’	7° 33.70’	30.11.07 20:28
75662	10.10.07 15:25	43° 34.40’	7° 27.57’	03.12.07 10:32
75663	10.10.07 14:16	43° 31.62’	7° 34.13’	03.12.07 09:37
75664	10.10.07 15:26	43° 34.95’	7° 27.62’	03.12.07 12:19
60212	10.10.07 17:03	43° 36.82’	7° 23.13’	03.12.07 10:30
60213	10.10.07 17:03	43° 36.82’	7° 24.05’	03.12.07 11:21

Table 2.3. Date and position of the drifters deployment.

Since the deployment sites were very close to the coast (in Table 2.3 the time and deploy position are listed), the simulated drifters reached the coast in a few days, then a restart of the simulations was needed (see Table 2.4). Figure 2.7 shows the trajectories reinitialized 4 days after the real drifters deployment.

ID Drifter	Re-initialisation Date (dd.mm.yy hh:mm)	Latitude (° ‘)	Longitude (° ‘)	Last signal (dd.mm.yy hh:mm)
75660	14.10.07 01:10	42° 52.22’	5° 55.90’	18.10.07 13:39
75661	14.10.07 01:12	42° 58.88’	6° 24.63’	30.11.07 20:28
75662	14.10.07 03:42	42° 48.37’	5° 53.36’	03.12.07 10:32
75663	14.10.07 01:12	42° 59.18’	6° 25.47’	03.12.07 09:37
75664	14.10.07 01:11	42° 47.76’	5° 56.83’	03.12.07 12:19
60212	14.10.07 01:10	42° 51.63’	5° 55.61’	03.12.07 10:30
60213	14.10.07 01:11	42° 53.22’	5° 57.78’	03.12.07 11:21

Table 2.4. Date and position of the drifters 4 days after the release.

Experiment Name	MERSEA-EXP1	MERSEA-EXP2	MERSEA-EXP3	MERSEA-EXP4	MERSEA-EXP5
Model	MFS	MFS	MFS	MFS	MFS
Horizontal resolution	6.5 km	6.5 km	6.5 km	6.5 km	6.5 km
Temporal frequency	Hourly fields	Hourly fields	Hourly fields	Hourly fields	Hourly fields
Current depth	0 m	0 m	0 m	0 m	30 m
Ageostrophic correction	0	1%	2%	3%	3%

Table 2.5. Table of the experiments designed to study the model sensitivity to the current depth and to the ageostrophic current correction.

In Figure 2.7 we present only two of the seven drifters trajectories. The behaviour of the seven drifters is similar: between 5° and 7°E all drifters move along the coast and between 4° and 5°E they are advected offshore towards the south, probably under the influence of winds.

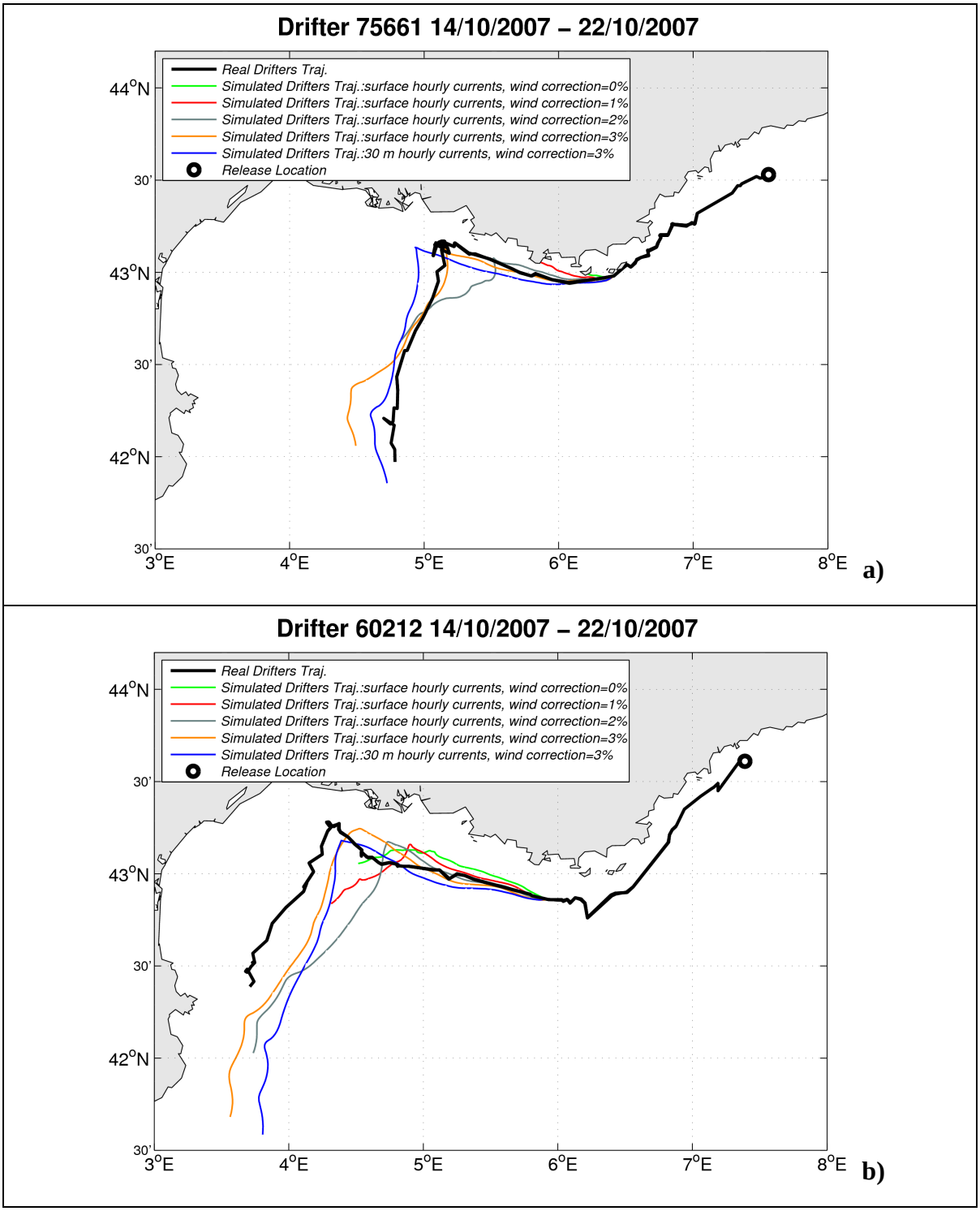

Figure 2.7. Observed drifter trajectory (black lines) and the Medslik-II trajectories from 14/10/2007 to 22/10/2007: a) drifter 75661, b) drifter 60212.

Figure 2.7 shows the observed drifters track (black line) and the MEDSLIK-II trajectories obtained using the MFS hourly currents using different wind correction of the ageostrophic

current. We can observe that increasing the wind correction, we can reproduce the movement offshore toward the south, which is not reproducible using only the currents produced by MFS. In this case the trajectories obtained using the 30m current depth and 3% wind correction (MERSEA-EXP5, blue lines) is similar to the trajectories obtained using the surface currents and the wind correction of 3%.

The best results are achieved using an "ageostrophic correction" of 3%. This can be due to the low resolution of the MFS model and to the proximity to the coast. In the coastal area the MFS surface currents could not contain a satisfactory representation of the surface ageostrophic currents. Moreover, the ageostrophic correction could be necessary in order to account for missing processes at the air-sea interface, such as the wind wave induced currents. Furthermore, we have to remember that the drifters used are SPHERE drifters, that are not completely underwater. Thus, they probably feel also a direct effect of the wind, that is not accounted in the surface currents. This could justify the necessity to add a percentage of the wind intensity to the surface currents in order to consider the wind drag on the emerged part drifter

2.6.2 Sensitivity to the Stokes' drift term.

Three OSD drifters have been launched on July 21 2009 at 9:40, at about 6 km from the coast, near Cesenatico (Northern Adriatic Sea). The OSD have been designed in order to be oil emulating drifters: their reduced submergence should allow them to follow the currents velocities of the first mm of the water column. The drifters are equipped with a GPS to acquire the geographical position every 10 minutes and a IRIDIUM satellite system to send data to a server.

The trajectory of one of the three drifters, the one that was at sea for the longer period (nearly a week), has been simulated using MEDSLIK-II. The simulations were carried out using the hourly current fields provided by the AFS model and the wind fields produced by the ECMWF (snapshot every 6 hours).

Several simulations were performed (see Table 2.6). First, we tried to use the surface current field (0 m) and we didn't add the wind drift (Figure 2.8, green lines). Second, we used the current fields adding 1% of the wind velocity to the current velocity (Figure 2.8, red lines). Then, we used the current fields adding the Stokes drift velocity (Figure 2.8, pink lines), calculated using the JONSWAP spectrum parameterization (see section 2.3.2).

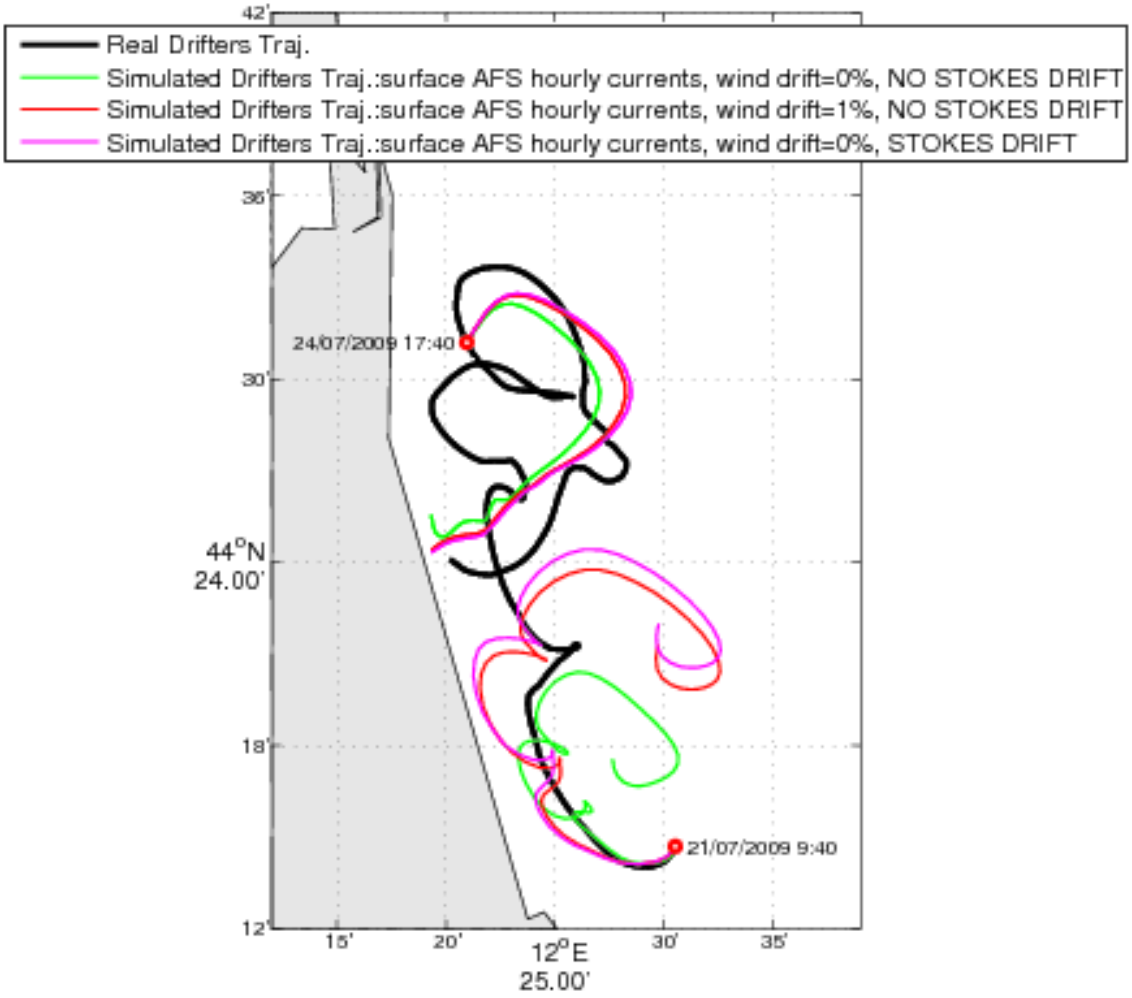

Figure 2.8. Observed drifter trajectory (black lines) and the Medslik-II trajectories obtained using the surface hourly AFS currents, from 21/07/2009 to 26/07/2009: (a) green lines are the trajectories simulated without adding the wind drift and the Stokes drift; (b) red lines are the trajectories simulated adding the 1% wind drift and without adding the Stokes drift; (c) the pink lines are the trajectories simulated considering the Stokes drift velocity and without adding the wind drift.

Since the simulated trajectories are integrals of the input fields (wind and current), their terminal locations bear an accumulation of the errors in those fields. Thus, as shown in Figure 2.8, we decided to re-initialize the position of the drifters 80 hours after the first deployment (see Table 2.7). As shown in Figure 2.8 re-initializing the simulations we are able to better reconstruct the real trajectory. As shown in Figure 2.8 the MEDSLIK-II simulated trajectory is shorter than the observed drifter trajectory, that's probably why the simulated velocities are too low in this region. Furthermore, the simulated trajectory is

erroneously directed in the east direction, this is probably due to the incorrect simulation of the inertial oscillations by the hydrodynamic model. Although, there isn't a strong evidence, we argue that the simulated trajectories, obtained adding the 1% of the wind intensity of the current velocities or considering the Stokes drift, are in better agreement with the observations. As shown in Figure 2.8 the simulated trajectories obtained adding the 1% of the wind intensity and considering the Stokes drift are almost overlapping, giving us the evidence that the wind-correction factor can be used to account for missing physics at the air-sea interface, such as the wind-wave-induced currents. Although, we have to remember that in our formulation the Stokes drift is a function of the wind velocity in the location of the slick or buoy, which is an useful assumption, but we are still missing the contribution from the long period swells.

Experiment Name	**OSD-EXP1**	**OSD-EXP2**	**OSD-EXP3**
Model	AFS	AFS	AFS
Horizontal resolution	2.2 km	2.2 km	2.2 km
Temporal frequency	Hourly fields	Hourly fields	Hourly fields
Current depth	0 m	0 m	0 m
Ageostrophic correction	0	1%	0%
Stokes Drift	NO	NO	**YES**

Table 2.6. Table of the experiments designed to study the model sensitivity to the Stokes drift velocity.

Date & time 1° release	21 July 2009 09:40 GMT
Simulation duration	80 hours
Coordinates	**Lat=** 44° 14.7' **Lon=** 12° 30.5'
Date & time 2° release	24 July 2009 17:40 GMT
Simulation duration	55 hours
Coordinates	**Lat=** 44° 31.20' **Lon=** 12° 20.95'

Table 2.7. Position, date and time of the simulated drifters releases (restart of the simulation after the beaching of the simulated drifter).

2.6.3 Sensitivity to the transformation processes.

In the framework of the MARCOAST project, the MFS forecasting system, coupled with the MEDSLIK-II oil spill model, has been used to support several requests from the Regional Marine Pollution Emergency Response Centre for the Mediterranean Sea (REMPEC) to forecast the dispersion of slicks detected by Synthetic-Aperture Radar

(SAR) images in the Tunisian and Algerian waters. The 6th of August 2008 at 9:50 a.m. oil spill has been detected with high confidence in the Algerian waters by the ENVISAT satellite, using a SAR sensor (red slick in Figure 2.9). After 25 hours a slick has been observed again in the same area by the MODIS TERRA satellite, using an optical sensor (green dots in Figure 2.11).

The SAR data (observation time and date, position of oil slick center, area and oil slick polygonal contour) has been provided by REMPEC, while the optical sensor data has been provided by Institute of Atmospheric Sciences and Climate (ISAC) of the Italian National Research Council (CNR). The slick information, such as the position of the centre of the slick, the slick polygonal coordinates, the time of the observation and the area of the slick are calculated by the satellite system and used by MEDSLIK-II. The age and thickness of the slick and the oil density are not provided by the satellite systems and they must be hypothesized in order to calculate the initial properties of the spill at time of the observation.

The input data provided by the satellite system and the input data hypothesized are listed in Table 2.9. The simulation was carried out using the surface currents from the MFS hourly analyses, while the winds are taken from ECMWF 6 hourly analyses.

Input data	
Observation Date	06/08/2008
Observation Time	09:51
Latitude (spill centre)	38° 17.39’
Longitude (spill centre)	5° 23.53’
Area	75712496 m2
Density (hypothesized)	0.898 tons/m3
Thickness (hypothesized)	0.0001 mm
Age (hypothesized)	0 and 24 hours
Current velocities	MFS 1 hourly Analysis
Wind forcing	ECMWF 6 hourly Analysis

Table 2.9. Oil spill simulation input data.

In order to consider the possible errors in the current fields, several simulations has been carried out varying the initial position of the slick. The initial position of the oil spill particles has been shifted 1 point grid (6.5 km) in 8 different position (1-North, 2-South, 3-East, 4- West, 5- North-East, 6- South-West, 7- South-East, 8- North-West). The best

agreement between the simulated and the observed slick has been obtained shifting the oil slick 1 point grid in the North-East direction from the original position and with a thickness of 0.0001 mm (volume equal to 6.8 tons).

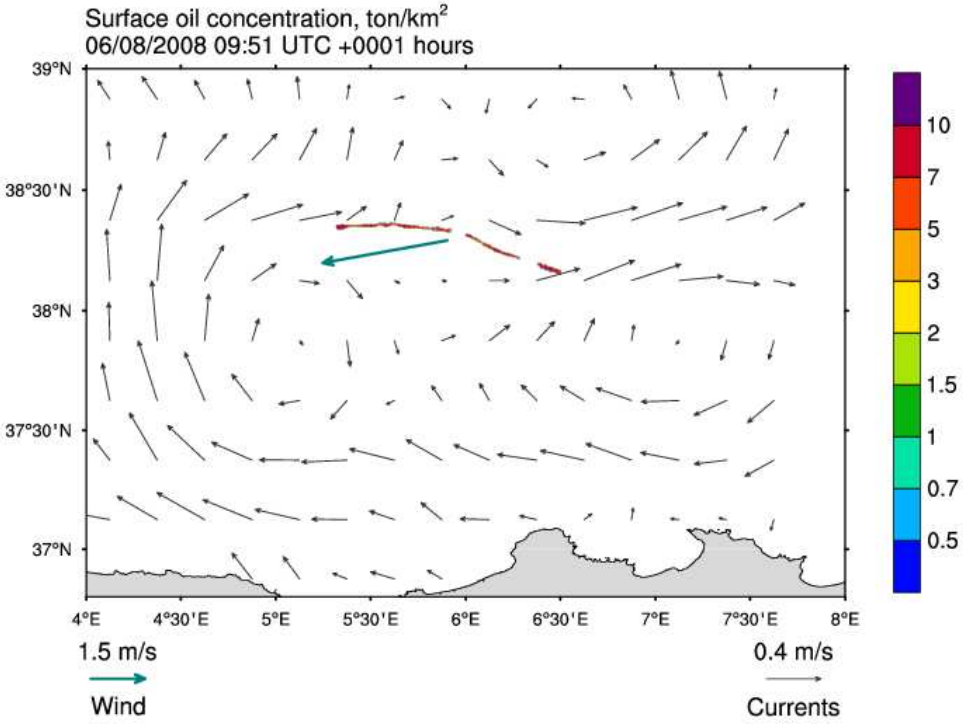

Figure 2.9. MFS current velocity (m/s) hourly analysis field at the surface at 9:51 of the 6th August 2008 and overlay of the slick observed by SAR (red).

As described in section 2.5.2 MEDSLIK-II allows to initialize the slick variables. Since we want to forecast the transport and weathering of an oil slick observed by satellite, the spill may have begun already to undergo the transformation due to the weathering processes. Since we didn't have any information about the age of the slick, we decided to perform two experiments, one considering the slick as just spilled (age= 0hrs) and the other simulating a slick with an age of 24 hrs. As shown in Figure 2.10-a and 2.10-b, one hour after the SAR observations (06/08/08 10:51) the area with an oil concentration higher than 0.1 m^3/km^2 is larger in the case we consider the slick as just spilled. We argued that it would be more feasible to detect the slick by satellite if the concentration of the surface oil on the water surface is higher. Thus, we think that the best experiment is the one considering the slick as just spilled.

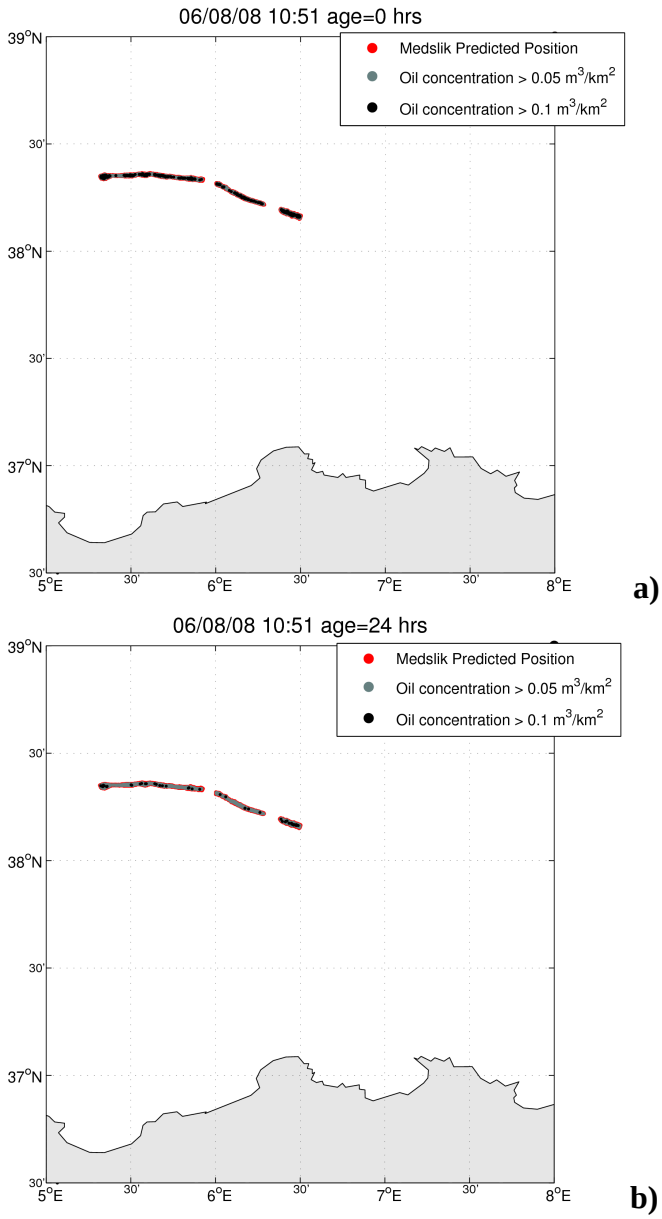

Figure 2.10. The position and shape of the oil slick predicted by MFS-MEDSLIK II on the August 6 10:51 GMT (upper panels) and August 7 12:51 GMT (lower panels). The simulation was carried out considering the slick as just spilled (left panels) and a slick age of 24 hours (right panels). The grey and black parts of the slick identifies the area where the oil concentration is higher.

In Figure 2.11 the simulated oil slick position (red), considering as starting point the position observed by the SAR satellite shifted one grid point in the North West direction, and the MODIS observation (green) of the 7th August 2008 are shown. We can see that the shape of the simulated slick is in agreement with the observed slick. In Figure 2.11 the grey and black part of the slick identifies the area where the oil concentration is higher. As shown in these pictures, the higher concentration area (the western part of the slick) is in

agreement with the position of the slick detected by the optical satellite sensor. The sensor probably didn't detect the lower oil concentration area. These results emphasize the importance of the transformation processes in the prediction of the oil slick fate, giving us the correct information about the persistence of the oil at sea. Without the simulation of the weathering processes the model cannot predict when and where the oil disappears from the sea surface.

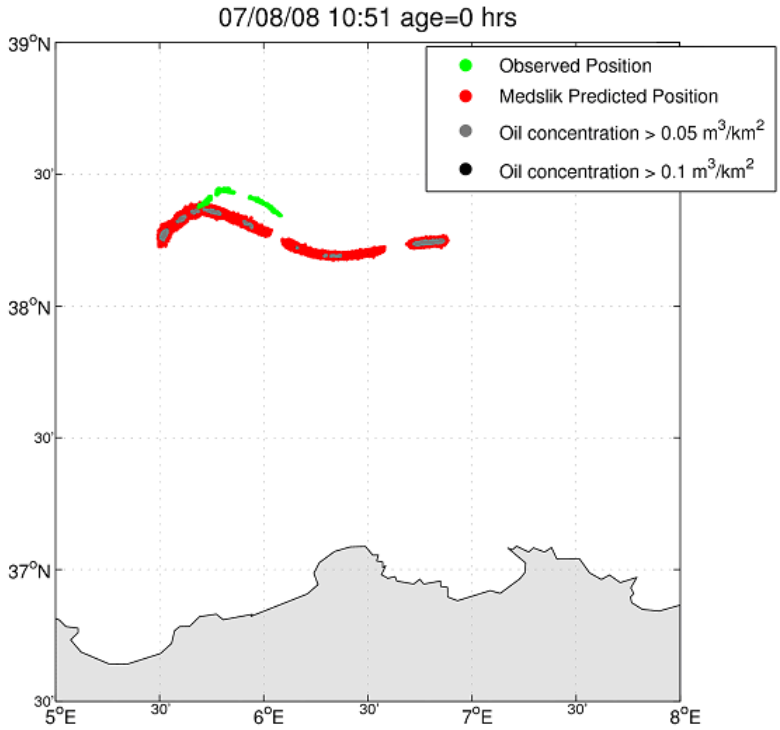

Figure 2.11. The position and of the oil slick after 25 hours predicted by MFS-MEDSLIK II (red), corresponding to August 7 2008 10:50 GMT compared with the slick observed by MODIS-TERRA (green). The simulation was carried out shifting the oil slick 1 point grid in the North-East direction from the original position. The grey and black parts of the slick identifies the area where the oil concentration is higher.

Chapter 3

3 Studies of Lagrangian drifters and oil spill observations

3.1 Introduction

The oil spill model, presented in Chapter 2, has been validated with surface drifter data, with satellite data and with in situ data in different Mediterranean regions. Verification of the oil spill forecasting is both a crucial issue and a difficult task to perform. It's difficult to obtain data of real transport of pollutants into the sea, for this reason the main objective of the cruise presented in this chapter, organized in the framework of the PRIMI project (PRogetto pilota Inquinamento Marino da Idrocarburi), was to visit oil slicks detected by satellite, in order to acquire in situ data for validation of the dispersion and transformation model. The area selected for the cruise was the central Mediterranean (southern Tyrrhenian Sea, Sardinia Channel, Sicily Channel, western Ionian Sea). Moreover, during the cruise different types of drifters were deployed at sea. The drifters are oceanographic instruments used to study the surface circulation and oceanographic dynamics, they are designed to be transported by ocean currents and these peculiarities make them useful tools for the validation of models of Lagrangian particle dispersion.

3.2 The PRIMI cruise

The cruise took place from August 6 to September 7, 2009, in the seas around Sicily (Tyrrhenian, Ionian Seas and Sicily Channel; Figure 3.1), an area with high frequency of illegal hydrocarbon discharge, as inferred from historical and PRIMI monitoring data. The main cruise objective was to visit oil slicks detected by the SAR and optical satellite observations and whose displacement was predicted by the MEDSLIK-II model, coupled with the oceanographic operational models available in the Mediterranean Sea, and acquire data on the oil-spill characteristics and composition. Besides Eulerian conventional hydrographic data, Lagrangian drifters were released in oil slicks for observation purposes, as well as for validation of the dispersion and transformation model. In particular, in order

to be able to distinguish between the uppermost meter of the water column and the purely superficial flow, representative of the near surface and of the oil spill dynamics, respectively, three types of drifting devices were used during the PRIMI cruise: 1) CODE-modified surface drifters, on the basis of the original design developed for the Coastal Ocean Dynamics Experiment (CODE) in the early 1980s (Davis, 1985), which provide measurements of surface currents in the topmost meter of the water column with an accuracy of few cm/s, 2) oil spill-following surface drifters (SPHERE) (see Price et al., 2003). The deployment was aimed at revealing the proportions in which the oil slick follows the wind and the current, respectively, 3) OSD drifters manufactured by the DICAM University of Bologna.

Finally, the cruise was dedicated to a systematic sampling of the hydrographic and biogeochemical characteristics of the area (not described here).

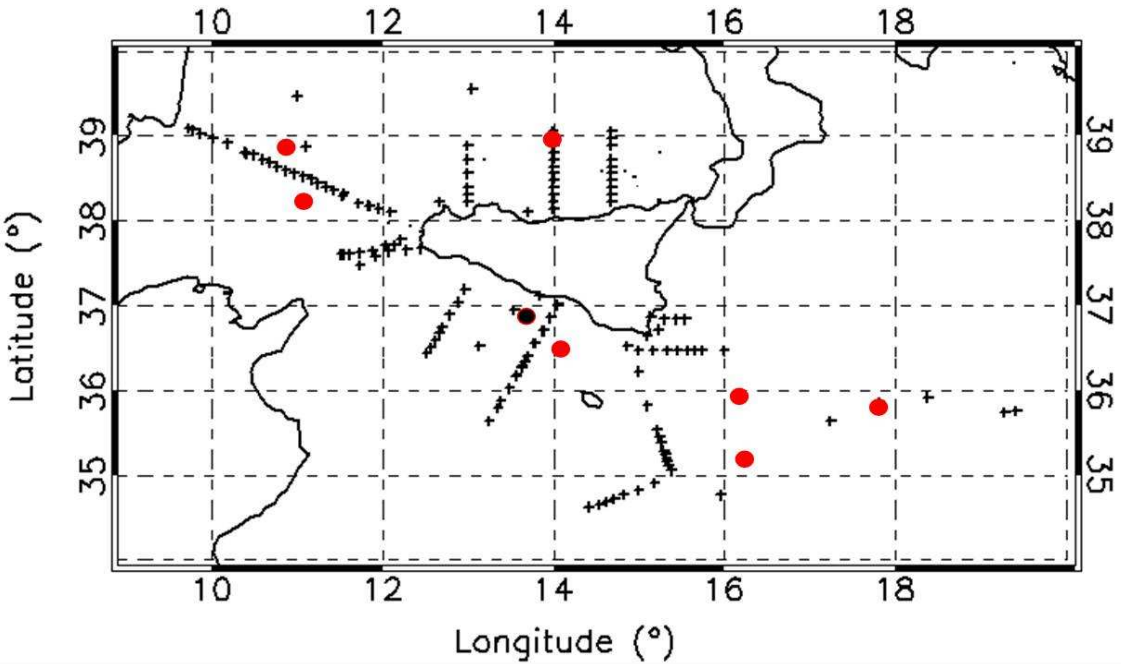

Figure 3.2. PRIMI cruise (Aug. 6 – Sep. 7 2009, R/V Urania) hydrographic stations (black crosses) and visited oil slicks (red dots).

The acquisition of SAR and optical imagery of the cruise area was planned for the cruise period. The ship track was conceived to have R/V URANIA (the ship) present (when possible) in each satellite scene at the time of acquisition and to subsequently search and sample detected oil spill candidates. Each image was searched for possible oil slicks.

MEDSLIK-II coupled with the oceanographic models was used operationally to optimize the research at sea of the oil slicks detected from satellite. Once the information about oil slicks observation from remote sensing monitoring system was received on board of R/V URANIA the staff decided which of the slicks should be search on the basis of the extension of the slicks and of the distance from R/V URANIA position. Then, the forecasters started the procedures to forecast the new position of the selected slicks at the time when R/V URANIA would reach the waypoint to start the visual research of the slick. This procedure was carried to search for 14 slicks and 4 of them have been found.
In the next section the forecasting and searching activities, during the PRIMI cruise 2009, of the 4 slick detected in situ are described.
Table 3.1 present the summary of the forecasting simulations carried out by INGV during the PRIMI cruise 2009.

3.2.1 Instruments

The drifter instruments commonly used during oceanographic cruise are modified CODE drifters'. The design is similar to the one developed for the Coastal Ocean Dynamics Experiment (CODE) in the early 1980s (Davis, 1985). The modified CODE drifter can be considered an efficient instrument to measure surface currents in the first meter of the water column with 1–2 cm/s accuracy (Davis, 1985). It is made of a 1 m long vertical buoyant tube with four wings coming out radially from the tube over its entire length. The buoyancy is provided by four small spherical floats attached on the upper extremities of the wings with a short flexible line (see Figure 3.2-a).
In the oceanographic survey presented in this chapter two other drifter types were used: the SPHERE drifters and the OSD (Oil Spill Drifters) drifter. The SPHERE drifters, which are oil spill-following surface drifters, conceived for oil spill tracking, 39.5 cm diameter spheres designed on the basis of earlier experiments carried out in the late 1980s and early 1990s (see Price et al., 2003). The SPHERE used in this work were equipped with IRIDIUM telemetry (Figure 3.2-c). The OSD drifter was manufactared by the DICAM University of Bologna (Archetti, 2009). The OSD is a 32cm diameter cylinder and it has been designed with a reduced submergence in order to follow or simulate oil spill or surface pollution (Figure 3.2-d). The drifters are equipped with a GPS to acquire the

geographical position every 10 minutes and a IRIDIUM satellite system to send data to a server.

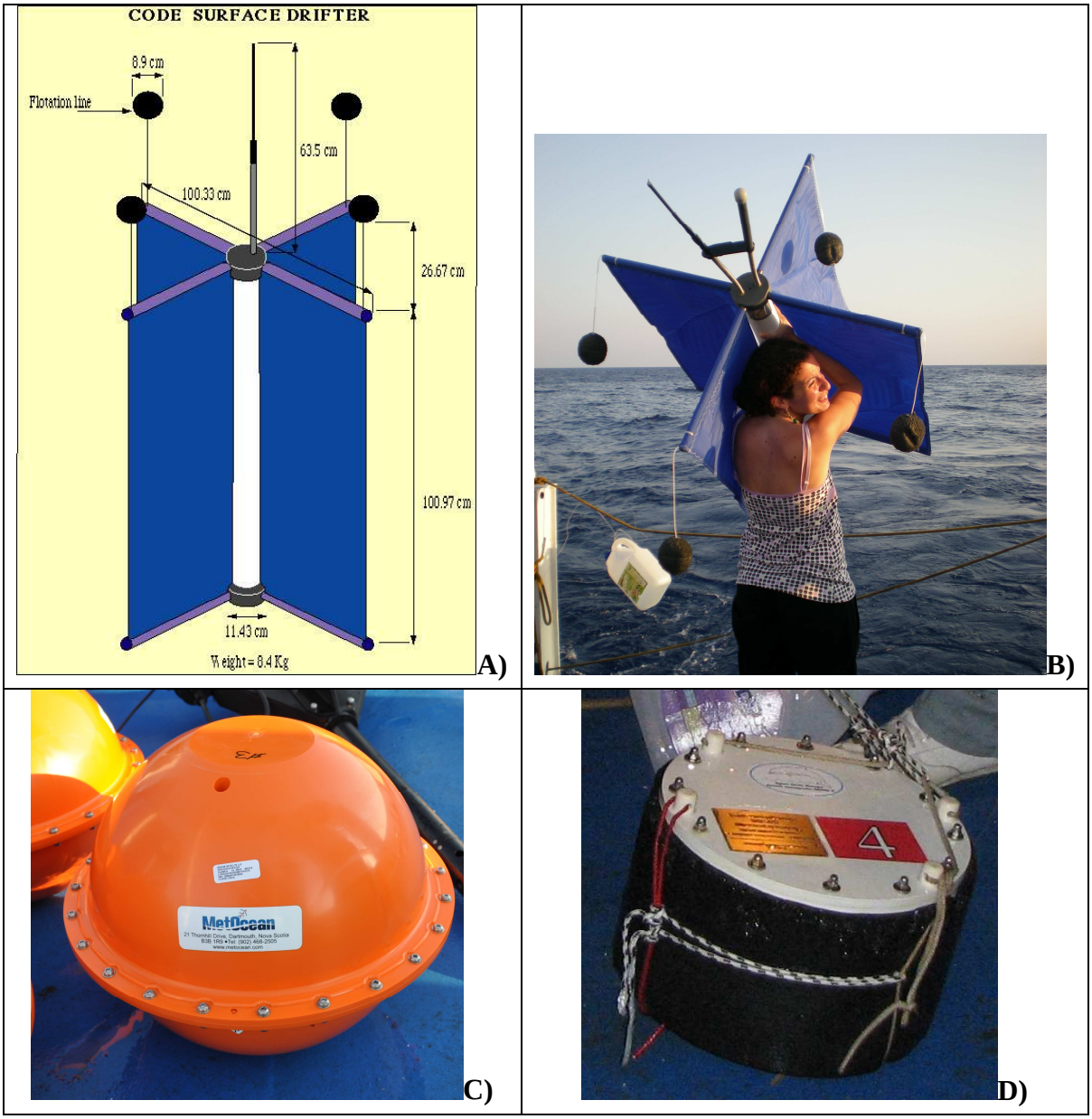

Figure 3.2 Surface drifters types: A) schematic diagram of the modified CODE drifter (image taken from the OGS website); B) deploying a modified CODE drifters; C) SPHERE drifter; D) OSD drifter.

Oil slick ID	Date and time of satellite observation and Mission ID	Distance of the forecasted and in situ slick position	COMMENTS
OS1	2009-08-07 04:58 COSMOSKYMED	More than 8 km	Visual confirmation. Thin film barely detectable by granules and iridescence. 2 samples taken.
OS2	2009-08-11 09:22 ENVISAT	Impossible to estimate	No certain visual confirmation. Slick presence is suggested by several RADAR roughness attenuation episodes, some simultaneous with LIDAR 403 nm band intensity lowering.
OS3	2009-08-15 04:57 COSMOSKYMED	No forecast needed	OS3 is found to be a thermal front with lower temperatures inshore by 0.1 – 0.2 °C.
OS4	2009-08-18 09:03 ENVISAT	Less than 1 km (6 hrs after the satellite observation)	Visual confirmation. Radar and Lidar signal alteration over slick. It is a clearly defined slick with iridescence, brown oil patches and floating tar balls, surely an illegal discharge resulting from ballast wash. 6 samples taken.
OS5	2009-08-24 05:16 COSMOSKYMED	6km	Simulation in Delay Time
OS6	2009-08-24 05:16 COSMOSKYMED		Not done
OS7	2009-08-26 21:06 ENVISAT	1km	Forecast 15h. Observed also in a 2°image on 27th August
OS8	2009-08-26 21:06 ENVISAT	Not found	
OS7	2009-08-27 12:07	1,4 km from the drifter, 6km from medslik forecast	
OS9	2009-08-29 09:45 MODIS AQUA	8km	Forecast 48h. Very small slick found at Way Point
OS10		Not found	No searching activities
OS11	2009-08-30 20:39 ENVISAT	Not found	Forecast 36h. Very small slick found at Way Point
OS12	2009-08-30 20:39 ENVISAT	Not found	Forecast 36h.
OS13	2009-09-02 20:45 ENVISAT	10 km	Found on the way to forecast Way Point. Very small slick found at Way Point
OS14	2009-09-02 20:45 ENVISAT	Not searched but seen again in MODIS	Not searched but seen again in MODIS

Table 3.1 Summary of the forecasting simulations carried out by INGV during the PRIMI cruise 2009.

3.2.2 The forecasting system

The forecast skill of the oil spill dispersal and fate is intimately connected to the accurate knowledge of the marine currents and the wind field. MEDSLIK-II can make use of atmospheric wind and oceanographic fields (i.e. currents, temperature) from several different sources. During the PRIMI cruise, MEDSLIK-II oil spill model used the output produced by the MFS (Mediterranean Forecasting System) (Pinardi et al. 2003), SCRM (Sicily Channel Regional Model) (Gaberšek et al. 2007), TYREMS (Tyrrhenian Regional Model) (Napolitano, in preparation) hydrodynamic models. The atmospheric forcing used has been provided by the ECMWF (horizontal resolution of 0.25°). The oil spill data required to define a numerical oil spill initial conditions are location, time and area of the spill. In the PRIMI system this information has been provided to MEDSLIK-II by the PRIMI satellite monitoring systems (optical and SAR). During the PRIMI cruise the hourly time resolution oceanographic fields were used by MEDSLIK-II. The Mediterranean Sea forecast at basin scale is produced on a daily basis by a complex system composed of an ocean general circulation model (OGCM), a data pre-processing and quality control scheme and an assimilation scheme that corrects the model initial guess with all the “in situ” and satellite available observations. The basin scale model is forced by ECMWF atmospheric fields, made available to INGV by the Italian Air Force Meteorological Office. The output of two other oceanographic models connected to MEDSLIK-II were available during the PRIMI cruise: the SCRM (Sicily Channel Regional Model, Gabèrsek et al., 2007) and the Tyrrhenian regional model (TYREMS, Napolitano et al., 2009). These models are nested within the Mediterranean model and downscale the current field down to 2 km resolution in most of the Italian sea areas, produce marine current and temperature forecasts once a day and for 5 days in the future. The model output from all these models has been coupled operationally with MEDSLIK-II.

Model Name		**MFS (Mediterranean Forecasting System)**
Institution providing the model		INGV
Type		OPA 8.2
Model region	**Geographical name**	Mediterranean Sea
	Geographical coordinates	-6°- 36°15' E 30°16' - 46°N
Grid spacing		1/16°x1/16°~6.5 Km
Model Name		**SCRM (Sicilian Channel Regional Model)**
Institution providing the model		**CNR-IAMC**
Type		POM98
Model region	**Geographical name**	Sicily Strait
	Geographical coordinates	9°-17°E 31°-39.5°N
Grid spacing		1/32°x1/32°~3.5 Km
Model Name		**Tyrrhenian Sea Model**
Institution providing the model		ENEA
Type		POM98
Model region	**Geographical name**	Tyrrhenian Sea
	Geographical coordinates	8.81° – 16.31°East36.68°– 44.51°North
Grid spacing		1/48°x1/48°~2 Km

Table 3.2. Oceanographic models main characteristics.

3.2.3 The operational procedures

During the cruise, oil spills were detected by the PRIMI observation system using near real time SAR (ERS-2, ENVISAT and COSMOSKYMED) as well as optical (MODIS and MERIS) imagery. The cruise plan was organized in order to have the ship within the selected image frames at acquisition time, so as to maximize the number of monitorable oil spills.

Each image was searched for possible oil spills by the PRIMI observation SAR and optical processing softwares, located at the ASI facility in Matera, Italy.

The images, the reports and the files containing the detailed slick information (such as the oil slick contour coordinates) generated by the PRIMI observation systems were received by e-mail on board.

Once the satellite information were received, the staff decided which of the slicks should be searched on the basis of the extension of the slicks and of the distance from R/V URANIA position.

Then, the forecasters started the procedures to forecast the new position of the selected slicks at the time when R/V URANIA would reach the waypoint to start the visual research of the slick.

If available, the oil slick contour provided by the PRIMI observation system were used as input in the oil spill model simulation, otherwise only the oil slick centre or an oil slick contour obtained on board from the satellite images could have been used as initial position of the oil slick.

The MEDSLIK-II model simulations were run on the cluster machine located at the INGV in Bologna, in order to minimize the download time of the oceanographic model outputs and the simulation time.

The step followed by the forecasters were:

- download of the MFS forecast and ECMWF forecast wind field;
- conversion of the satellite information in format suitable to the MEDSLIK-II model;
- run of the MEDSLIK-II model;
- download of the SCRM and TYREMS models forecast (if the SCRM and/or the TYREMS model covered the area of the slick observation);
- run of the MEDSLIK-II models coupled with the higher horizontal resolution currents.

The R/V URANIA staff on the basis of the oil spill forecasted position decided the research area (considering the possible error of the forecasted position) and the ship track to be followed within the area (zig-zag).

Once the ship was moved to the indicated spill area, the oil slick searching via visual and instrumental (Lidar and radar) was carried on.

In the case the oil spill was found, oil samples were collected and in the more severe oil spill the drifters were released.

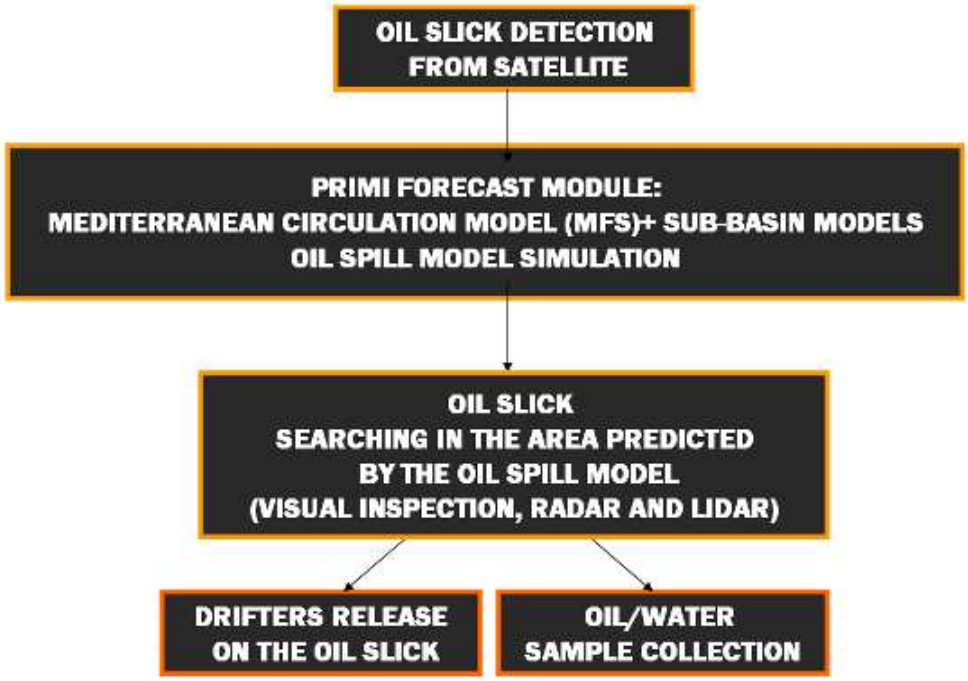

Figure 3.3. Scheme of the operational procedures.

3.2.4 Real time model validation: forecasting of the detected oil slicks

3.2.4.1 PRIMI Oil Slick 1

Diary of the pollution event

1) Satellite image: COSMOSKYMED 07.08.2009 at 04:48 UTC.
2) Reception of the PRIMI SAR report 4726.
3) Reception of the CSKS2_DGM_B_WR_01_HH_RA_SF_20090807045814_20090807045829_SAROSA image and XML data.
4) Release of the OS1 MFS-MEDSLIK forecast.
5) In situ oil slick visual detection and sample collection.

Description of the OS1 pollution event

On the 7th of August 2009 at 09:00 UTC the report related to the image SAR COSMOSKYMED CSKS2_DGM_B_WR_01_HH_RA_SF_20090807045814_20090807045829_SAROSA was received on board. At 10:00 UTC the XML files containing the detailed information

about the spill were received on board. The slick 1 in PRIMI SAR report 4726 (see Figure 3.4), called in this report OS1, was chosen as the one to be searched. The OS1 centre coordinates are 38° 55' 36.314'' N 013° 43' 32.758'' E. At 23:00 UTC the R/V URANIA ship left the previous route (NE Sicily) in order to reach oil spill 1 (OS1) detected in SAR COSMOSKYMED image and the ship steamed to OS1 forecasted position for 08/08/09 10:00 UTC (38' 50.000' N 13° 48.000' E).

On the 8th of August 2009 at 05:00h UTC the ship arrived, before the planned time, on OS1 forecasted position for 08/08/09 10:00 UTC (38' 50.000' N 13° 48.000' E). The searching for OS1 started with E-W tracks in zone delimited by 38° 50.000' N, 38° 55.000' N, 13° 48.000' E, 13° 51.000' E. The tracks were spaced by 1 nm in N-S direction. The arrival time in the predicted position was supposed to be at 10:00 08.08.09. Actually the ship was in the position 5 hours before, but the searching area wasn't updated. Anyway the searching activity were carried on in the area approximately for 5 hours. In Figure 3.5a and 3.5b the searching area, the predicted slick position at 05:00 UTC and 10:00 UTC are shown.

At 09:00h UTC the searching activity in the above zone was stopped and no oil spill was detected. Following the captain suggestion, the ship was moved in order to search east of above zone due to strong eastward current present in the area (about 1 knot). At 09:25h UTC a slick was found: thin film barely detectable by surface granules and iridescence. At 09:25 UTC a sample (OS1_1) was taken (38° 57.814' N 13° 59.070' E) end at 09:33h UTC another sample a sample (OS1_2) was collected (38° 57.889' N 13° 59.141' E).

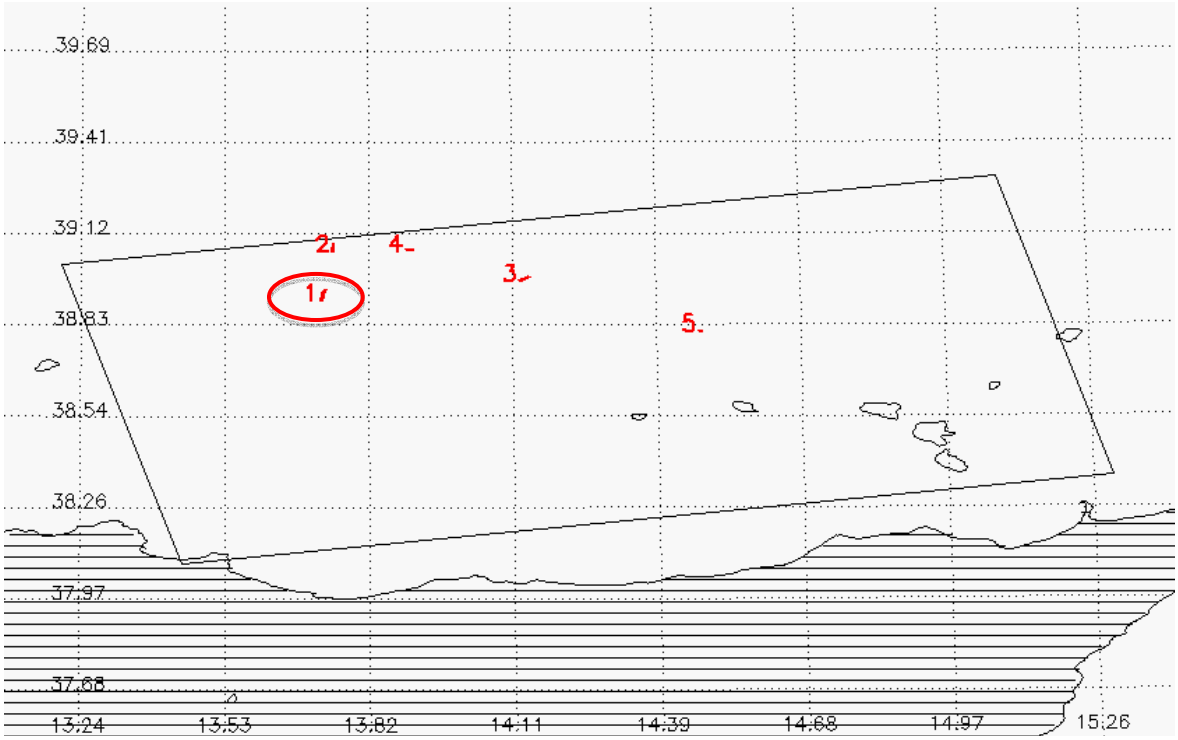

Figure 3.4. Report of COSMOSKYMED 07.08.2009 04:58 UTC passage. 5 slicks were detected in the area. The slick 1 was chosen as the one to be searched.

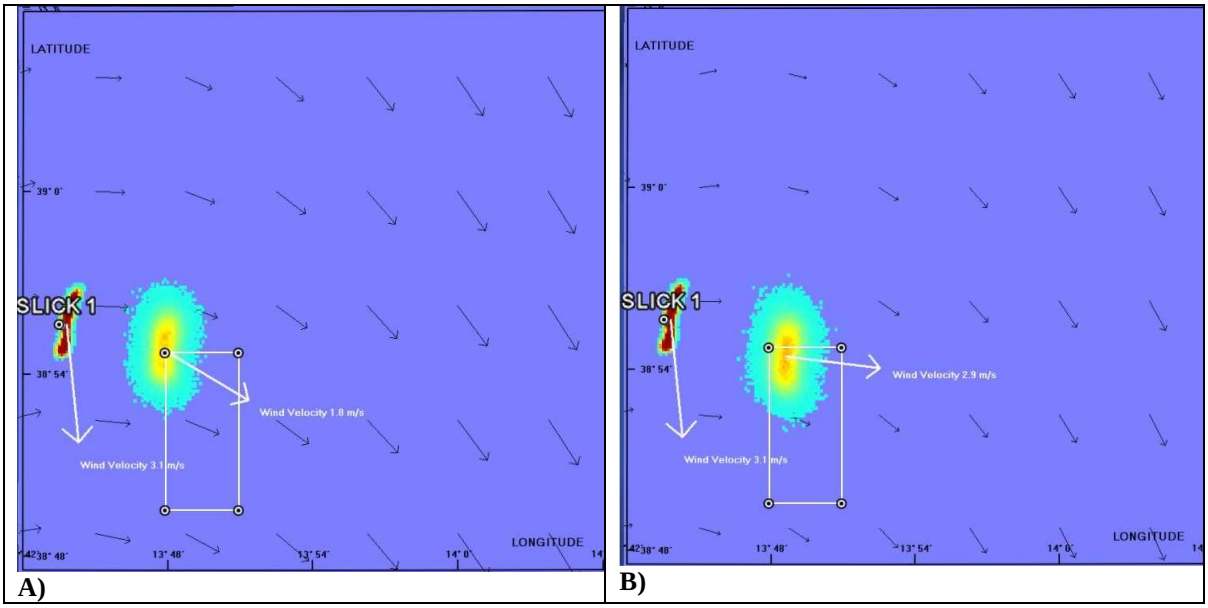

A) **B)**

Figure 3.5. Searching area (white rectangle) and predicted position A) after 24 hours (08.08.09 05:00 UTC) B) after 29 hours (08.08.09 10:00 UTC). Simulation done using the MFS surface currents and wind drift equal to 0%.

Figure 3.6. Photo of the oil slick OS1

Forecasting of OS1

The simulation of the oil slick OS1 has been done after the reception on board of the CSKS2_DGM_B_WR_01_HH_RA_SF_20090807045814_20090807045829_SAROSA image and XML data (07.08.09 10:00 UTC). The first simulation have been performed using the MFS forecast current fields produced the 7th of August 2009, using the surface currents and a wind drift equal to 0. The result of the simulation (position of the slick after 29 hours, 08.08.09 10:00 UTC expected time the ship would have been in the area) is shown in the figure 3.5. The oil spill searching area is indicated by the white rectangle.

However slick 1 and 2 in the PRIMI SAR report 4726 (Figure 3.4) are separately classified, they might be one slick. The forecast of the slick 2 (done in delay mode) indicates that the slick observed in situ might be the slick 2 of the report 4726: the predicted position 29 hours after the satellite passage of the slick 2 is close to the position of the observed slick. After the observation in situ of the slick, in delay mode the following simulations were done:

- simulation of the transport of the slick 1 using the MFS hourly 30 m-currents and 3% wind drift (Figure 3.7);
- simulation of the transport of the slick 2 using the MFS hourly surface currents and 0% wind drift (not shown);

- simulation of the transport of the slick 2 using the MFS hourly 30 m-currents and 3% wind drift (Figure 3.7);
- simulation of the transport of the slick 1 using the TYREMS hourly 30 m-currents and 3% wind drift (Figure 3.8);
- simulation of the transport of the slick 2 using TYREMS hourly 30 m-currents and 3% wind drift (Figure 3.8);

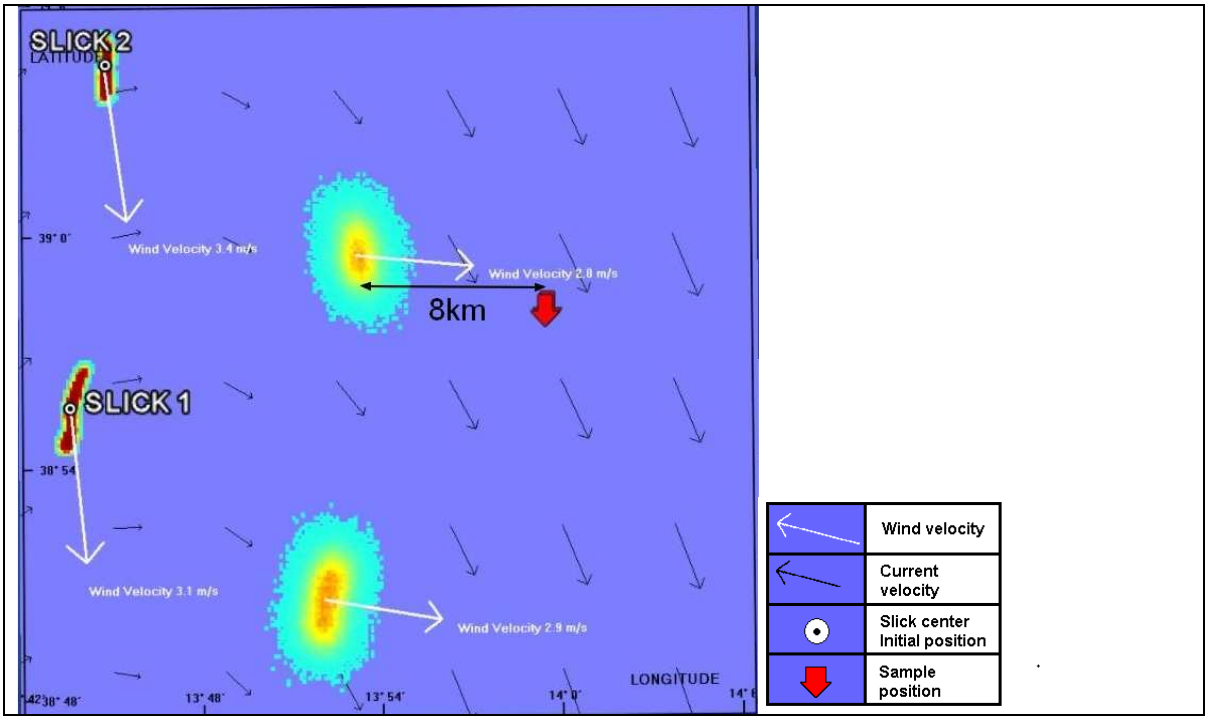

Figure 3.7. Scheme of the evolution of oil slick OS1. The oil spill labelled "slick1" and "slick2" corresponds to the slick1 and 2 of the COSMOSKYMED image (slick1 is OS1). The wider two slicks are the predicted positions by MFS-MEDSLIK 29 hours after (08.08.09 09:00) the COSMOSKYMED image detection. The red arrows represent the sample collection positions the 08.08.09 at 9:30. Simulations done using the MFS 30 m currents and wind drift equal to 3%.

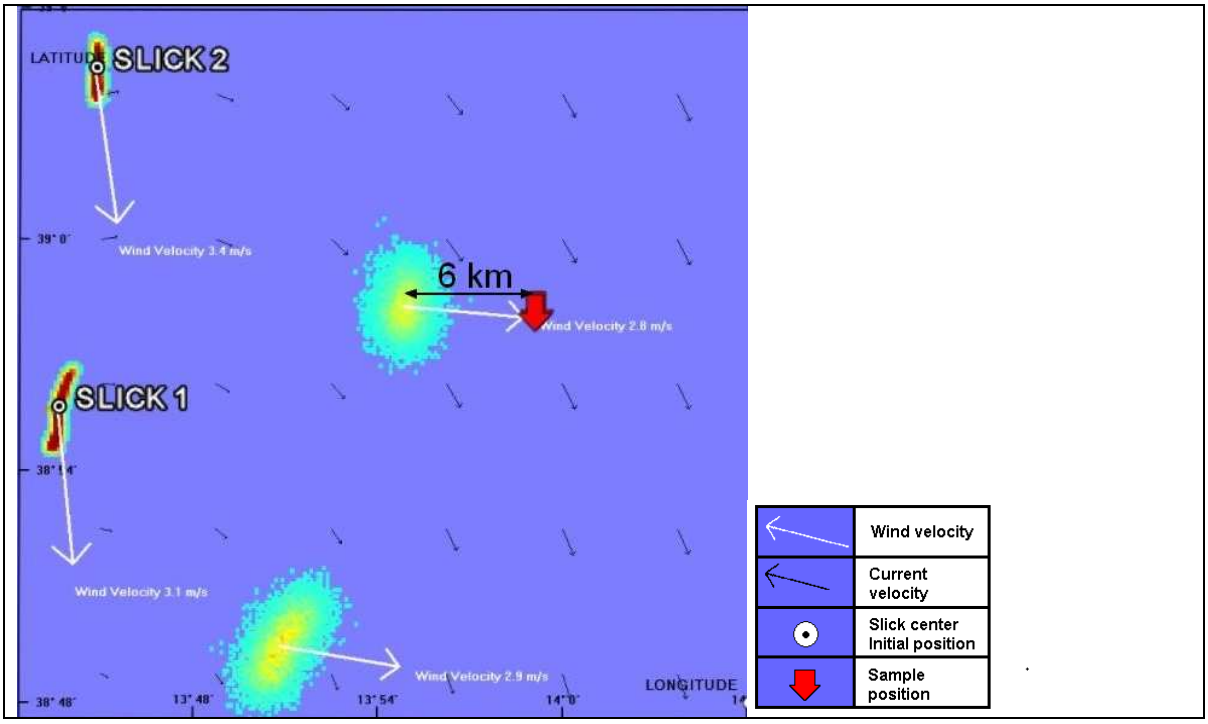

Figure 3.8. Scheme of the evolution of oil slick OS1. The oil spill labelled "slick1" and "slick2" corresponds to the slick1 and 2 of the COSMOSKYMED image (slick1 is OS1). The wider two slick are the predicted position by TYREMS-MEDSLIK 29 hours after (08.08.09 09:00) the COSMOSKYMED image detection. The red arrows represent the sample collection positions the 08.08.09 at 9:30. Simulations done using the TYREMS 30 m currents and wind drift equal to 3%.

In Figure 3.7 and 3.8 the oil spill labelled "slick1" and "slick2" correspond to the slick1 and 2 of the COSMOSKYMED image (slick1 is OS1). The wider two slick are the predicted position by MEDSLIK 29 hours after (08.08.09 10:00) the COSMOSKYMED image detection. The red arrows represent the sample collection position the 08.08.09 at 9:30.

The distance between the simulated position, using the MFS currents, of the slick 2 and the observed slick position is approximately 8 km (figure 3.7). The distance between the simulated position, using the TYREMS currents, of the slick 2 and the observed slick position is approximately 6 km (figure 3.8). The better agreement with the in situ observation was obtained using the TYREMS 30 m-currents and 3% wind drift.

The comparison of model simulation results with in situ observations shows that the oil spill simulated were moving slower than the real slick.

Table 3.3 present the details of the performed simulations.

FORECAST MODE	OPERATIONAL	DELAY TIME	DELAY TIME	DELAY TIME	DELAY TIME	DELAY TIME
OIL SLICK ID	SLICK 1	SLICK 1	SLICK 2	SLICK 2	SLICK 1	SLICK 2
SPILL DATE	2009-08-07	2009-08-07	2009-08-07	2009-08-07	2009-08-07	2009-08-07
OBSERVATION TIME	04:58 UTC	04:58 UTC	04:58 UTC	04:58 UTC	04:58 UTC	04:58 UTC
SLICK CENTER COORDINATE	38° 55' 36.314" N 13° 43' 32.758" E	38° 55' 36.314" N 13° 43' 32.758" E	39° 4' 29.042" N 13° 44' 47.022" E	39° 4' 29.042" N 13° 44' 47.022" E	38° 55' 36.314" N 13° 43' 32.758" E	39° 4' 29.042" N 13° 44' 47.022" E
AREA	1354387.5 m^2	1354387.5 m^2	859612.50 m^2	859612.50 m^2	1354387.5 m^2	859612.50 m^2
THICKNESS (HYPOTHESIS)	0.1 mm	0.1 mm	0.1 mm	0.1 mm	0.1 mm	0.1 mm
DENSITY (HYPOTHESIS)	API=26 (MEDIUM) 0.898 tons/m^3	API=26 (MEDIUM) 0.898 tons/m^3	API=26 (MEDIUM) 0.898 tons/m^3	API=26 (MEDIUM) 0.898 tons/m^3	API=26 (MEDIUM) 0.898 tons/m^3	API=26 (MEDIUM) 0.898 tons/m^3
POINT SOURCE OR AREAL SOURCE	AREAL SOURCE	AREAL SOURCE	AREAL SOURCE	AREAL SOURCE	AREAL SOURCE	AREAL SOURCE
CURRENT VELOCITIES	**MFS 1 HOURLY CURRENTS FORECAST (SURFACE CURRENTS) Forecast production Date: 07.08.09**	**MFS 1 HOURLY CURRENTS FORECAST (30 M CURRENTS) Forecast production Date: 07.08.09**	**MFS 1 HOURLY CURRENTS FORECAST (SURFACE CURRENTS) Forecast production Date: 07.08.09**	**MFS 1 HOURLY CURRENTS FORECAST (30 M CURRENTS) Forecast production Date: 07.08.09**	**TYREMS 1 HOURLY CURRENTS FORECAST (30 M CURRENTS) Forecast production Date: 07.08.09**	**TYREMS 1 HOURLY CURRENTS FORECAST (30 M CURRENTS) Forecast production Date: 07.08.09**
WIND FORCING	ECMWF 6 HOURLY FORECAST	ECMWF 6 HOURLY FORECAST	ECMWF 6 HOURLY FORECAST	ECMWF 6 HOURLY FORECAST	ECMWF 6 HOURLY FORECAST	ECMWF 6 HOURLY FORECAST
WIND FACTOR	0%	3%	0%	3%	3%	3%

Table 3.3. Description of simulations for OS1. The "Forecast Mode: Operational" indicates the oil spill model simulations done before the searching activities, The "Forecast Mode: Delay Mode" indicates the oil spill model simulations done after the detection in situ of the slick. The "Initial slick position: Areal Source" indicates the simulations initialized with the oil slick contour coordinates provided by the satellite systems. The "Initial slick position: Point Source" indicates the simulations initialized with the oil slick barycentre.

3.2.4.2 PRIMI Oil Slick 4

Diary of the pollution event

1) Satellite image: ENVISAT 18.08.2009 at 09:03 UTC
2) Reception of the PRIMI SAR report 6358
3) Reception of the ASA_WSM_1PNACS20090818_090325_000000592081_00408_39039_0001_SARO SA image and XML data
4) Release of the OS4 MFS-MEDSLIK forecast (predicted position for 18.08.09 15:00 UTC)

5) In situ oil slick visual detection and sample collection
6) Drifters (I-SPHERE and CODE) release

Description of the OS4 pollution event

On the 18th of August 2009 at 09:55 UTC the report related to the image SAR ENVISAT ASA_WSM_1PNACS20090818_090325_000000592081_00408_39039_0001_SAROSA was received on board. In the image five slicks were present. The slick 3 in PRIMI SAR report 6358 (see Figure 3.9), called in this document OS4, was chosen as the one to be searched. The ship track was modified in order to reach the OS4. The OS4 centre coordinates are 35° 16' 55.26'' N 16° 24' 52.438" E. The estimated travel time was 8 hours.

At 11:41 UTC the XML files containing the detailed information about the spill were received on board. The forecasted position for 18/08/09 17:00 UTC was 35' 18.000' N 16° 27.000' E (Figure 3.10).

Actually, the ship was in the searching area 2 hours before the expected time. At 14:45 UTC the ship was proceeding to zigzag inside the rectangle containing the slick when a first visual contact with the slick was possible. Radar and Lidar signal alteration were measured over the slick. The slick was a well defined slick with iridescence, brown oil patches and floating tar balls, surely an illegal discharge from ballast wash (Figure 3.11). Six sample were taken (see Table 3.3 and 3.9).

Sample name	Day	Time UTC	Lat	Lon
OS4_1	18/08/09	14 45	35° 17.150' N	16° 25.440' E
OS4_2	18/08/09	15 07	35° 18.196' N	16° 27.188' E
OS4_3	18/08/09	15 14	35° 18.225' N	16° 27.016' E
OS4_4	18/08/09	15 18	35° 18.143' N	16° 27.091' E
OS4_5	18/08/09	15 33	35° 17.840' N	16° 27.162' E
OS4_6	18/08/09	15 33	35° 17.840' N	16° 27.162' E

Table 3.4. Position of the collected samples.

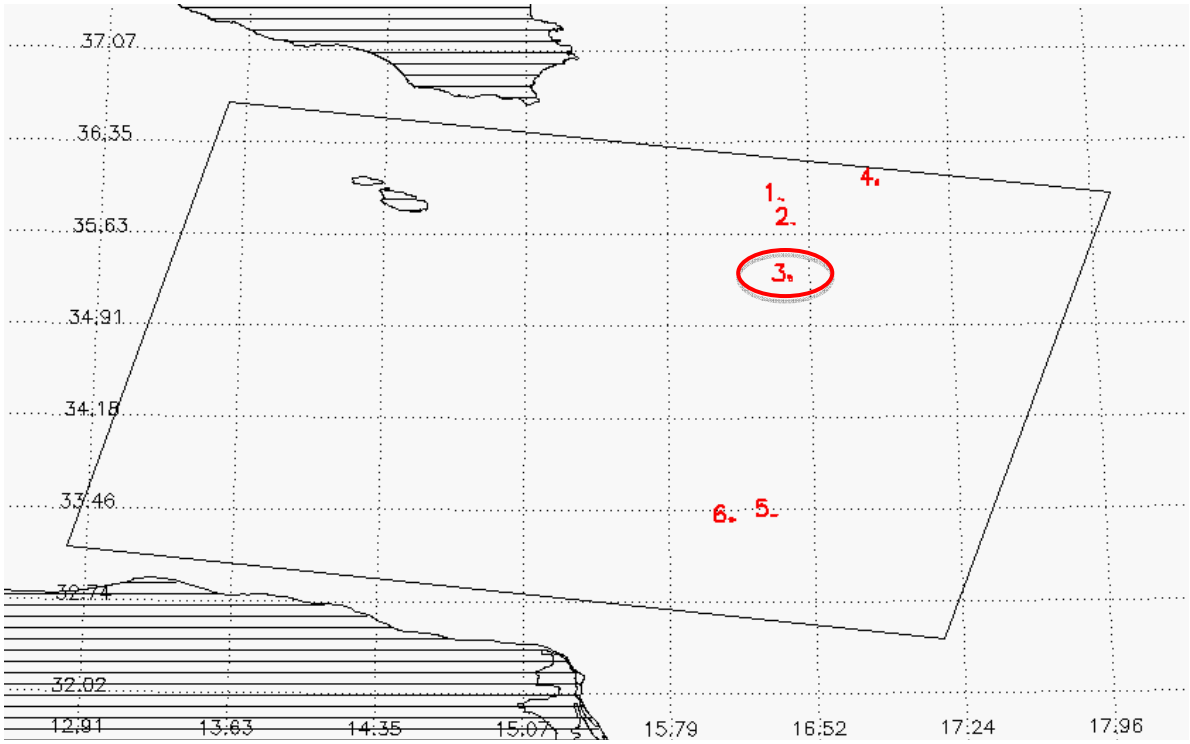

Figure 3.9. Report of ENVISAT 18.08.2009 at 09:03 UTC.

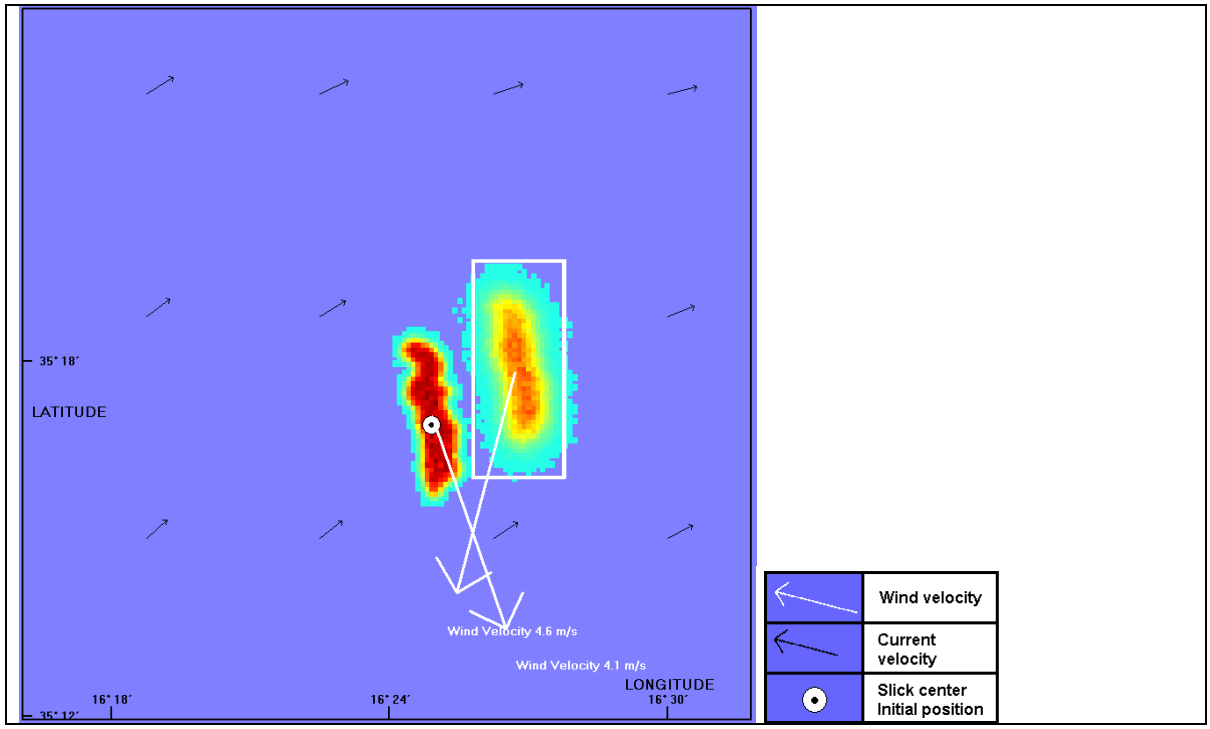

Figure 3.10. Searching area (white rectangle) and predicted position after 8 hours (18.08.09 17:00 UTC). Simulation done using the MFS surface currents and wind drift equal to 0%.

Figure 3.11. Photos of the oil slick OS4

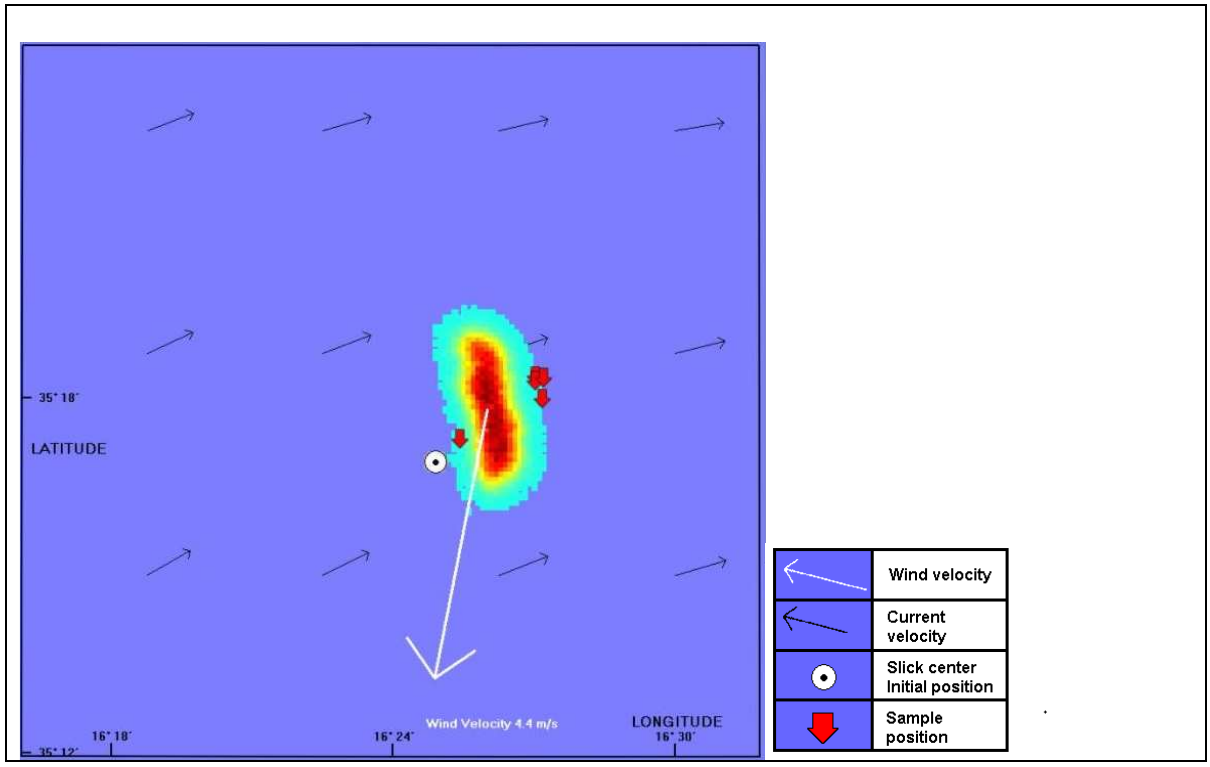

Figure 3.12. Predicted position after 6 hours (18.08.09 15:00 UTC). Simulation done using the MFS surface currents and wind drift equal to 0%. The red arrows represent the position of the collected samples.

Forecasting of OS4

The simulation of the oil slick OS4 has been done after the reception on board of the ASA_WSM_1PNACS20090818_090325_000000592081_00408_39039_0001_SAROSA image and XML data.

The first simulation have been performed using the MFS forecast current fields produced the 18th of August 2009, using the surface currents and a wind drift equal to 0.

The result of the simulation (position of the slick after 8 hours, 18.08.09 17:00 UTC expected time the ship would have been in the area) is shown in the Figure 3.10. The oil spill searching area is indicated by the white rectangle.

Table 3.5 presents the details of the performed simulations.

FORECAST MODE	**OPERATIONAL**	**DELAY TIME**	**DELAY TIME**	**DELAY TIME**
OIL SLICK ID	**SLICK 1**	**SLICK 1**	**SLICK 1**	**SLICK 1**
SPILL DATE	2009-08-18	2009-08-18	2009-08-18	2009-08-18
OBSERVATION TIME	09:03 UTC	09:03 UTC	09:03 UTC	09:03 UTC
SLICK CENTER COORDINATE	35° 16' 55.261" N 16° 24' 52.438" E	35° 16' 55.261" N 16° 24' 52.438" E	35° 16' 55.261" N 16° 24' 52.438" E	35° 16' 55.261" N 16° 24' 52.438" E
AREA	4972500 m^2	4972500 m^2	4972500 m^2	4972500 m^2
THICKNESS (HYPOTHESIS)	0.1 mm	0.1 mm	0.1 mm	0.1 mm
DENSITY (HYPOTHESIS)	API=26 (MEDIUM) 0.898 tons/m^3	API=26 (MEDIUM) 0.898 tons/m^3	API=26 (MEDIUM) 0.898 tons/m^3	API=26 (MEDIUM) 0.898 tons/m^3
POINT SOURCE OR AREAL SOURCE	AREAL SOURCE	AREAL SOURCE	AREAL SOURCE	AREAL SOURCE
CURRENT VELOCITIES	**MFS 1 HOURLY CURRENTS FORECAST (SURFACE CURRENTS) Forecast production Date: 18.08.09**	**MFS 1 HOURLY CURRENTS FORECAST (30 M CURRENTS) Forecast production Date: 18.08.09**	**SCRM 1 HOURLY CURRENTS FORECAST (SURFACE CURRENTS) Forecast production Date: 18.08.09**	**SCRM 1 HOURLY CURRENTS FORECAST (30 M CURRENTS) Forecast production Date: 18.08.09**
WIND FORCING	ECMWF 6 HOURLY FORECAST	ECMWF 6 HOURLY FORECAST	ECMWF 6 HOURLY FORECAST	ECMWF 6 HOURLY FORECAST
WIND FACTOR	**0%**	**3%**	**0%**	**3%**

Table 3.5. Description of simulations for OS4. The "Forecast Mode: Operational" indicates the oil spill model simulations done before the searching activities, The "Forecast Mode: Delay Mode" indicates the oil spill model simulations done after the detection in situ of the slick. The "Initial slick position: Areal Source" indicates the simulations initialized with the oil slick contour coordinates provided by the satellite systems. The "Initial slick position: Point Source" indicates the simulations initialized with the oil slick barycentre.

After the observation in situ of the slick, in delay mode the following simulation was done:

- simulation of the transport of the OS4 using the MFS 30 m-currents and 3% wind drift (not shown);
- simulation of the transport of the OS4 using the SCRM 30 m-currents and 3% wind drift (not shown);
- simulation of the transport of the OS4 using the SCRM surface currents and 0% wind drift (not shown);

The better agreement with the in situ observation was obtained using the MFS surface currents and 0% wind drift (Figure 3.12). The distance between the sample collection position and the predicted slick centre is approximately 1 km. As in the case of OS1, the comparison of model simulation results with in situ observations shows that the oil spill simulated were moving slower than the real slick.

3.2.4.3 PRIMI Oil Slick 5 and PRIMI Oil Slick 6

The in situ observation of OS5 showed that the slick moved north-west with respect to the position observed by SAR COSMOSKYMED satellite. The simulation of the oil slick OS5 has been done in delay mode due to a delay in the forecasting products delivery. The simulations of the OS5 have been performed anyhow and have been used to calibrate/validate the oil spill forecasting system. OS5 was forecasted to drift toward a north-west direction by the forecasting system. Also the drifter released on the OS5 showed a north-west direction but it seemed to move faster that the model prediction. The LIDAR measurements at 21:24 UTC suggested that the drifter is 750 m apart from the oil.

Diary of the pollution event

1) Satellite images: COSMOSKYMED 24.08.2009 at 05:16:15 UTC
2) Reception of the COSMOSKYMED Quick Look at 7:18 UTC 24.08.2009
3) Release of the OS5 MFS-MEDSLIK forecast: in delay mode on 26.08.09 due to a delay in the production of MFS-INGV forecast. For OS6 no simulation has been done.
4) In situ oil slick visual detection:
   a. Slick 5 (PRIMI OS5) 10:24 LAT: 38° 40.792'N LON: 10° 43.355'E
   b. Slick 2 (PRIMI OS6) 17:52 LAT: 38° 33.713'N-LON: 10° 22.368'E.
5) Launch and collection of OSD drifter:
   c. launched at 12:30 UTC 24.08.2009 recovered at 12:55 UTC 24.08.2009
   d. launched at 14:30 UTC 24.08.2009 recovered at 00:17 UTC 25.08.2009
6) Lidar oil detection at night 21:24 UTC at the position: 38° 44.695'N, 10° 38.606'E

Description of the OS5 and OS6 pollution event

The first report (report 21427) showed 2 oil slicks: slick 5 (Primi OS5) and slick 2 (Primi OS6) (see Figures 3.13 and 3.14). As soon as the report was received, the search for OS5 started. The slick was found and visually inspected at 10:24 UTC on 24.08.2009 at the position 38° 40.792'N 10° 43.355'E. The presence of oil at sea was confirmed by radar and Lidar instruments.

The OSD drifter was launched on the slick as a test at 12:30 UTC and soon recovered (12:55 UTC), then the operational launch was performed at 14:55 again on the slick.

After having observed the slick OS5, at 15:00 UTC the R/V URANIA moved towards the observed position of OS6. The latter has been found and observed in situ by visual inspection at 17:52 UTC 24.08.2009 and confirmed by Lidar and radar observation in the position 38° 33.713'N 10° 22.368'E.

MEDSLIK-MFS simulation have been done in delay mode since MFS-INGV forecast production was released with delay. Simulation of OS5 have been done using as initial position the barycentre of the slick as observed in the COSMOSKYMED Quick Look image mentioned above.

While recovering the OSD drifter at night, the Lidar observed the presence of oil at sea at 21:24 UTC on 24.08.2009 in the position 38° 44.695'N, 10° 38.606'E. The distance between the position of oil detected by the Lidar and the drifter is around 600 m.

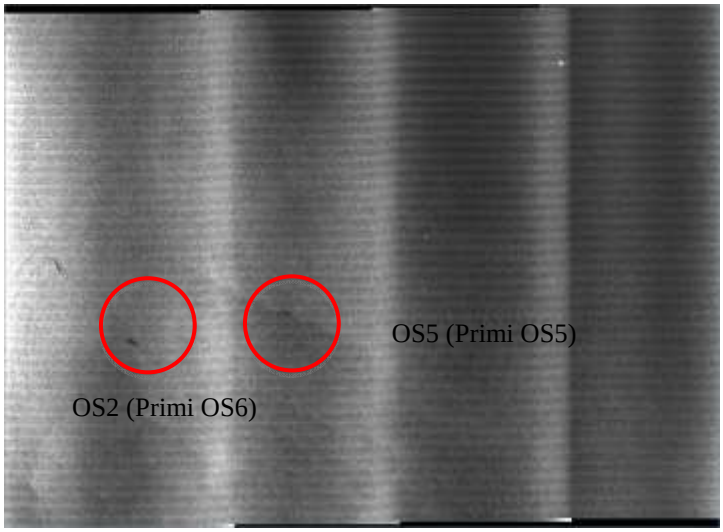

Figure 3.13. COSMOSKYMED 24.08.2009 Quick look 05:16:15 UTC. The red circles highlight the two oil slicks 5 (Primi OS5) and 2 (Primi OS6).

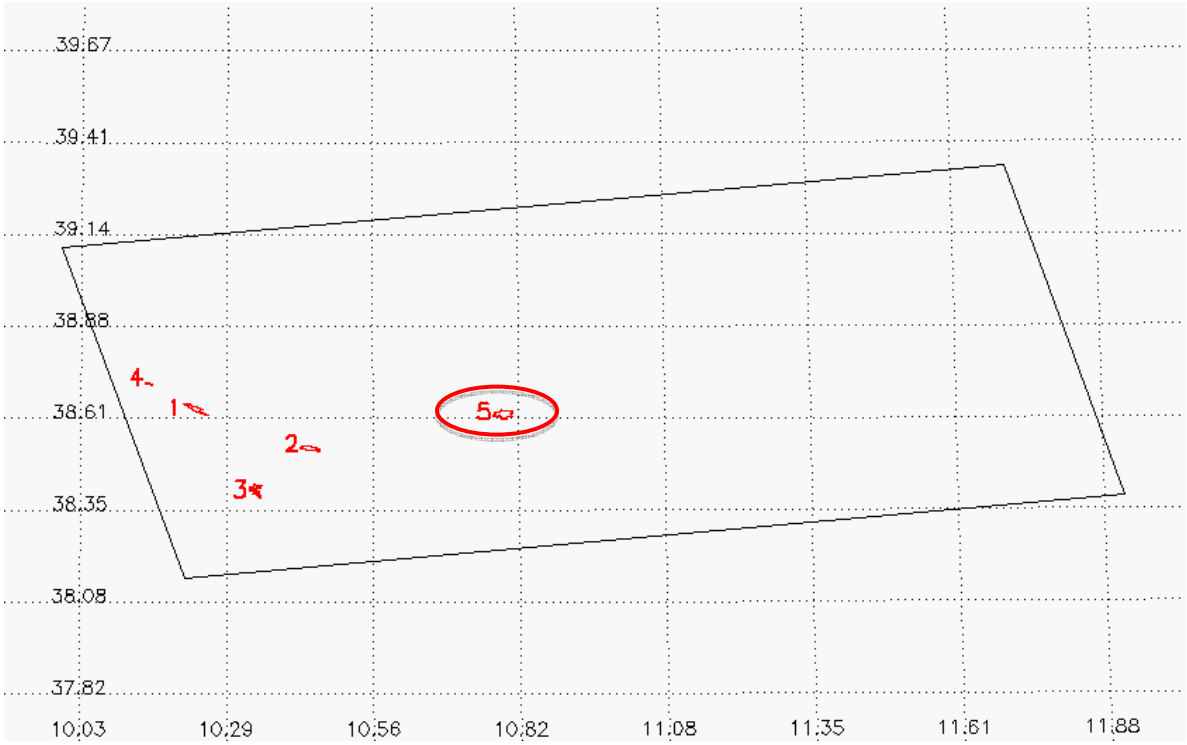

Figure 3.14. Report of COSMOSKYMED 24.08.2009 05:16:15 UTC passage.

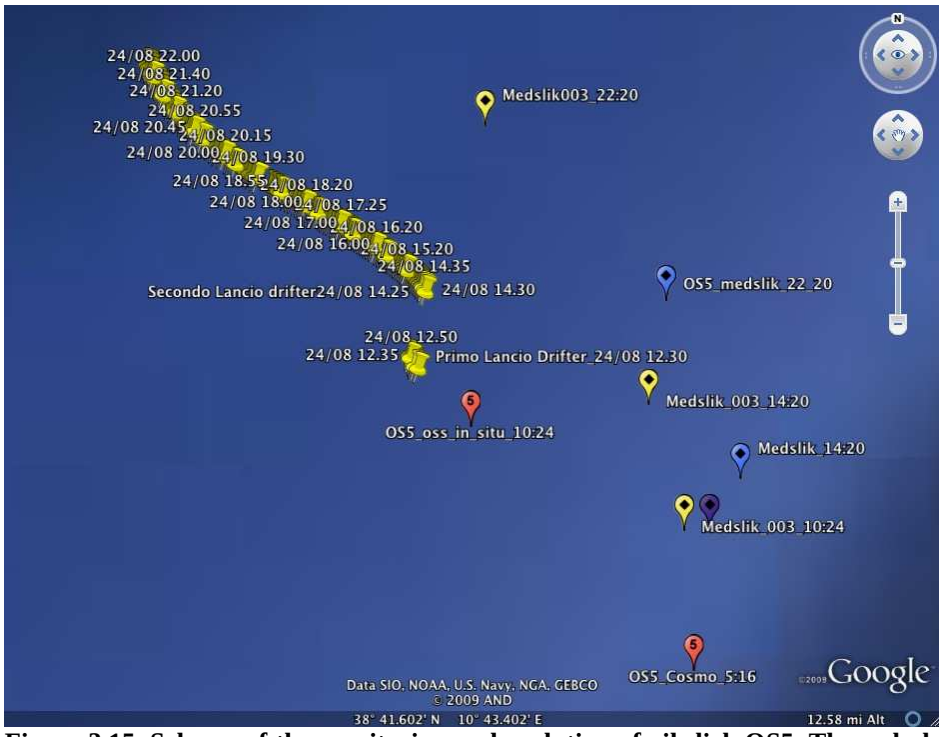

Figure 3.15. Scheme of the monitoring and evolution of oil slick OS5. The red placemark in the right-bottom part of the figure represents the position where the slick has been observed by COSMOSKYMED. The yellow placemarks represent the position of the slick forecasted by MFS-MEDSLIK using drift factor equal to 3%, at the different time (10:24, 14:20 e 22:20 UTC). The blue placemarks represent the position of the slick forecasted by MFS-MEDSLIK using drift factor equal to 0%, at the different time (10:24, 14:20 e 22:20 UTC).

Figure 3.16. Photo of the oil slick OS5 (Primi OS5).

Launch at sea of the OSD drifter on OS5

After the in situ visual inspection of the slick OS5 at 10:24 UTC on 24.08.2009 the drifter OSD was launched twice during that day, both time on the oil slick.

A first launch was performed at 12:30 UTC (38° 41.380'N 10° 42.378'E) and the drifter was then recovered at 12:55 UTC (38° 41.557'N 10° 42.227'E).

A second launch was performed at 14:25 UTC (38° 42.409'N 10° 42.515'E) on the oil slick. The OSD drifter follows a direction towards 310° and was recovered at 00:17 UTC on 25.08.09 (38° 45.494'N 10° 37.752'E) after having cover a distance of 9 km. Since the recovery of the OSD drifter was done at night no visual inspection was possible to see if oil was present at sea in proximity of the drifter, but the LIDAR confirmed the presence of oil at sea at 21:24 UTC in the position: 38° 44.695'N, 10° 38.606'E. At that time the drifter was in the position 38° 44.907'N, 10° 38.173'E, resulting 750 m north-west of the LIDAR observation.

Forecasting of OS5

Simulation have been initialized with the centre of the oil slick OS5, since the report with the shape file has not been received on time on board.

Two types of simulation have been performed to evaluate the sensitivity of results to the wind drift factor which has been chosen equal to 0% and equal to 3%. MFS surface current field have been used in the MEDSLIK-II simulations.

Results of the simulation are shown in Figure 3.15: the yellow placemarks represent the position of the slick forecasted by MFS-MEDSLIK using drift factor equal to 3%, at the different time (10:24, 14:20 e 22:20 UTC). The blue placemarks represent the position of the slick forecasted by MFS-MEDSLIK using drift factor equal to 0%, at the different time (10:24, 14:20 e 22:20 UTC).

The comparison of model simulation results with in situ observations and drifters observation shows that the model simulations are moving slower than observation. Among the two simulations the one with the drift equal to 3% show results similar to observations. Table 3.6 present the details of the performed simulations.

FORECAST MODE	**DELAY TIME**	**DELAY TIME**
OIL SLICK ID	**OS5**	**OS5**
SPILL DATE	2009-08-24	2009-08-24
OBSERVATION TIME	05:16 UTC	05:16 UTC
SLICK CENTER COORDINATE	38° 37' 28.535" N 10° 47' 33.191" E	38° 37' 28.535" N 10° 47' 33.191" E
AREA	5106825.0 m^2	5106825.0 m^2
THICKNESS (HYPOTHESIS)	0.1 mm	0.1 mm
DENSITY (HYPOTHESIS)	API=26 (MEDIUM) 0.898 tons/m^3	API=26 (MEDIUM) 0.898 tons/m^3
POINT SOURCE OR AREAL SOURCE	POINT SOURCE	POINT SOURCE
CURRENT VELOCITIES	**MFS 1 HOURLY CURRENTS FORECAST (SURFACE CURRENTS) Forecast production Date: 26.08.09**	**MFS 1 HOURLY CURRENTS FORECAST (SURFACE CURRENTS) Forecast production Date: 26.08.09**
WIND FORCING	ECMWF 6 HOURLY FORECAST	ECMWF 6 HOURLY FORECAST
WIND FACTOR	**3%**	**0%**

Table 3.6. Description of simulations for OS5. The "Forecast Mode: Operational" indicates the oil spill model simulations done before the searching activities, The "Forecast Mode: Delay Mode" indicates the oil spill model simulations done after the detection in situ of the slick. The "Initial slick position: Areal Source" indicates the simulations initialized with the oil slick contour coordinates provided by the satellite systems. The "Initial slick position: Point Source" indicates the simulations initialized with the oil slick barycentre.

3.2.4.4 PRIMI Oil Slick 7

OS7 was observed from satellite on 26.08.2009 and then a successful forecasted by MFS-MEDSLIK allowed to find the slick on 27.08.2009. After in situ sample collection and observation the OSD drifter was launched on the slick and was then recovered the day after (28.08.2009). The slick was found again close to the drifter. OS7 was forecasted to drift in the north-west direction by the forecasting system. Also the drifter showed a north-west direction but it moved following an anti-cyclonic pattern that is not represented by the model.

Diary of the pollution event

1) Satellite passage ENVISAT 26.08.2009 at 21:05:56 UTC
2) Second satellite passage over the same area ENVISAT 27.08.09 at 09:20:17.
3) At 9:01 UTC on the 27.08.2009 reception of the report 7951 of the satellite passage ENVISAT 26.08.2009 at 21:05:56 UTC
4) At 10:45 UTC on the 27.08.2009 release of the first forecast (MFS-MEDSLIK forecast simulations of OS7).
5) At 12:06 UTC on the 27.08.2009 OS7 was visually observed (36° 52.563'N 13° 29.111'E) (900 m away from predicted slick position)
6) At 12:07 UTC on the 27.08.2009 LIDAR: slight Raman signal variation was observed, OS7 slick present at surface.
7) At 12:12 UTC on the 27.08.2009 ships entered the slick in the position 36° 52.17’N 13° 30.03’E
8) At 12:22 UTC on the 27.08.2009: R/V Urania entered the thicker part of slick in the position 36° 12.31’N, 13° 30.29’E. Vacuum cleaner sampling is carried out at 38° 52.48’N, 13° 30.34’E
9) At 13:10 UTC on the 27.08.2009 13:10 UTC: Lagrangian experiment with bio-spheres and OSD drifter at 36° 52.841'N 13° 30.623'E.
10) At 16:05 UTC on the 27.08.2009: stop of the Lagrangian experiment with bio-spheres at 36° 54.238'N 13° 33.271'E. (OSD DRIFTER experiment continues)
11) At13:35 UTC on the 28.08.09 recovery of OSD drifter at position 36° 53.839'N 13° 26.639'E at 1,4 km from the afterwards observed slick.

12) At13:35 UTC on the 28.08.09 first visible detection of oil at position 36° 54.414'N 13° 26.020'E
13) At13:57 UTC on the 28.08.09 LIDAR signal variation was observed, oil slick present at surface.
14) At 14:47 UTC on the 28.08.09 last visual detection of the slick at position 36° 55.712' 13° 22.272'E (comparing the first and final position of detection the slick OS7 appeared to be 4.6 km long)

Description of the OS7 pollution event

On the 27th of August 2009 at 09:00 UTC the report related to the image SAR ENVISAT ASA_WSM_1PNACS20090826_210556_000000612082_00029_39161_0001_SAROSA (ENVISAT image of the 26.08.2009 at 21:05:56 UTC) was received on board. In the image three slicks were present. The slick 3 in PRIMI SAR report 7951 (see Figure 3.17), called in this document OS7, was chosen as the one to be searched. The ship track was modified in order to reach the detected position of OS7, while INGV started the procedures to forecast the new position of OS7. The estimated arrival time was at 12:00 UTC on the 27.08.09. The forecasted position was 36° 52.31'N, 13° 29.70'E.

R/V URANIA arrived in the forecasted position 15 hours after the detection (12:00 UTC 27.08.2009) after detection . The slick was found in the area, by visual observation (see Figure 3.20) and by Lidar measurements at 12:07 UTC of 27.08.2009 in the position 36° 52.563'N and 13° 29.111'E, 900 m away from the predicted slick position.

At 13:10 UTC of 27.08.2009 the OSD drifter is launched in the position 36° 52.841'N 13° 30.623'E in the core of the slick.

On the 27th August 2009 at 10:15 a second report (report 10379)related to the image SAR ENVISAT ASA_IMP_1PNACS20090827_092017_000000152082_00036_39168_0001_SAROSA (ENVISAT image of the 27.08.2009 at 09:20 UTC) was received on board. In the image several oil spill were present, it's reasonable because of the shape, of the position and of the results of the MEDSLIK simulations, to suppose that the slick 6 in the report 10379 (figure 3.18) is the evolution of the OS7.

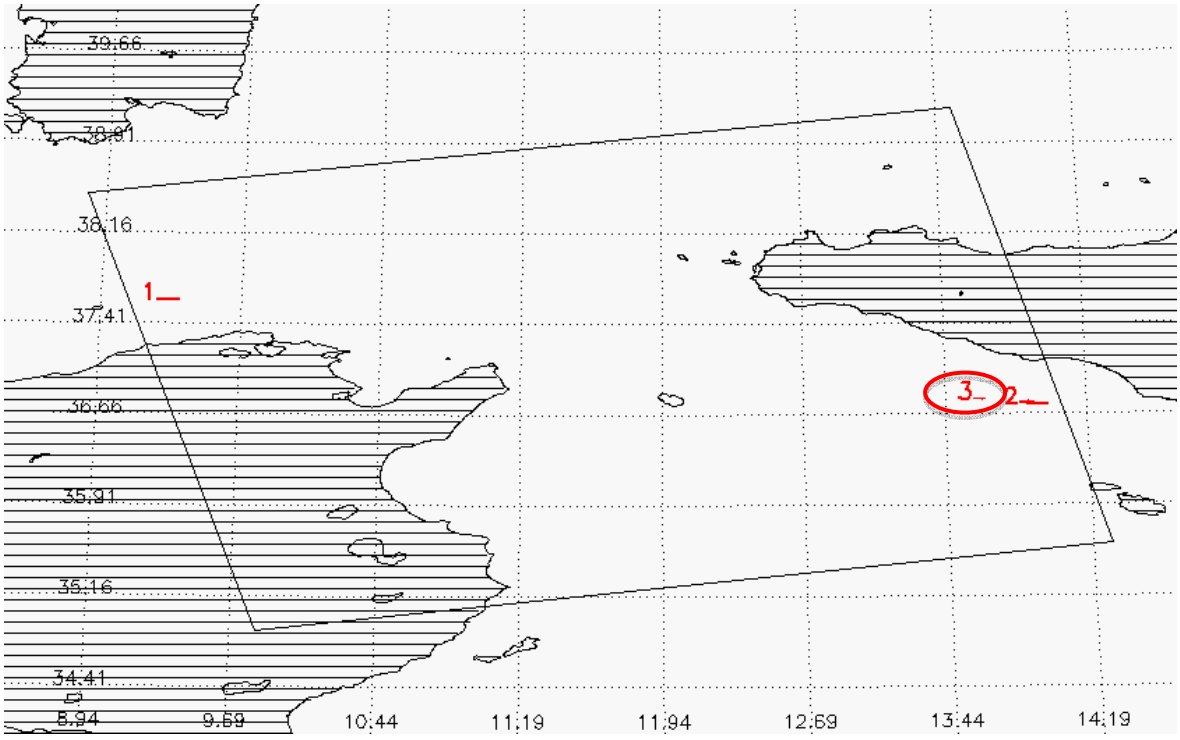

Figure 3.17: Report of the ENVISAT passage 26.08.2009 at 21:05:56 UTC.

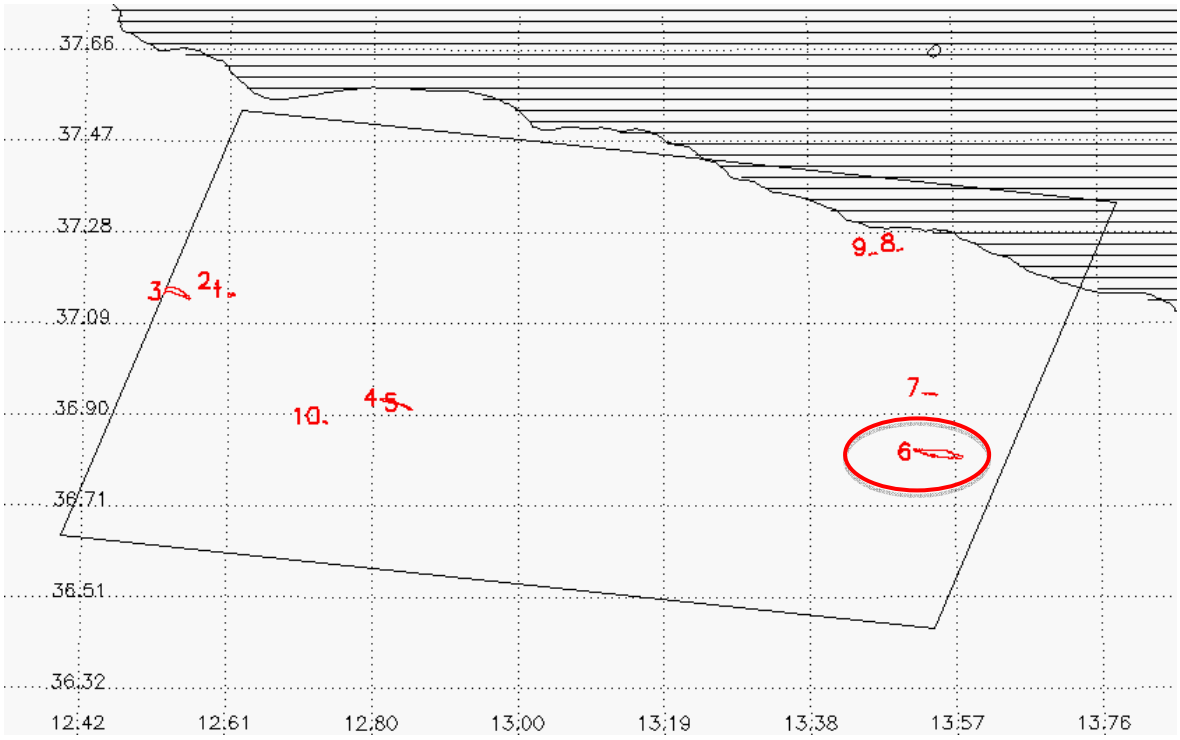

Figure 3.18: Report of the ENVISAT passage 27.08.09 at 09:20:17 UTC

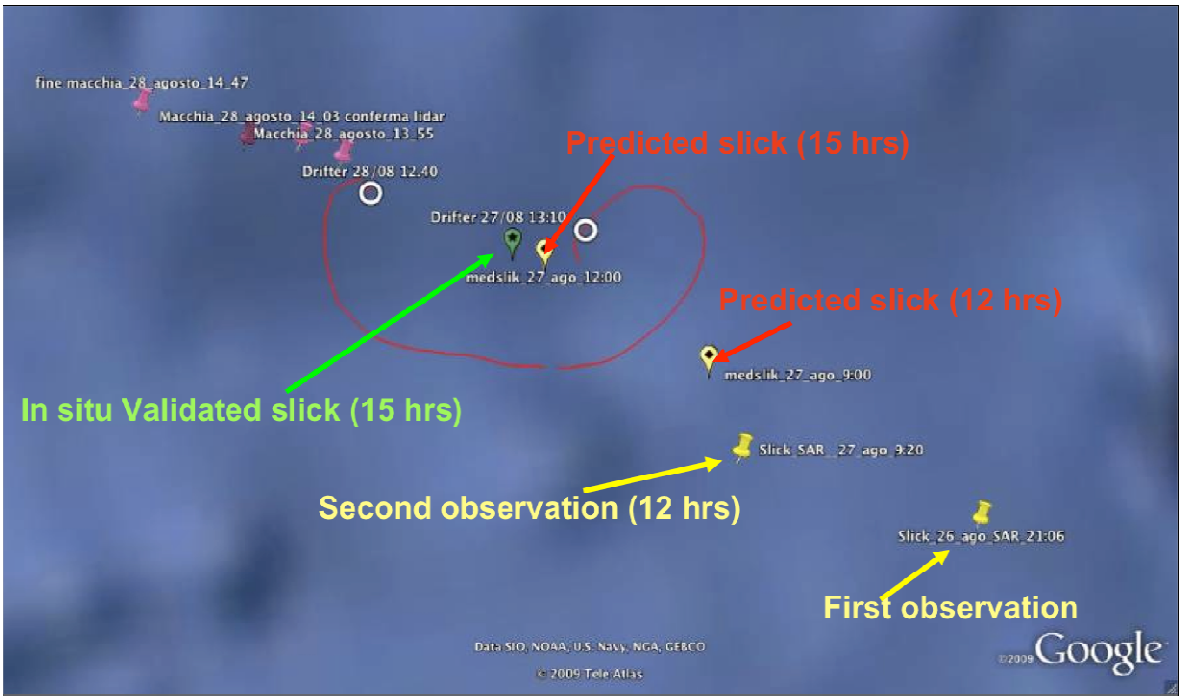

Figure 3.19. Scheme of the monitoring and evolution of oil slick OS7. The yellow placemark in the right-bottom part of the figure ("First Observation") represents the position where the slick has been observed by SAR ENVISAT 26.08.2009 at 21:05:56 UTC. The second yellow placemark represents the position of the slick as observed by SAR ENVISAT del 27.08.09 at 09:20:17 UTC ("Second Observation"). The two yellow placemarks calles "Predicted slick" present the position of the slick as forecasted by MEDSLIK-MFS after 12 and 15 hours.
The green placemark presents the position of the slicks as observed in situ from R/V URANIA RV.
The white circle on the right is the position where the OSD drifter is launched on the 27.09.2009 at 13.10 UTC, the red line represents the trajectory of the slick and the second yellow circle on the left represents the position where the drifter has been collected after 24 hours on 28.09.2009 at 12.40 UTC.
The purple placemarks on the left side of the picture represent the positions of in situ observations of oil slicks just after the drifter collection on 28.08.2009.

Figure 3.20. Photo of the oil slick OS7

Launch at sea of the OSD drifter on OS7

After the in situ visual inspection of the slick OS7 the drifter OSD was launched at 13:10 UTC on 27.08.2009 in the oil slick. The OSD drifter followed an anti-cyclonic patterns and it was collected at 12:40 UTC on 28.08.09 (see Figure 3.19). After the recovery of the OSD drifter, oil was found in proximity of the drifter.

Forecasting of OS7

The simulation of the oil slick OS7 has been done in real time on 27.08.09. Simulation have been initialized with the centre of the oil slick OS7, since the report with the shape file has not been received on time on board. Results of the simulation are shown in Figure 3.19: the yellow placemarks represent the position of the slick forecasted by MFS-MEDSLIK after 12 and 15 hours.

FORECAST MODE	**OPERATIONAL**
OIL SLICK ID	**OS7**
SPILL DATE	2009-08-26
OBSERVATION TIME	21:06 UTC
SLICK CENTER COORDINATE	36° 47' 12.455" N 13° 37' 14.488" E
AREA	2452500.0 m^2
THICKNESS (HYPOTHESIS)	0.1 mm
DENSITY (HYPOTHESIS)	API=26 (MEDIUM) 0.898 tons/m^3
POINT SOURCE OR AREAL SOURCE	POINT SOURCE
CURRENT VELOCITIES	**MFS 1 HOURLY CURRENTS FORECAST (SURFACE CURRENTS) Forecast production Date: 26.08.09**
WIND FORCING	ECMWF 6 HOURLY FORECAST
WIND FACTOR	**3%**

Table 3.7. Description of simulations for OS7. The "Forecast Mode: Operational" indicates the oil spill model simulations done before the searching activities, The "Forecast Mode: Delay Mode" indicates the oil spill model simulations done after the detection in situ of the slick. The "Initial slick position: Areal Source" indicates the simulations initialized with the oil slick contour coordinates provided by the satellite systems. The "Initial slick position: Point Source" indicates the simulations initialized with the oil slick barycentre.

The comparison of model simulation results with in situ and satellite observations (it's realistic to suppose that the slick 6 in the report 10379 -Figure 3.18- is the evolution of the OS7) shows that the model performed well and the simulation was successfully used to search the slick and the forecasted position was less than 1 km far from the in situ observed slick.

3.2.5 I-Sphere and CODE release

A line of alternated 5 CODE and 4 I-SPHERE (see Figure 3.22) drifters 250 m apart, along slick length, inside slick (see Figure 3.21 and Table 3.8) was released in the slick OS4. The line pattern was chosen because of slick narrowness (approx. 50-100 m).

Unfortunately, only 2 of the five CODE drifters released were transmitting their position.

In Figure 3.23 the overlay of the observed drifters trajectories (the solid red lines are the SPHERE drifters trajectories and the dashed red lines are the CODE drifters trajectories) and the MEDSLIK-II trajectories from 18/08/2009 to 21/08/2009 are shown. The blue solid lines represent the simulated drifters trajectories obtained using the MFS surface daily currents analysis and 0% wind drift. These trajectories represent the paths of the CODE drifters, because the CODE drifters are completely underwater and don't experience the direct effect of the wind.

The dashed lines represent the simulated drifters trajectories obtained using the MFS surface daily currents analysis and 1% wind drift. These trajectories represent the SPHERE drifters, that are not completely underwater and are transported not only by the surface currents, but feel also the effect of the wind.

Buoy type	**s/n**	**Release date**	**Time UTC**	**Lat**	**Lon**
ARGO	33200	18/08/09	16 34	35° 18.254' N	16° 27.595' E
I-SPHERE	300034012578040	18/08/09	16 38	35° 18.371' N	16° 27.626' E
ARGO	33201	18/08/09	16 42	35° 18.507' N	16° 27.668' E
I-SPHERE	300034012489470	18/08/09	16 44	35° 18.630' N	16° 27.716' E
ARGO	33205	18/08/09	16 47	35° 18.738' N	16° 27.753' E
I-SPHERE	300034012480560	18/08/09	16 49	35° 18.790' N	16° 27.790' E
ARGO	33206	18/08/09	16 52	35° 18.946' N	16° 27.818' E
I-SPHERE	300034012659810	18/08/09	16 55	35° 19.055' N	16° 27.847' E
ARGO	33209	18/08/09	16 57	35° 19.163' N	16° 27.877' E

Table 3.8. Position of drifters release.

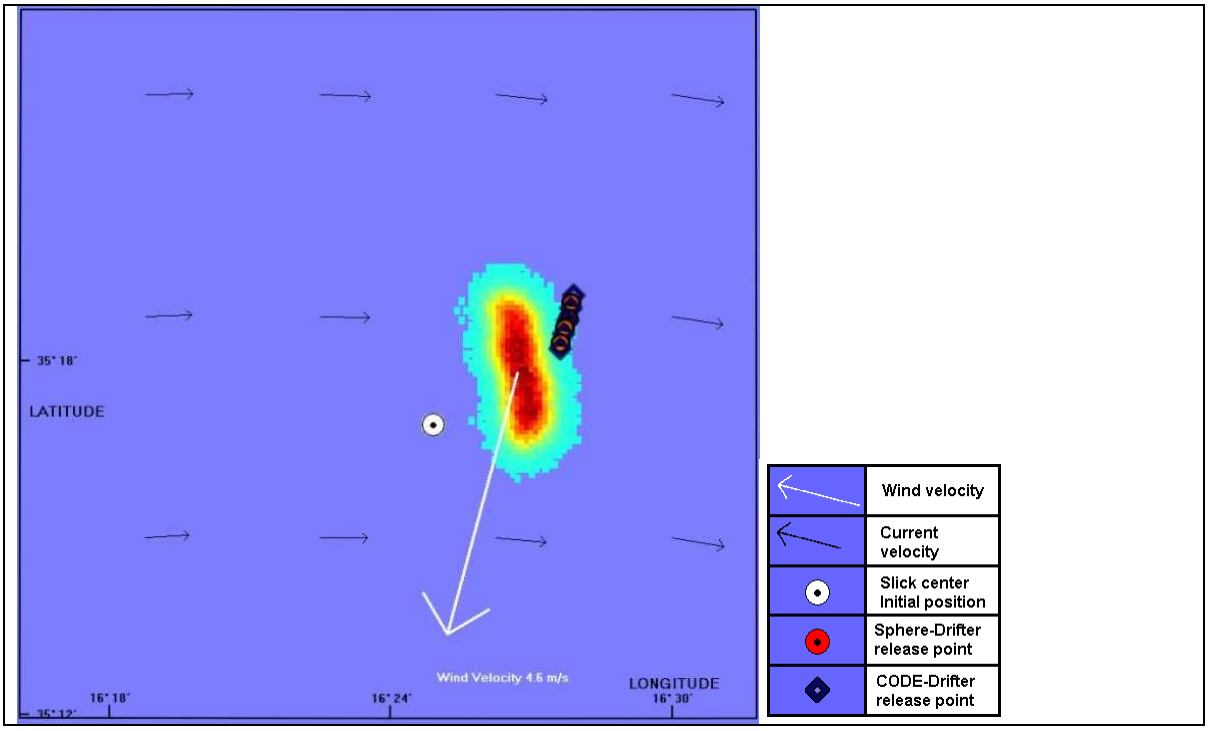

Figure 3.21. Predicted position of slick OS4 after 8 hours (18.08.09 17:00 UTC) and drifters release position. Simulation done using the MFS surface currents and wind drift equal to 0%.

Figure 3.22. Photos of the released drifters (the blue drifters are the CODE drifters, the orange drifters are the SPHERE drifters).

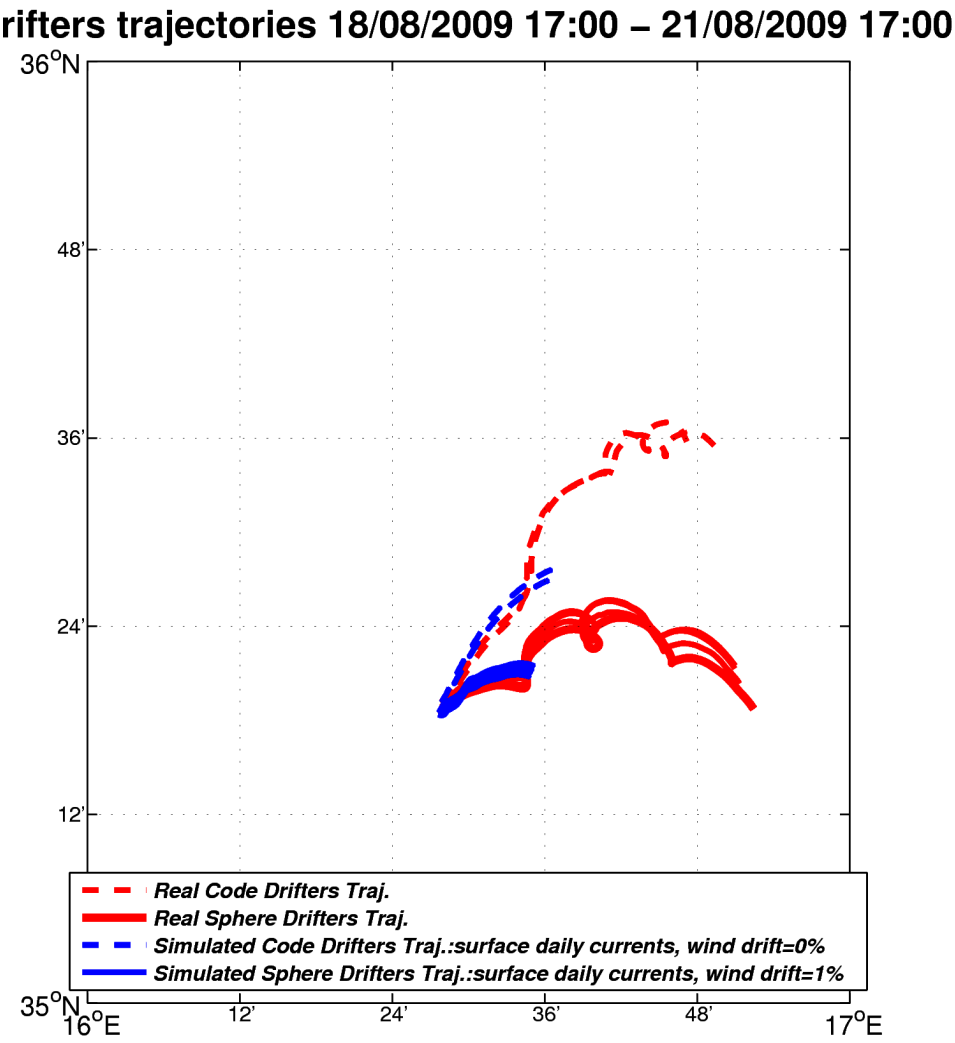

Figure 3.23. Overlay of the observed drifters trajectories (1- solid red lines: SPHERE drifters; 2- dashed red lines: CODE drifters) and the Medslik trajectories from 18/08/2009 to 21/08/2009. The blue solid lines represent the simulated drifters trajectories obtained using the surface daily currents and 0% wind drift and the dashed lines represent the simulated drifters trajectories obtained using the MFS surface daily currents analysis and 1% wind drift.

Chapter 4

4 Estimates of Lagrangian horizontal diffusivity from drifter data

4.1 Introduction

In recent years there has been a growth of interest for the prediction of particle trajectories in the sea. One important application is the forecast of oil spills.

Transport and dispersion processes can be simulated using a Lagrangian particle model coupled with Eulerian Ocean General Circulation Models (OGCM). Using this approach each particle displacement is described by a deterministic and stochastic part, corresponding to an average and a fluctuating part, respectively. The first one represents the advection associated with the Eulerian current field while the second describes the sub-grid scale processes, due to unresolved scales in the OGCMs, and the turbulent diffusion.

The focus of this study is to quantify the diffusivity K and the time scales T, to be used as input parameters for dispersion in oil spill models. To this end the first step has been to compute K and T using the drifters deployed during the Marine Rapid Environmental Assessment 2007-2008 (MREA) exercise in the Ligurian Sea. The second step is the analysis of the relation between the horizontal diffusivity and the wind and current field, which can be provided by Eulerian models. This last analysis has been performed using the drifters, deployed in the Adriatic Sea as part of the Dynamics of Localized Currents and Eddy Variability in the Adriatic (DOLCEVITA) project (2002 – 2004). The final aim is to find a parametric law for the calculation of the horizontal diffusivity to be used for the simulation of Lagrangian trajectories in realistic Eulerian flow field simulations.

An accurate calculation of the Lagrangian transport is important for a number of practical problems, such as the dispersion of oil at sea. In order to understand Lagrangian motion at sea, surface drifter data (Poulain & Niiler 1989), (Poulain 2001), (Falco et al. 2000), (Ursella et al. 2006), (Poulain & Zambianchi 2007) are usually analysed and transport parameters are computed that could be used in Lagrangian particle models.

In the statistical approach to understand and model the Lagrangian transport, the flow field

has two distinct components: a large scale mean flow **u** and a turbulent field **u'**. Thus, the tracer particles are moved by two separated processes, an average advection by **u** and a fluctuating transport due to **u'**, in which the turbulent velocity or eddy Lagrangian velocity is modelled as a random walk process. The mean displacements might be calculated using the current velocity fields provided by the Eulerian ocean general circulation models, such as the Mediterranean Forecasting System (MFS) (Pinardi et al. 2003) or higher horizontal resolution regional model. These models do not correctly simulate the horizontal sub-grid scale diffusion due to an unrealistic horizontal diffusivity, which is necessary to the numerical convergence. In the MFS model the horizontal diffusivities are set to the value of $7 \cdot 10^5$ cm^2/s in both directions (Tonani et al. 2008).

The stochastic model is represented by a zero order, linear, ordinary differential equation, characterized by some simple transport parameters such as the diffusivity. The purpose of this study is to correctly estimate the turbulent transport parameters using drifter data sets. The work is organized as follows. The drifter dataset will be described in the next section. Lagrangian statistics will be presented in the third section of this chapter. The Lagrangian properties as computed from satellite-tracked drifters data in the northwestern Mediterranean Sea (2007-2009) are presented in the forth section of this chapter while the essential results of the analysis of the relation between the horizontal diffusivity and the wind and current fields, for the Adriatic Sea, are discussed in the last section.

4.2 Drifters data

4.2.1 The MREA07-MREA08 cruises (Ligurian sea)

Drifters are considered to be quasi-Lagrangian instruments because they do not perfectly follow the water particles due to wind/wave interactions. In good approximations, however they follow rather well the horizontal surface currents and can be thus viewed as surface passive tracers. The drifter dataset used in this work has already been used for the description of the surface circulation in the Liguro-Provencal basin (Poulain et al., 2010 in preparation).

The drifters were deployed as part of the Marine Rapid Environmental Assessment (MREA) exercises in small clusters (1 km) of 3-5 units at a single location in the open Ligurian Sea in the vicinity of the ODAS buoy (9.17° E 43.79° N).

The drifters employed were provided by NATO Undersea Research Centre (NURC), by the Istituto Nazionale di Geofisica e Vulcanologia (INGV), by Centro Nazionale Ricerche (CNR) and by the Istituto Nazionale di Oceanografia e di Geofisica sperimentale (OGS). The drifter design is similar to that used in the COastal Dynamics Experiment (CODE) in the early 1980s (Davis, 1985). These drifters have been localized by Global Positioning System (GPS) at hourly intervals and their data telemetered via the ARGOS system. The scheme of the released drifter positions was a cross, one central drifter in the vicinity of the ODAS buoy and the other 4 drifters 500 m far from the central buoy in direction North, South, East and West.

The surface drifters were deployed in the Ligurian Sea in May and June 2007 during the MREA07 and LASIE (Ligurian Air-Sea Interaction Experiment) experiments by the Italian Navy Vessel Galatea and R/V R/V Urania . Three drifter clusters, each consisting of five drifters, were launched in three different periods, a first cluster was launched on 14 May, a second cluster was deployed on 17 June and the last cluster was released on 22 June. In 2008, during the MREA08 experiment, which took place in the Ligurian Sea from the 29th of September until the 22nd of October, on board of Italian Navy Vessel Magnaghi, other three clusters of CODE drifters, each consisting of three drifters, were released in three different period. A first cluster was launched on 1 October, a second cluster was deployed on 11 October, and the last cluster was released on 22 October. Some drifters stranded on the Italian and French coasts and were successfully redeployed. Considering that some drifters failed transmitting right after deployments and those others were recovered and redeployed, we have a total of 32 trajectories.

Drifter ID	Start date	Start time	End date	End time	Total days
MREA07					
a74871	14/05/2007	13.44	16/06/2007	3.00	33
a74872	14/05/2007	13.55	26/09/2007	19.01	135
a74873	14/05/2007	14.00	15/06/2007	5.00	32
a74874	14/05/2007	14.22	27/05/2007	20.02	13
a74875	14/05/2007	14.28	23/07/2007	13.00	70
b74874 (redeployed)	30/05/2007	10.01	22/06/2007	15.00	23
b74875 (redeployed)	13/08/2007	15.00	01/09/2007	3.00	19
c74875 (redeployed)	19/09/2007	8.30	27/09/2007	13.00	8
a06950	17/06/2007	10.07	01/07/2007	13.00	14
a06952	17/06/2007	10.19	24/06/2007	10.00	7
a06955	17/06/2007	10.26	30/07/2007	14.00	43
a06957	17/06/2007	10.38	19/10/2007	2.00	124
a12582	17/06/2007	10.57	24/06/2007	4.02	7
b06950 (redeployed)	17/07/2007	6.33	07/09/2007	12.02	52
a12583	22/06/2007	11.00	12/08/2007	0.20	51
a12584	22/06/2007	11.11	06/07/2007	22.10	14
a12587	22/06/2007	11.18	01/07/2007	16.00	9
a12591	22/06/2007	11.27	01/07/2007	7.00	9
a14648	22/06/2007	11.34	01/07/2007	11.00	9
b12587 (redeployed)	17/07/2007	6.27	12/10/2007	17.00	87
b12591 (redeployed)	17/07/2007	6.30	13/08/2007	21.00	27
b14648 (redeployed)	17/07/2007	6.37	10/08/2007	4.00	24
c12591 (redeployed)	16/08/2007	1.04	08/10/2007	22.00	53
MREA08					
a85193	01/10/2008	6.34	08/12/2008	10.55	68
a85747	01/10/2008	6.33	08/12/2008	22.18	68
a85743	01/10/2008	6.19	08/12/2008	20.35	68
a85194	11/10/2008	15.20	08/12/2008	22.19	58
a85744	11/10/2008	15.36	08/12/2008	17.52	58
a85745	11/10/2008	15.41	02/11/2008	15.32	22
a85746	22/10/2008	23.21	29/10/2008	21.06	7
a85748	22/10/2008	23.29	08/12/2008	22.17	47
b85742	22/10/2008	23.20	31/10/2008	9.24	9

Table 4.1. Coordinates and release data of theMREA07 and MREA08 drifters.

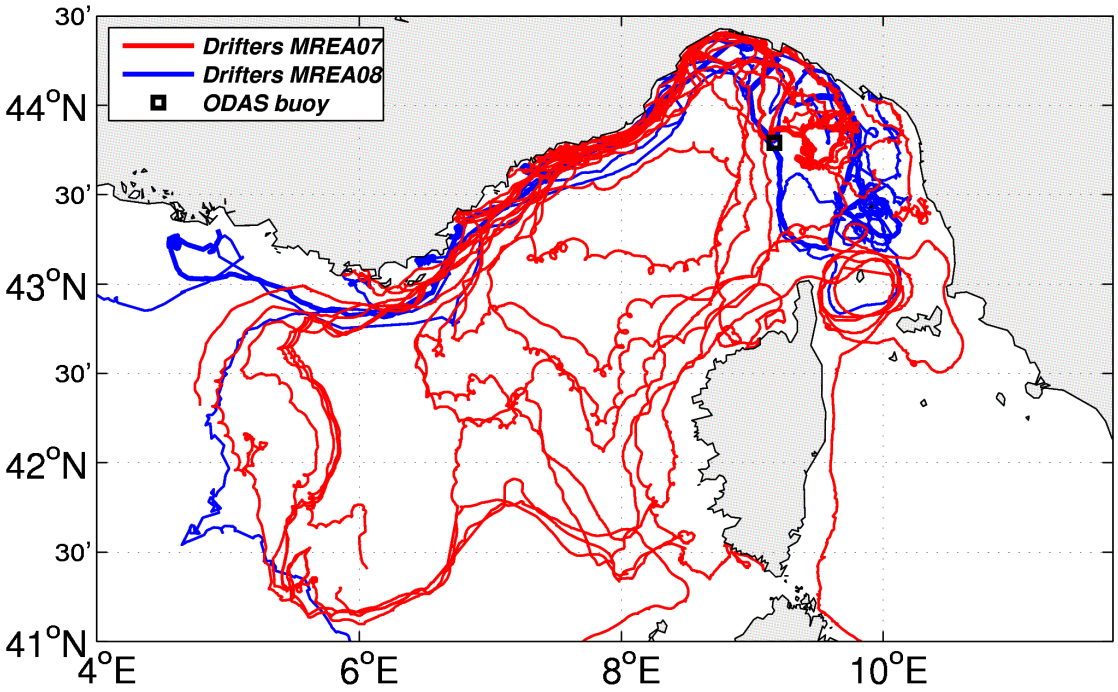

Figure 4.1. Position diagram of the drifter data and the ODAS buoy.

4.2.2 Hystorical data: DOLCEVITA cruise (Adriatic Sea)

The observations derived from the surface drifters deployed in the Northern and Central Adriatic between September 2002 and March 2004. A total of 124 drifting buoys were launched during the international DOLCEVITA project, corresponding to 188 deployments because some drifters were recovered and redeployed several times. The main objective of the DOLCEVITA project was to quantify the kinematic and dynamic properties of the northern and middle Adriatic Sea and to define the mesoscale variability with special attention to coastal Italian current.

Two versions of the CODE drifters (Davis, 1985; Poulain, 1999, 2001) were used, with ARGOS telemetry and GPS systems which permit a finer resolution in space (~10 m) and time (Barbanti et al., 2005) to be obtained. The position sampling for GPS-CODE drifters, transmitted to the ARGOS satellite system, was programmed at 1-hour intervals. These surface drifters are considered efficient instruments for measuring and describing ocean circulation due to their accuracy in following the surface current at 1-2 cm/s.

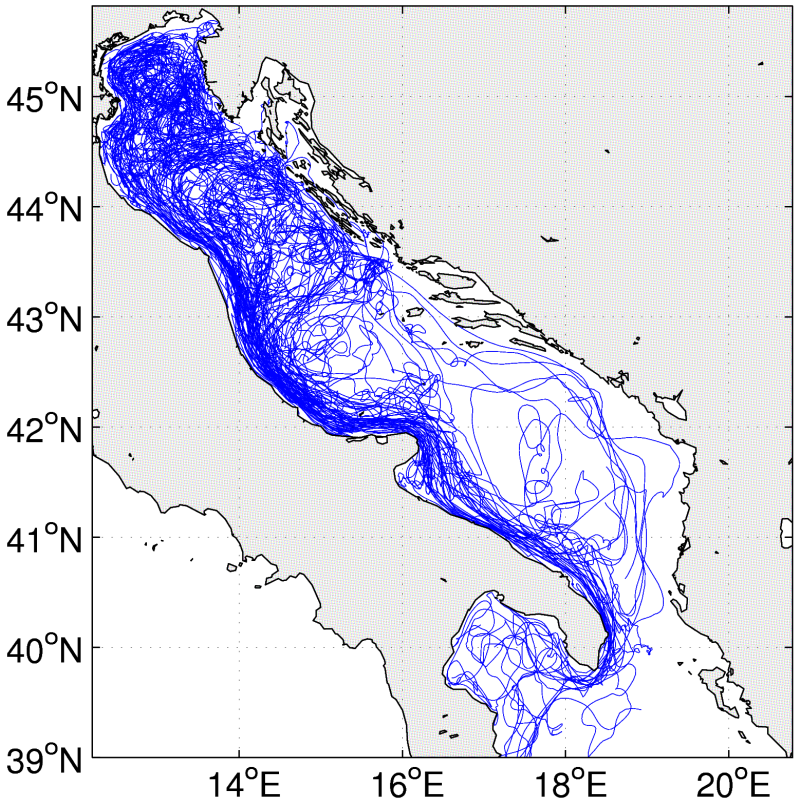

Figure 4.2. Position diagram of the drifter data

4.3 Lagrangian statistics

The quasi-Lagrangian nature of the drifter tracks is exploited to obtain Lagrangian scales of variability and to describe diffusive transport by the eddy field. Lagrangian scales of variability from individual drifters are calculated. Let $\mathbf{u}(\mathbf{x}_0,t)$ be the velocity at time t of the drifter passing trough x0 at the initial time t0. The Lagrangian autocorrelation is defined (Poulain & Niiler 1989):

$$R_{ii}(\tau, T, t_0, \mathbf{x}_0) = \frac{\frac{1}{T}\int_{t_0}^{t_0+T} u_i'(\mathbf{x}_0, t)u_i'(\mathbf{x}_0, t+\tau)dt}{\frac{1}{T}\int_{t_0}^{t_0+T} u_i'(\mathbf{x}_0, t)u_i'(\mathbf{x}_0, t)dt} = \frac{\langle u_i'(\mathbf{x}_0, t)u_i'(\mathbf{x}_0, t+\tau)\rangle_L}{\langle u_i'(\mathbf{x}_0, t)^2\rangle_L} \qquad (4.1)$$

where $\mathbf{u'}(\mathbf{x}_0,t)$ is a residual velocity and

$$\langle \quad \rangle_L = \frac{1}{T}\int_{t_0}^{t_0+T} dt$$

is a Lagrangian average, where T is the interval time over which the average is performed.

For homogeneous and stationary fields, the dependence on T, $\mathbf{x}_0$ and t_0 vanishes. Residual velocity, $\mathbf{u}' = \mathbf{u} - \langle \mathbf{u} \rangle_L$, are defined by removing the mean velocity for each drifter. There is a large variability in the individual autocorrelation functions. Most of these have significant negative lobes and approach a zero value at small time lag. The Lagrangian integral time and space scales are the time and the distance over which a drifter remembers its velocity. They are defined by:

$$T_i^L = \int_0^t R_{ii}(\tau) d\tau \qquad (4.2)$$

$$L_i^L = \left[\langle u_i'^2 \rangle_L \right]^{1/2} \int_0^t R_{ii}(\tau) d\tau = \left[\langle u_i'^2 \rangle_L \right]^{1/2} T_i^L \qquad (4.3)$$

The integral of the autocorrelation which appears in these definitions is generally time dependent and does not approach a constant limit as t increases. A usual practice is to integrate from zero to the time when the autocorrelation reaches for the first time a value lower than 1/e. This corresponds to the first maximum of the integral scales and the values can be considered as upper bound to the true scales.

4.4 Lagrangian properties in the northwestern Mediterranean Sea as computed from satellite-tracked drifters data (2007-2009)

The trajectories described by 32 drifters between May 2007 and December 2008 were used to study the transport properties in the Liguro-Provencal basin (see 3.3). Since the acquisition period was not regular, the drifter data were quality controlled and interpolated at 1-h uniform interval using a linear interpolation and the velocities were then calculated as finite differences of the positions. Lagrangian scales of variability from individual drifters were analyzed and Lagrangian single-particle statistics were computed from the edited and interpolated 1-hourly drifter position and drifter data.

The main quantities computed are the autocorrelation, the integral time scale, T_i^L, and the diffusivity, K_{ii}. Since all the quantities are expressed as vector components, the choice of the coordinates system is expected to play a role in the presentation of the results. The mean flow could influence the turbulent features, resulting in an anisotropy of statistics. Thus, the best choice is to use a natural Cartesian system, which is obtained rotating locally along the mean flow axes. So, at each time step t the mean flow velocity has been computed as the average of the drifter velocities over 4 days, centred at the time t. The

coordinate system has been oriented along the direction of the 4 days mean flow velocity. The two components of a quantity in that system are the along current component and the across-current component. As example, the Lagrangian autocorrelations of drifters a74871 and a85743 are plotted in Figure 4.3. The drifter a74871 shows the streamwise component of the autocorrelation higher than zero for more than 2 days, while the across stream component reaches a first zero value after few hours. The trajectory of the drifter a85743 shows higher decorrelation time scales: about 1 day in the across current direction and more than 3 days in the along current direction.

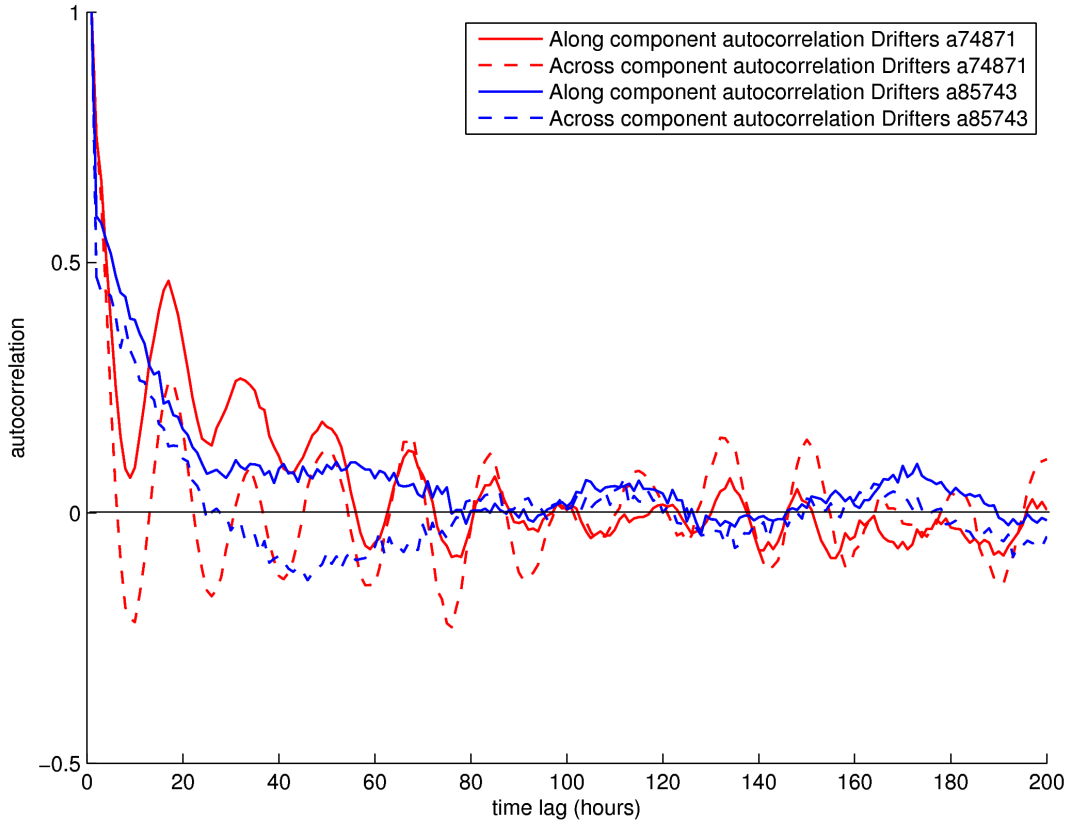

Figure 4.3. Lagrangian autocorrelations versus time lag in natural coordinates: a) along component (solid); b) across component (dashed) for drifters a74871 and a85743.

This variability reflects the inhomogeneous structure of the flow field. Average diffusivities values are about $1.7 \cdot 10^7$ cm^2/s and $5.1 \cdot 10^6$ cm^2/s in the along and across current directions, respectively. The average streamwise component of the integral time scale is equal to 9 hours, while the across component is equal to 4.4 hours.

The probability density of particle displacements $p(\mathbf{x},t;\mathbf{x}_0,t_0)$ plays a major role in the

transport of the mean concentration of a passive scalar property (Davis 1983).
Its second moment is the displacement covariance and is defined as:

$$\left\langle d'_i{}^2 \right\rangle(t) = \int_A p(\mathbf{x}, t; \mathbf{x}_0, t_0) d'_i \, d'_i \, (d\mathbf{x}_0)^3 \qquad (4.4)$$

where $\mathbf{d}' = \mathbf{x} - \mathbf{x}_0 - \langle \mathbf{u} \rangle (t - t_0)$ is a residual displacement, $p(\mathbf{x}, t; \mathbf{x}_0, t_0)$ is the probability density that a particle released at ($\mathbf{x}_0$, t_0) reaches ($\mathbf{x}$, t) and A is the domain of all the possible initial conditions. For homogeneous and stationary fields, a simple formula relates the single-particle diffusivity (K_{ii}), defined as the time rate of change of the displacement covariance, to the integral of the Lagrangian autocorrelation. This relation, first derived by Taylor (1921) is expressed as:

$$K_{ii}(t) = \frac{1}{2} \frac{d}{dt} \left\langle d'_i{}^2 \right\rangle = \left\langle u'_i{}^2 \right\rangle \int_0^t R_{ii}(\tau) d\tau = \left\langle u'_i{}^2 \right\rangle T_i^L \qquad (4.5)$$

Equation (4.5) approaches two independent limits:

- Initial dispersion:

$$\text{If } t << T_i^L, \text{ then } \frac{1}{2} \frac{d}{dt} \left\langle d'_i{}^2 \right\rangle = \left\langle u'_i{}^2 \right\rangle t \qquad (4.6)$$

- Random walk regime:

$$\text{If } t >> T_i^L, \text{ then } \frac{1}{2} \frac{d}{dt} \left\langle d'_i{}^2 \right\rangle = \left\langle u'_i{}^2 \right\rangle T_i^L \qquad (4.7)$$

In spite of the non-uniform nature of the observations, we begin the analysis with the simplest approach of assumed homogeneity and steadiness. A large number of independent tracks are necessary to calculate reliable statistics. Since the decorrelation time scale of the individual drifter track is less than 7 days, any two locations of the same drifter separated in time by more than 7 days are independent and they can be considered as the origins of two independent tracks. Thus, the number of degrees of freedom was increased by considering subtracks whose origins are taken every 7 days, along the 32 original trajectories, giving a total of 169 segments. Using the segmented tracks data, we calculated again the diffusivity and time scale. The values obtained for the diffusivity are $1.4 \cdot 10^7$ cm^2/s and $3.1 \cdot 10^6$ cm^2/s in the along and across current directions, respectively. These values are slightly lower than the ones obtained using the individual tracks. This is due to

the different means taken out in the calculation of the velocity fluctuations, the latter calculated by removing the average velocity of the segment of the drifter trajectory. The average integral time scale is about 10 hours and 3.5 hours in the along and across current directions, respectively.

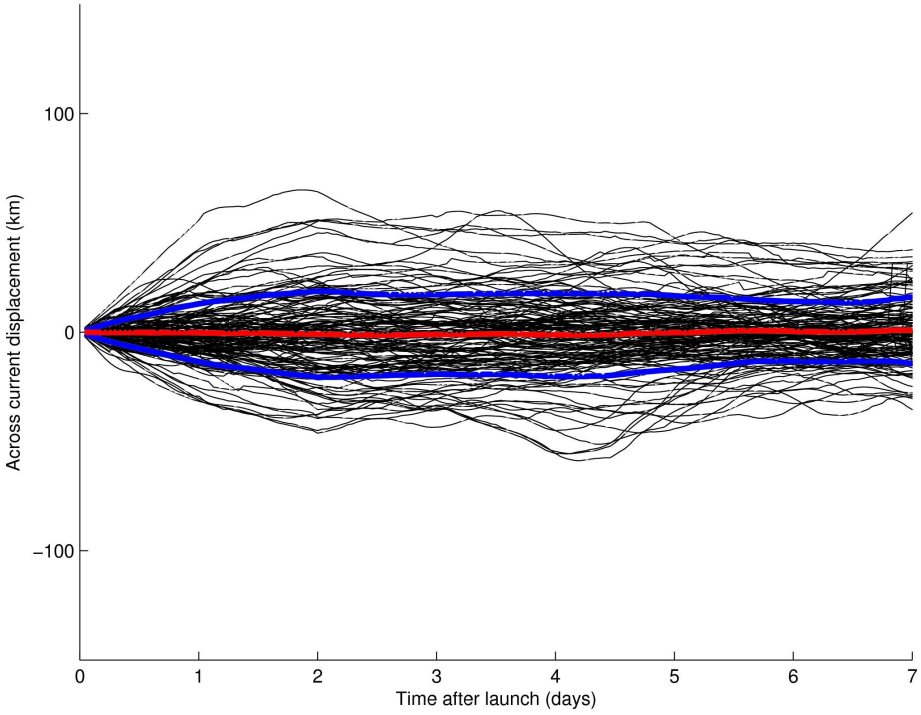

Figure 4.4. Displacements across component in natural coordinates versus time after deployment for the segmented drifter tracks (black lines); time series of the mean displacements (red line) and associated rms intervals (blue lines)

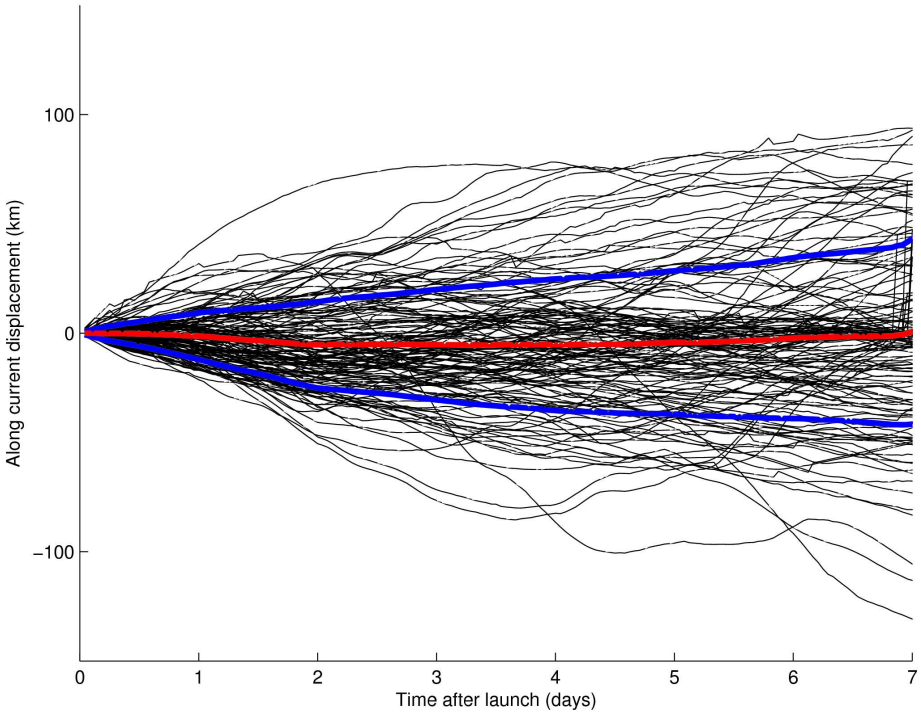

Figure 4.5. Displacements along component in natural coordinates versus time after deployment for the segmented drifter tracks (black lines); time series of the mean displacements (red line) and associated rms intervals (blue lines).

Then, the evolution in time of the displacement of each drifters from the release point were calculated. The original and segmented displacement series are plotted versus time after deployment in Figures 4.4 and 4.5. Mean and rms displacements are displayed versus time and superimposed over the displacements series. The picture looks like a diffusing plume of dye from a continuous source. It is possible to recognize the two different dispersion regimes, described in equations 6 and 7. Equation 6 can be rewritten as $\left\langle d'^{2}_{i} \right\rangle^{1/2} = \sqrt{2\left\langle u'^{2}_{i} \right\rangle} t$. Thus, for the initial dispersion range there is a linear evolution in time of the rms of the residual displacements, plotted in Figure 4.6a. The initial dispersion (equation 6) law holds until 1 days after deployment. Equation 7 can be expressed as $\left\langle d'^{2}_{i} \right\rangle = 2\left\langle u'^{2}_{i} \right\rangle T_{i}^{L} t = 2K_{i} t$ The variance of the residual displacements are plotted in Figure 4.6b. The two red lines correspond to the integration of Taylor's theorem: the slope of the curve is equal to the double of the diffusivity components, obtained using the segmented tracks.

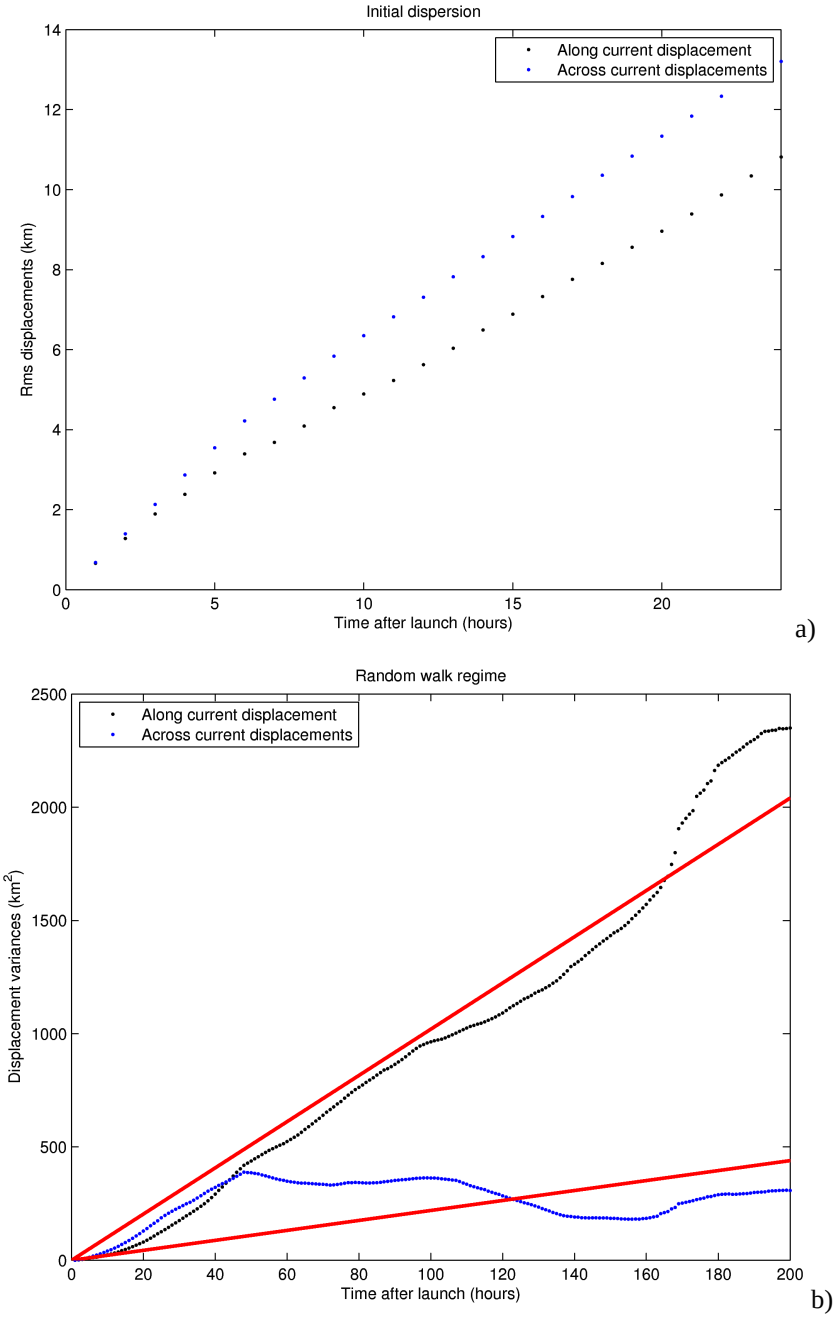

Figure 4.6. (a) Initial dispersion regime: Rms displacements versus time; (b) Random walk regime: displacement variances versus time. Taylor's theorem predicts the dispersion depicted by the red lines.

The value of along current component of the diffusivity ($1.4 \cdot 10^7$ cm^2/s) is in agreement with the results obtained in the Adriatic sea by (Falco et al. 2000), (Poulain 2001), (Ursella et al. 2006). They found values of K in the range of $1\text{-}2 \cdot 10^7$ cm^2/s in the along basin direction. Similar values (diffusivities ranging in 1-5 10^7 cm^2/s) have been estimated in the

central Mediterranean Sea by Poulain & Zambianchi 2007.

The strong mean flow (the coastal current which flows along the Italian and French coasts in the westward direction) determines the existence of a privileged direction, resulting in anisotropy of the fluctuation, with more energetic events in the direction of the mean.

4.5 Estimates of the horizontal diffusivity from satellite-tracked drifters data in the Adriatic Sea (2002-2004)

The previous section represents just the first step in the estimation of the diffusivities.

From direct observations it's possible to determine the diffusivity, but it would be advantageous if one could instead infer the diffusivity independently of observations, for example from the currents and winds produced by Eulerian models. Thus, the final goal is to obtain a general formulation for the diffusivity coefficient to be used in the parameterization of the stochastic component of the Lagrangian equation describing the turbulent parcels displacements. In order to parameterize the diffusion coefficient depending on the Eulerian current velocity shear and wind velocity, the relation between local winds and drifter-derived diffusivities will be explored using high resolution analysed winds and the current velocities from an OGCM. In this section the horizontal diffusivity has been quantified using the drifter data deployed in the Adriatic Sea as part of DOLCEVITA project (see 4.2.2).

The drifter data positions have been subjected to quality control. The data have been interpolated at 1 hour intervals with linear interpolation method. Then the surface velocities have been calculated as finite differences of the position data. The data sets analyzed in this work span from September 2002 to March 2004. The Northern and Central Adriatic are well covered by drifters, with a maximum of density in the northernmost part of the basin, while the south Adriatic shows a limited drifter distribution.

4.5.1 Adriatic division into sub-domains

The circulation of the Adriatic Sea has been investigated by studies of the last decades using both direct observations (Artegiani et al. 1997a), (Artegiani et al. 1997b), (Poulain 2001) and numerical simulations (Zavatarelli et al. 2002), (Zavatarelli & Pinardi 2003), (Oddo et al. 2005). The Adriatic Sea mean surface flow is globally cyclonic, with three

main cyclonic gyres located in the southern, central and northern sub-basin, named, respectively, Southern, Middle and Northern Adriatic gyres (Artegiani et al. 1997b). The three cells are interconnected with two costal currents: the Eastern Adriatic Current (EAC) which flows along the eastern side from the eastern Strait of Otranto to as far north as the Istrian Peninsula and the Western Adriatic Current (the WAC) which flows to the southeast along the western coast. The Northern part of the basin is characterized by very shallow water with gently sloping bathymetry with an average bottom of about 35 metres. The central part is 140 m deep on average, with two small bottom depressions (the Pomo and Jacuba Pits) having a maximum depth of 250 m. The southern part is characterized by a wide depression deeper than 1100 m.

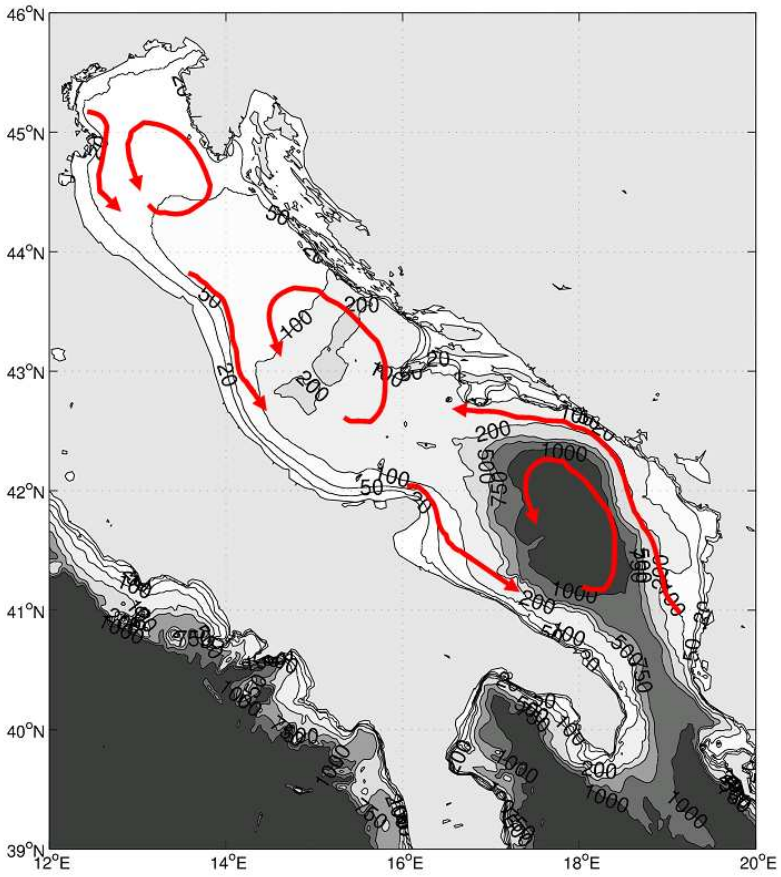

Figure 4.7. Bathymetry of the Adriatic Sea and schematic map of the circulation (bathymetric data provided by General Bathymetric Chart of the Oceans -GEBCO-, resolution 1 minute).

The analysis of drifters data can be influenced by the non –homogenous character of the flow and by the existence of different regimes of dispersion. The framework of this analysis is the Taylor's (1921) theory of stationary and homogenous turbulence, but the motion of drifters is affected by the space non-homogeneities and by non-steadiness of the Eulerian velocity field. Thus, averaging among long trajectories experiencing a mixture of different flow regimes can lead to misleading results. To avoid a mixture of different regimes a first step is to try to identify, using a previous knowledge of the velocity field, some geographical sub-domains, which can be considered, in a first approximation, homogeneous. Then, the mean statistical properties can be computed considering only trajectories belonging to the same "dynamical class": as pointed out by (Rupolo 2007), often the simple observation of the shape of the trajectory informs about the underlying dynamics of the flow much more that the statistical indices computed from the velocity series. Thus, considering the general circulation of the Adriatic Sea and following a "trajectory shape" approach we can divide the Adriatic Sea in three main sub-regions.

We can classify the shape of the trajectories in three main categories. The drifters trajectories characterized by high frequency variability, which very often rapidly whirl, will be called "turbulent" trajectories. The "looping" drifters are those characterized by meandering around large-scale structures, which could be trapped in the coherent eddies and rotate or experience only sporadic looping behaviour. The drifters which do not experience looping behaviour will be called "linear", like the ones trapped in the WAC. The "turbulent" trajectories are mainly concentrated in the Northern Adriatic, while the "looping" trajectories are located in the central part of the Adriatic Sea and along the east coast. The "linear" trajectories are those trapped in the WAC.

Based on the oceanographic characteristics and on the shape classification, three regions have been defined and separately analyzed: the WAC region, between the Po delta and Otranto Strait along the Italian coast; the Northern region, delimited by 100 m bathymetry north of the Jabuka Pit; the Middle-South region including the EAC and the Middle and Southern gyre.

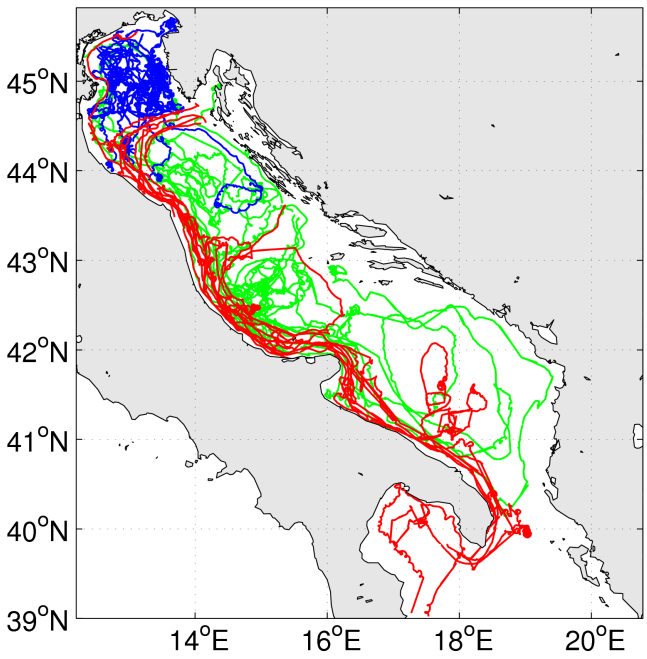

Figure 4.8. Adriatic division into sub-domains (a) northern Adriatic, blue trajectories; (b) WAC current, red trajectories; (c) middle and southern Adriatic gyres, green trajectories.

4.5.2 Diffusivity calculation procedure and energy spectra.

The application of the diffusion theory of Taylor implies the homogeneity and stationarity of the turbulent velocity field. These concepts are related to the spatial or temporal scale used in the statistical estimation. By reducing the spatial or temporal scale over which statistics are estimated, the condition of homogeneity can be assumed. If observations are taken over long periods the associated statistics can be considered stationary.

The correct scale could be chosen if an energy gap exists between the low-frequency fluctuations and the dominant frequency of the signal. Thus, we decided to analyze the Lagrangian energy spectra: we considered all the drifters trajectories together and we divided the time serie into 70 pieces of 1000 hours, computing the spectra for each piece and averaging over the number of pieces. Results are displayed in Figure 4.9. The horizontal axis of the figure is the frequency (hours^{-1}). In case of oceanographic data the variations of fixed frequencies such as tides would appear as distinctive peaks. In fact, the tidal components in Figure 4.9 appear as distinctive peaks at about 0.04 hours^{-1} (period of 24 hours) and 0.08 hours^{-1} (period of 12 hours). The former two are diurnal (once a day) and semi-diurnal (twice a day) tides. Moreover, the inertial oscillations with a period of 18

hours at our latitudes are clearly present, they are identified by the peak around 0.05 hours^{-1}. Other peaks are present between 0.1 hours^{-1} and 0.2 hours^{-1}, corresponding to a period between 10 and 5 hours, these peaks could be associated to the mesoscale structures (identified by a Rossby radius of 5-8 km in the Adriatic Sea).

It's not possible to identify a clear spectral gap between the resolved scales and the turbulent scales of motion. This may mean that in the ocean there isn't a clear spectral gap like in the atmosphere or it can be due to the low temporal resolution of the data sampling. Since we have the velocity values only every 1 hour, we cannot know if the spectral gap is located in the higher frequency range. The absence of an energy gap implies a difficulty in choosing the interval time over which the average should be performed for the calculation of the mean velocity.

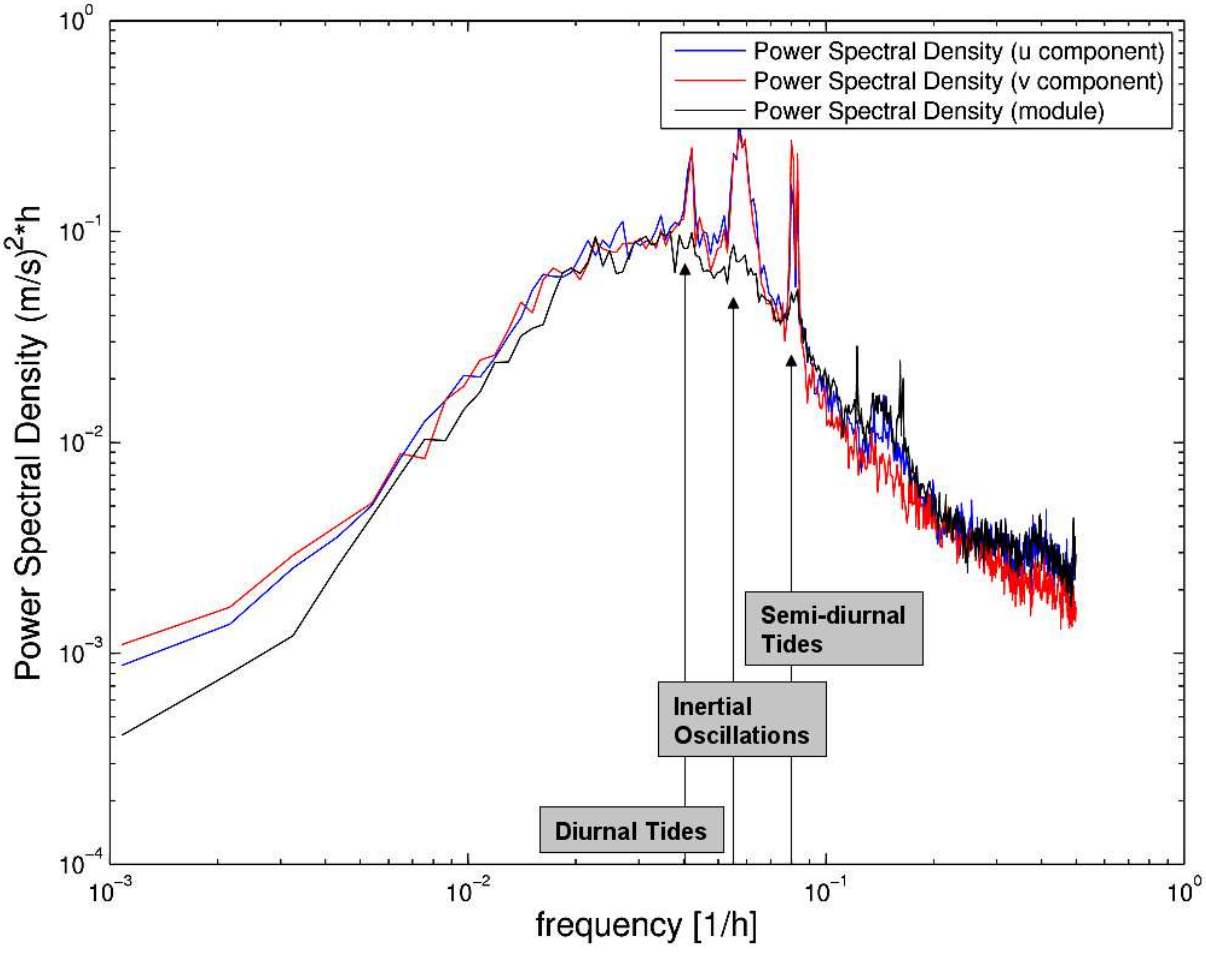

Figure 4.9. Lagrangian spectra calculated from all drifters trajectories.

We decided to subdivide the original drifters trajectories into overlapping segments 4 days long, whose origin are taken every 1 day. Reducing the length of the segments will generate problems with the autocorrelation function calculation: for large lag the autocorrelation should be computed by averaging over only a limited number of pairs of observation and should be very noisy. Increasing the length compromises the homogeneity assumption. Thus, we believed the length of 4 days was the optimal. In this way we are not far from the assumptions of homogeneity and steadiness.

The residual velocities are calculated by removing the mean velocity for each drifter, i.e. the mean velocity is calculated averaging the drifters velocities over a time window of 24 hours. If we consider a mean drifter velocity of 10-20 cm/s, the corresponding displacement in 24 hours is about 10-20 km. So our results of T and K will be valid for motions at scales less than 10-20 km.

The integral time scale has been calculated as the integral of the velocity autocorrelation until the first zero-crossing. The horizontal diffusivity values were, then, calculated using the formula (4.5), as the product of the velocity variance and the integral time scale.

4.5.3 Estimates of the Lagrangian diffusivity from observed drifters trajectories.

The Lagrangian integral time scale, the Lagrangian diffusivity and the Lagrangian EKE were computed for each 4 days segment.

Both the diffusivity and the integral time scale are expressed as vector components (the meridional and zonal component) in a Cartesian system. A "scalar" diffusivity has been also computed from the diffusivity components as $\sqrt{K_x^2 + K_y^2}$ and it has been compared with the wind intensity, the currents velocity rms and EKE.

First, the effect of wind on the horizontal diffusivity has been examined using the wind field provided by the LAMI (Limited Area Model Italy), produced by the Servizio IdroMeteorologico dell'Emilia Romagna (ARPA-SIM, Bologna). The model grid has an horizontal resolution of 6.5-7 km (Figure 4.10), latitude and longitude respectively, and a temporal frequency of 3 hours.

At each drifter position has been related the wind speed provided by the LAMI model: the bilinear interpolation of the Eulerian wind velocity from the grid model to the location of a drifter has been performed using the four grid points around the position.

For each 4-days segment the average value of diffusivity and wind intensity has been calculated. In figure 4.12 the relation between the wind speed and the horizontal diffusivity, expressed as “scalar diffusivity”, is shown.

The wind intensity is not strongly correlated to the drifter mean velocity intensity (Figure 4.11). As consequence the horizontal diffusivity is not correlated with the wind speed (Figure 4.12). This weak correlation cannot justify the formulation of a generic law relating the wind field to the diffusivity or integral time scale.

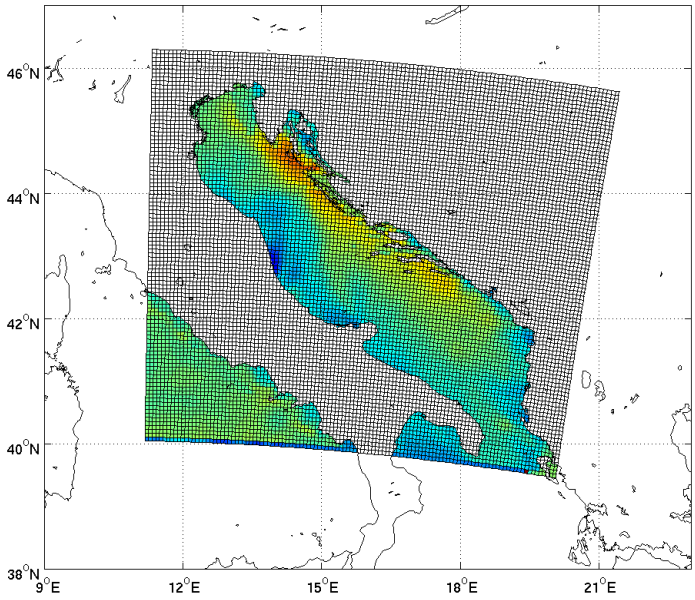

Figure 4.10. LAMI model domain.

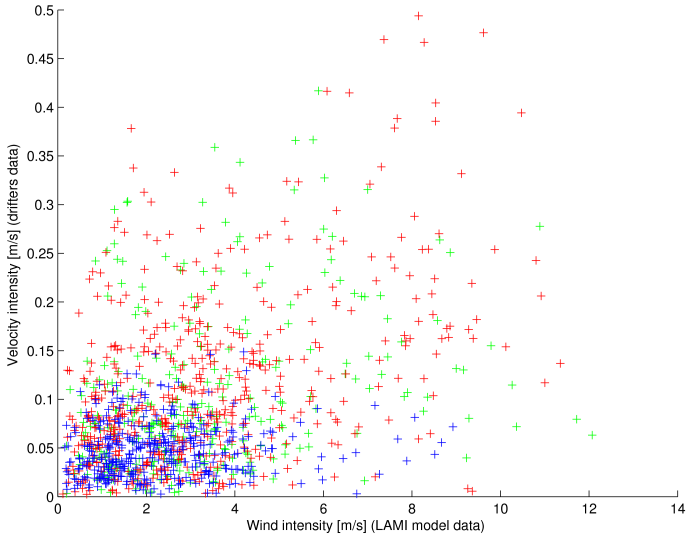

Figure 4.11. Average wind speed over 4 days (provided by the LAMI model) versus the drifter velocity intensity averaged over 4 days. (1- northern Adriatic, blue dots; 2- WAC current, red dots; 3- Middle and Southern Adriatic gyres, green dots).

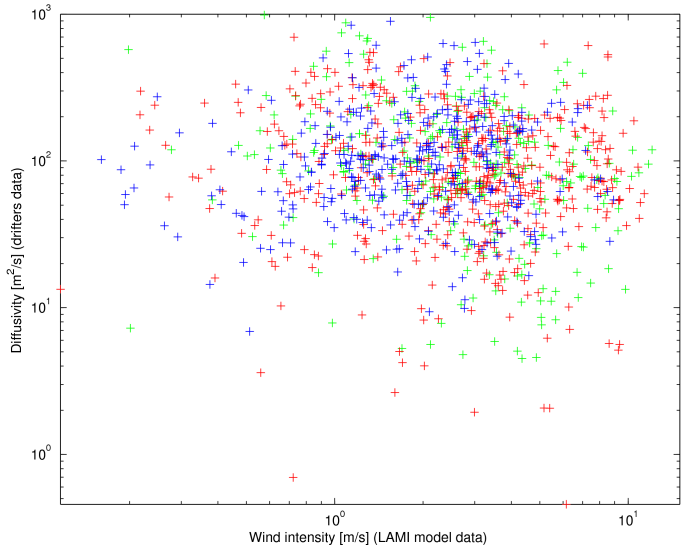

Figure 4.12. Average wind speed over 4 days (provided by the LAMI model) versus the drifter diffusivity ("scalar" diffusivity) (1- northern Adriatic, blue dots; 2- WAC current, red dots; 3- Middle and Southern Adriatic gyres, green dots).

Next, the relation between the Lagrangian properties and the currents has been examined. The average value of the T (average over all the basin) calculated from the observations is about 2.4 hours for both the zonal and meridional components, ranging from 0.4 to 6 hours for the both components. Figure 4.13-a and 4.10-b show the T versus u' (the velocity rms): the integral time scale is nearly constant for the Northern Adriatic trajectories, ranging from 3 and 4 hours, (blue dots), while it spans a wider range of values for the drifters in the

other two regions (red and green dots). For all the regions the time scale doesn't depend on the velocity rms.

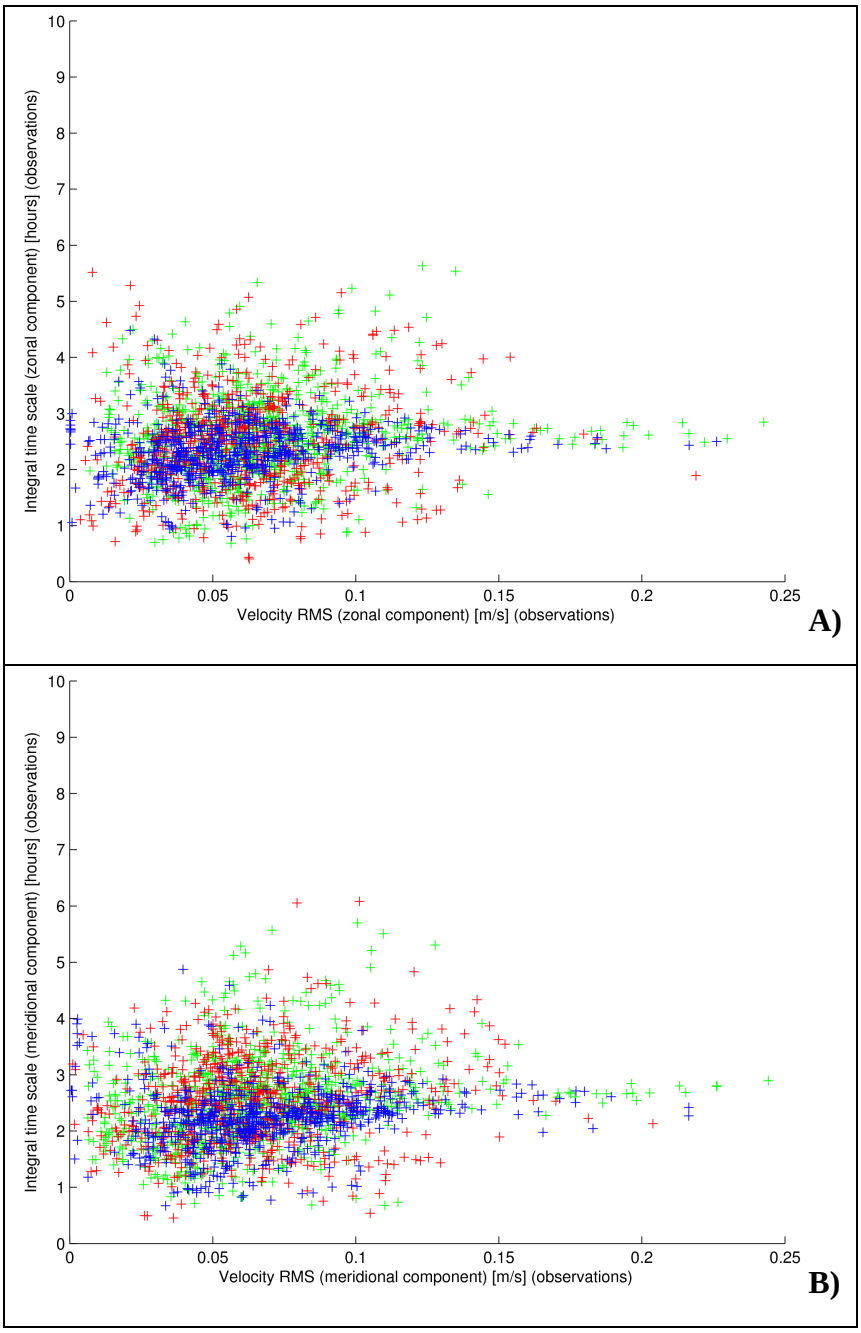

Figure 4.13. Relation between the integral time scale and the velocity rms calculated from: (a) zonal component (b) meridional components (1- northern Adriatic, blue dots; 2- WAC current, red dots; 3- Middle and Southern Adriatic gyres, green dots).

From the observations we obtained an average values of the diffusivity (averaging over the all basin) equal to 88 m^2/s and 82 m^2/s, in the zonal and meridional direction respectively (the maximum value of the diffusivity is 833 m^2/s and 840 m^2/s, in the zonal and meridional direction respectively).

In the literature the diffusivity estimated using drifters data is about 10-50 10^2 m^2/s (Falco et al. 2000), (Poulain 2001), (Ursella et al. 2006), (Poulain & Zambianchi 2007). In the abovementioned works the drifter data were sub-sampled every 6 hours and the residual velocities were calculated by removing a mean velocity, calculated averaging the drifters velocities over long time periods. The diffusivity values found in the literature are high and do not represent the diffusivity to be used in an oil spill model. The diffusivity to be introduced in an oil spill model should represent only the turbulent processes and the sub-grid scale processes, which are not resolved by the Eulerian models. That's why we decided to use hourly drifters data and to calculate the mean velocity over a shorter period, averaging the drifters velocities over a time window of 24 hours. This choice has led to diffusivity values 1 or 2 order of magnitude smaller that those found in the literature.

In figure 4.14 the relation between the "scalar" diffusivity and the velocity intensity is shown. The diffusivity increases with the velocity intensity.

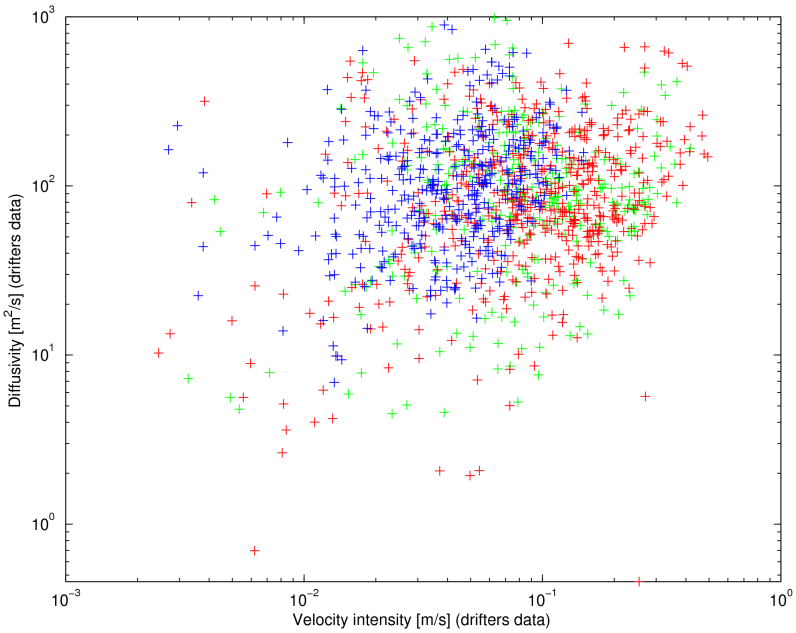

Figure 4.14. Relation between the "scalar" horizontal diffusivity and the velocity intensity calculated from the drifter data: (1- northern Adriatic, blue dots; 2- WAC current, red dots; 3- Middle and Southern Adriatic gyres, green dots).

Next we tried to investigate if the diffusivity can be parameterized simply in terms of the Eddy Kinetic Energy (EKE). Some studies indicate the diffusivity scales with EKE (Poulain & Niiler 1989), (Figueroa & Olson 1989), which would make sense if T is a constant time scale. If a constant-T rule were universal, it would be great value, diffusivity could be estimated directly from distribution of EKE. Subsequent studies found that a constant-T rule did not apply elsewhere and suggested that the diffusivity scales with the rms velocity (Krauss & Boning 1987), (Brink et al. 1991), (Zhang et al. 2001), in this case the length scale, L, would be constant. As shown in figure 4.15, in our case the diffusivity doesn't scale with the rms velocity.

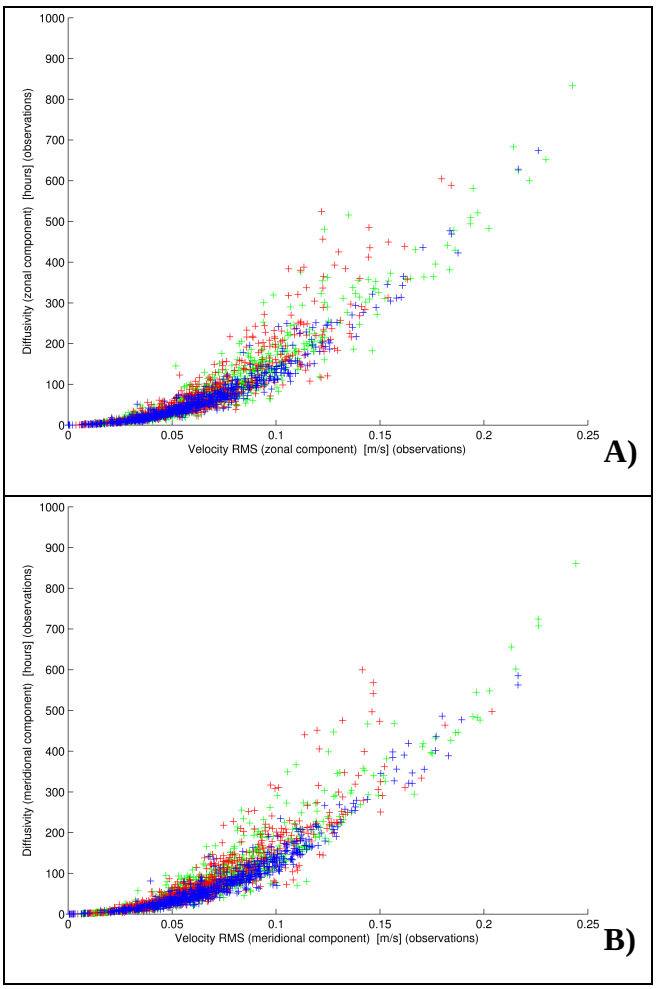

Figure 4.15. Relation between the velocity rms and the diffusivity calculated from the drifter data: A) the zonal components of rms velocity and diffusivity, B) the meridional components of rms velocity and diffusivity (1- northern Adriatic, blue dots; 2- WAC current, red dots; 3- Middle and Southern Adriatic gyres, green dots).

In figure 4.16 and 4.17 the relation between EKE and diffusivity is shown, we found the constant-T case. For the simulated and observed drifters trajectories, the diffusivity scales with the Lagrangian EKE, where the Lagrangian EKE is calculated from the drifters residual velocities as

$$EKE = \left\langle \frac{1}{2}\left(u'u'+v'v'\right) \right\rangle_L \qquad (4.8)$$

where u' and v' are the component of the residual velocity and $\langle\ \rangle_L$ indicates the average along the four days trajectory. In Figure 4.16-a and 4.16-b the black line represents the line with a slope equal to the average integral time scale for all the basin. Thus, we can say that the diffusivity increases with EKE, with a slope equal to the average integral time scale.

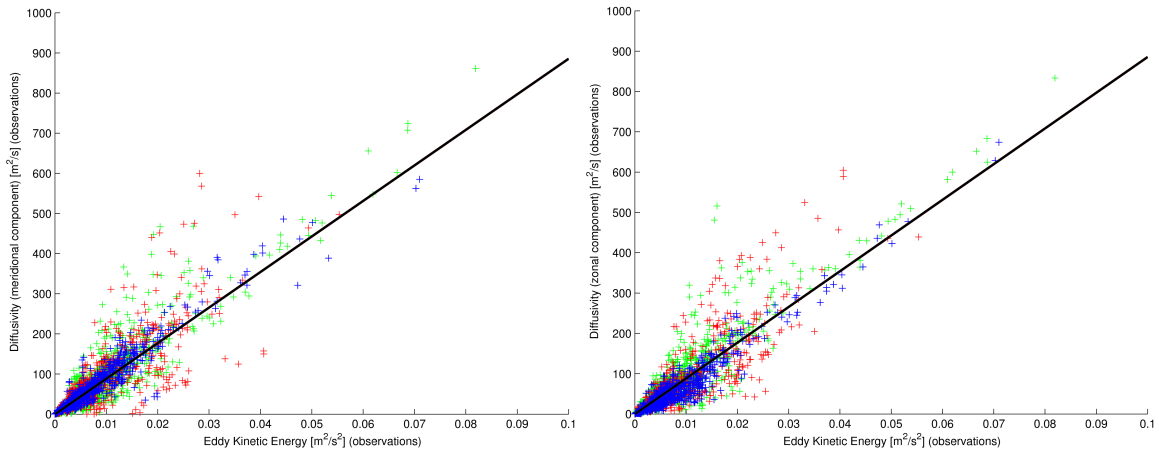

Figure 4.16. Relation between the EKE and the horizontal diffusivity calculated from: (a) zonal components, (b) meridional components.

In Figure 4.17 the relation between EKE and "scalar" diffusivity is shown: using the "scalar" diffusivity the data are less scattered.

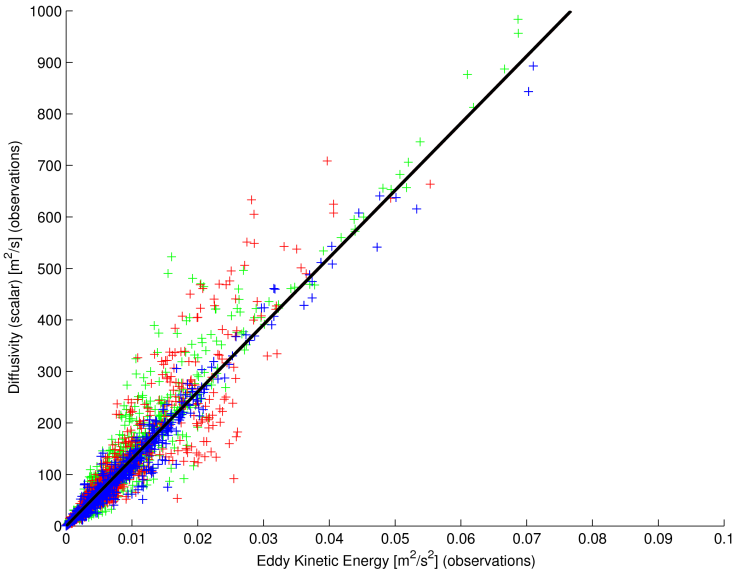

Figure 4.17. Relation between EKE and the "scalar" horizontal diffusivity calculated from the drifter data (1- northern Adriatic, blue dots; 2- WAC current, red dots; 3- Middle and Southern Adriatic gyres, green dots).

In conclusion, the new calculation method, implemented for the DOLCEVITA drifters, has led to diffusivity values 1 or 2 order of magnitude smaller that those found in the literature. These values would be the correct values to be introduced in an oil spill model.

Moreover, we found that there is a linear relationship between the EKE and horizontal diffusivity, both calculated from the experimental observations of drifters. Thus, we found the link between the diffusivity and the currents: the diffusivity increases with EKE, with a slope equal to the average integral time scale. However, as pointed out in other studies, this rule is not universal and in the future remains to determine what are the dynamics that makes it regionally applicable.

Chapter 5

5 Conclusions

In this work the problem of transport and dispersion of hydrocarbons in the marine environment has been approached from different points of view: from numerical modeling studies, passing through experimental observations, up to more theoretical studies.

The development of the numerical model, representing the transport and dispersion of an oil spill, was mainly dedicated to the study of the correct representation of the deterministic component of the flow: the oil slick movement due to eulerian ocean horizontal currents that are the result of the combined effect of buoyancy forcing, winds and waves.

Thanks to the coupling with the operational oceanographic models, like MFS and higher resolution operational hydrodynamic models, the oil spill model, MEDSLIK-II, now can take account of a proper representation of high frequency currents and wind fields in the advective components of the lagrangian trajectory model. Using drifter trajectories, the influence of the horizontal resolution and frequency of the current field has been examined. We found that increasing frequency and horizontal resolution of the current fields allows greater accuracy in the reproduction of the real trajectories.

In the past the drift velocity of the surface oil was considered to be the sum of a fraction of the wind velocity and the eulerian velocity field, supposed to represent the deeper (geostrophic) velocity field. The wind correction was necessary in order to reproduce the surface Ekman currents, which was not properly resolved by low resolution hydrodynamic models. Nowadays, with the advent of accurate operational oceanographic circulation models, a correct representation of the ageostrophic current velocity field can be provided by the Ocean General Circulation Model (OGCM). Thus, comparing the MEDSLIK-II simulations with drifters trajectories observations, we proved that there is no need to add a

"wind correction" to reconstruct a correct Ekman current, because if the surface water current velocities are derived from an high resolution state-of-the-art OGCM, they already contain a rather satisfactory representation of the surface ageostrophic currents.

The use of the wind correction can still be justified only with non accurate oceanographic models or in particular strong wind conditions. Furthermore, there are still some lacks in our understanding of the wind interactions with the surface oil. First, we still have to investigate on the possible direct effect of the wind on the slick. Second, some further investigation are needed on the correct representation of the physics of the first mm of the water column, such thin viscous layer could be important in the transport dynamics of an oil spill.

Usually in the oil spill models wind and wave effects are normally lumped together and represented by the wind drag coefficient, but the specific role of waves in the slick's drift is important especially in near-shore areas. In MEDSLIK-II the transport by waves (Stokes drift) has been introduced using an analytical formulation that depends from the wind amplitude (using the JONSWAP wave spectrum), but in the future the model will use the Stokes drift from the output of a complete numerical wave model.

The advance of the oil spill model was also dedicated in the correct representation of the weathering processes, taking also advantages of the innovative opportunity to couple the oil spill model with remote sensing data. In the case of a simulation of a slick observed by satellite, the initial spill should cover the entire slick area observed by the satellite. In addition, since the spill has usually already begun to undergo the transformations due to the weathering processes, we should consider a slick age and calculate the initial properties of the spill at the time of the observation. Now, MEDSLIK-II allows to reproduce the real shape of the slick and to consider the initial slick age, giving us a more realistic oil slick propagation over the water surface.

Using the information of a slick observed by satellite in two subsequent days, we verified the importance of the representation of the physical and chemical processes that transform the oil (evaporation, emulsification, dispersion in water column, adhesion to coast) together with the possibility to consider the slick age and the use of the remote-sensing data as initial conditions. Comparing the MEDSLIK-II results with real satellite observations, we highlighted the importance of the transformation processes and the use of

the slick age as the initial conditions in the prediction of the oil slick fate, giving us the correct information about the persistence of the oil at sea. Without the simulation of the weathering processes the model cannot predict when and where the oil disappears from the sea surface. Moreover, using the remote sensing data as initial conditions we were able to reproduce the evolution of the slick shape closer to reality.

Verification of the oil spill forecasting is both a crucial issue and a difficult task to perform, because it's difficult to obtain data of real transport of pollutants into the sea. For this reason the main objective of the cruise organized in the framework of the PRIMI project (presented in Chapter 3) was to visit oil slicks detected by satellite, in order to acquire in situ data for validation of the dispersion and transformation model. The data collected were in situ observations of oil slicks and drifters trajectories. This dataset was utilized to verify the oil spill model performances and to analyze the roles of wind and current in the oil drift. A total of about 30 slicks were detected by 14 SAR passages in the area during the PRIMI Cruise. Some oil spills were also confirmed in MODIS and/or MERIS imagery when the sky was clear. Eight oil spills were visited and confirmed by in situ measurements. Even if the ship was in the vicinity of the detected oil spill, the oil spill forecasting system component, which consists of the oceanographic models MFS, TYREMS and SRCM coupled with MEDSLIK-II oil spill model, proved crucial to find the oil slick within the next 12-24 hours, even if the oil spill model usually under-estimated the displacement of the oil slicks. The position of the detected oil slick moved several tens of km in few hours and the ship had to be moved toward the predicted oil spill position in order to validate the detection and the forecast.

The three most polluted oil spills, i.e. those which contained thick, dark oil patches and floating solid hydrocarbon particles were chosen for drifter release. The SPHERE, CODE and OSD drifters were released in the more severe spills, in order to verify the roles of wind and current in spill drift. A preliminary analysis of the trajectories showed that the area was dominated by inertial oscillations; in addition, the short-term wind forcing did not appear to be the main factor affecting the surface dynamics, at least in the first couple of days, in which the drifter behaviour did not display a pure Ekman dynamics. The analysis of the behavior of the different drifters (CODE and SPHERE) reveals an extreme

sensitivity of the trajectories to the shape of the drifters. The CODE drifters are completely underwater and their movement probably experience the effect of the first meter of the water currents, while the SPHERE drifter, which are not completely underwater, maybe feel the direct effect of wind. In the MEDSLIK-II simulation, the addition of the correction term of the wind seemed to be important for the SPHERE drifters, thus the correction might be important for thin or just released slick.

In the experiment a key part is missing: further investigation is needed in order to determine what type of drifters moved together with the oil slicks. The CODE drifters are designed to be transported by ocean currents (Davis 1985) and they are considered to behave as passive tracers, but we don't know if they also follow the oil slicks movements. Some previous studies ((Price 2003), (Reed 1994)) demonstrated that the SPHERE drifters move on the ocean surface like consolidated oil slicks under light to moderate winds.

One way to verify the behavior of drifters and oil slicks is to release the drifters on an oil slick, as done in the PRIMI cruise, and to acquire information on the slick evolution using satellite imagery in the subsequent days. During the PRIMI cruise, unfortunately, the satellite images over the area of interest weren't available for those days. Thus, we cannot know if any type of the drifters was moving together with the slick. Another cruise should be conceived in order to have the satellite acquisitions following the slick. Only combining the satellite, in situ and drifters information we can have a complete comprehension of the slick and drifters dynamics.

The drifters observations, collected during the MREA07/08 experiment and during the DOLCEVITA drifter program (presented in chapter 4), were used to improve our understanding of the turbulent processes, in order to arrive to a better representation of the stochastic component of transport. The final goal was to find the diffusivity value to be introduced in an oil spill model, which represents only the turbulent processes and the sub-grid scale processes, which are not resolved by the Eulerian models. From the experimental observations of drifters trajectories in the Ligurian Sea (MREA 07/08) and in the Adriatic Sea (DOLCEVITA) it was possible to determine a value for the horizontal diffusivity, K, and time scales, T.

The diffusivity values found in the literature are high (around $1\text{-}2\cdot10^7$ cm^2/s) and do not represent the diffusivity to be used in an oil spill model. Thus, we decided to implement a new method of diffusivity calculation from observed drifters trajectories.

First, using the dataset of MREA07/08 we implemented two different methods for the diffusivity calculation, based on the Taylor (1921) formulation. From the comparison between the two different methods we tested the robustness of our method of computation.

Next, we extended the drifters database in order to obtain a robust statistical analysis. Using the drifters collected during the DOLCEVITA project, the analysis of the power spectral density calculated from the drifters velocity has been performed. The variations of fixed frequencies such as tides and the inertial oscillations appear as distinctive peaks in the energy spectra. Moreover, from the analysis of the power spectral density wasn't possible to identify a clear spectral gap between the resolved scales and the turbulent scales of motion. This may mean that in the ocean there isn't a clear spectral gap like in the atmosphere or it can be due to the low temporal resolution of the data sampling (since the sampling is every hour, we cannot know if the spectral gap is located in the higher frequency range). The absence of an energy gap implies a difficulty in choosing the interval time over which calculate the mean velocity and this could lead to an overestimation of the diffusivity value.

The diffusivity value obtained from the DOLCEVITA drifters is around $8\text{-}9\cdot10^5$ cm^2/s. Thus, the new calculation method, implemented for the DOLCEVITA drifters, has led to diffusivity values 1 or 2 order of magnitude smaller that those found in the literature. These values can be introduced in an oil spill model.

Finally, since it would be advantageous if one could determine the diffusivity independently of observations, for example from the currents and winds produced by eulerian models we tried to find a general formulation that parameterize the diffusivity as function of wind or currents properties. We found that the diffusivity cannot be easily correlated with the wind field, while examining the relation between the currents velocity and the diffusivity, both calculated from the drifters observations, we found a relation between the EKE and the diffusivity. The diffusivity increases with EKE, with a slope equal to the average integral time scale. However, this rule could not be universal and in the future remains to determine what are the dynamics that makes it regionally applicable.

REFERENCES

Al-Rabeh, A.H., Lardner, R.W. & Gunay, N., 2000. Gulfspill Version 2.0: a software package for oil spills in the Arabian Gulf. *Environmental Modelling and Software*, 15(4), 425-442.

Al-Rabeh, A., 1994. Estimating surface oil spill transport due to wind in the Arabian Gulf. *Ocean Engineering*, 21(5), 461-465.

Ambj\örn, C., 2007. Seatrack Web, Forecasts of Oil Spills, a New Version. *Environmental Research, Engineering and Management*, 3(41), 60–66.

Apel, J.R. 1987. Principles of ocean physics. Academic Pr.

Archetti. R., 2009. Design of surface drifter for the oil spill monitoring. *REVUE PARALIA. Conférence Méditerranéenne Côtière et Maritime Coastal and Maritime Mediterranean Conference. HAMMAMET, TUNISI. 2-5 Dec 2009*. Vol. 1, pp. 231 - 234

Artegiani, A. et al., 1997a. The Adriatic Sea general circulation. Part I: Air-sea interactions and water mass structure. *Journal of Physical Oceanography*, 27(8), 1492–1514.

Artegiani, A. et al., 1997b. The Adriatic Sea general circulation. Part II: baroclinic circulation structure. *Journal of Physical Oceanography*, 27(8), 1515–1532.

ASCE, 1996. State-of-the-Art Review of Modeling Transport and Fate of Oil Spills. *Journal of Hydraulic Engineering*, 122(11), 594-609.

Blumberg, A.F. & Mellor, G.L., 1987. A description of a three-dimensional coastal ocean circulation model. *Three-dimensional coastal ocean models*, 4, 1–16.

Boughton, B.A., Delaurentis, J.M. & Dunn, W.E., 1987. A stochastic model of particle dispersion in the atmosphere. *Boundary-Layer Meteorology*, 40(1), 147–163.

Brink, K.H. et al., 1991. Statistical properties of near-surface flow in the California coastal transition zone. *Journal of Geophysical Research*, 96(C8), 14693.

Buist, I., 1979. *An experimental study of the dispersion of oil slicks into the water column. MA Sc*. Thesis, Dept Chem. Engng., Univ. of Toronto.

Coppini, G. et al., 2010. Hindcast of Oil Spill Pollution during the Lebanon Crisis, July-August 2006. *Marine Pollution Bulletin*.

Craik, A.D.D., 1985. *Wave Interactions and Fluid Flows, 322 pp*, Cambridge Univ. Press, New York.

Crone, T.J. & Tolstoy, M., 2010. Magnitude of the 2010 Gulf of Mexico Oil Leak. *Science*.

Daniel, P. et al., 2003. Improvement of drift calculation in Mothy operational oil spill prediction system. In *International Oil Spill Conference (Vancouver, Canadian Coast Guard and Environment Canada).*

Davis, R.E., 1983. Oceanic property transport, Lagrangian particle statistics, and their prediction. *Journal of Marine Research*, 41(1), 163–194.

Davis, R.E., 1985. Drifter observations of coastal surface currents during CODE: The method and descriptive view. *Journal of Geophysical Research*, 90(C3), 4741–4755.

Desaubies, Y., 2009. Preface - The Mersea Project. *Ocean Sci.*, 5(2), 173-190.

Falco, P. et al., 2000. Transport properties in the Adriatic Sea as deduced from drifter data. *Journal of Physical Oceanography*, 30(8), 2055–2071.

Figueroa, H.A. & Olson, D.B., 1989. Lagrangian statistics in the South Atlantic as derived from SOS and FGGE drifters. *Journal of Marine Research*, 47(3), 525–546.

Gaberšek, S. et al., 2007. The Sicily Channel Regional Model forecasting system: initial boundary conditions sensitivity and case study evaluation. *Ocean Sci.*, 3(1), 31-41.

Hackett, B., Breivik, Ø. & Wettre, C., 2006. Forecasting the Drift of Objects and Substances in the Ocean. In *Ocean Weather Forecasting*. pagg. 507-523. Available at: http://dx.doi.org/10.1007/1-4020-4028-8_23 [Consultato Maggio 14, 2010].

Haidvogel, D.B. & Beckmann, A., 1999. *Numerical ocean circulation modeling*, Imperial College Pr.

Hasselmann, K. et al., 1973. Measurements of wind-wave growth and swell decay during the Joint North Sea Wave Project (JONSWAP). *Ergnzungsheft zur Deutschen Hydrographischen Zeitschrift Reihe*, A8–12.

Krauss, W. & Boning, C.W., 1987. Lagrangian properties of eddy fields in the northern North Atlantic as deduced from satellite-tracked buoys. *Journal of Marine Research*, 45(2), 259–291.

Lumpkin, R., Treguier, A.M. & Speer, K., 2002. Lagrangian eddy scales in the northern Atlantic Ocean. *Journal of Physical Oceanography*, 32(9), 2425–2440.

Lardner, R., Zodiatis, G., Hayes, D., Pinardi, N., 2006. Application of the MEDSLIK Oil Spill Model to the Lebanese Spill of July 2006. *European Group of Experts on Satellite Monitoring of Sea Based Oil Pollution. European Communities.*

Lenn, Y.D. & Chereskin, T.K., 2009. Observations of Ekman currents in the Southern Ocean. *Journal of Physical Oceanography*, 39(3), 768–779.

Mackay, D., Paterson, S. & Nadeau, S., 1980. Calculation of the evaporation rate of volatile liquids. In *Proceedings National Conference on Control Hazardous Material Spills*. pagg. 361–368.

Molcard, A. et al., 2009. Comparison between VHF radar observations and data from drifter clusters in the Gulf of La Spezia (Mediterranean Sea). *Journal of Marine Systems*, 78, S79–S89.

Morales-Caselles, C. et al., 2007. Comparing sediment quality in Spanish littoral areas affected by acute (Prestige, 2002) and chronic (Bay of Algeciras) oil spills. *Environmental Pollution*, 146(1), 233–240.

Nittis, K. et al., 2006. Operational monitoring and forecasting for marine environmental applications in the Aegean Sea. *Environmental Modelling & Software*, 21(2), 243-257.

Noye, J., 1987. Numerical methods for solving the transport equation. *Numerical Modelling: Application to Marine Systems*, 145, 195–229.

Oddo, P. et al., 2006. The Adriatic basin forecasting system. *Acta Adriatica*, 47, 169–184.

Oddo, P., Pinardi, N. & Zavatarelli, M., 2005. A numerical study of the interannual variability of the Adriatic Sea (2000-2002). *Science of the Total Environment*, 353(1-3), 39–56.

Pedlosky, J., 1986. The buoyancy and wind-driven ventilated thermocline.

Phillips, O.M., 1977. *The Dynamics of the Upper Ocean, 336 pp*, Cambridge Univ. Press, New York.

Pinardi, N. et al., 2003. The Mediterranean ocean forecasting system: first phase of implementation (1998-2001). In *ANNALES GEOPHYSICAE-EUROPEAN GEOPHYSICAL SOCIETY*. pagg. 3–20.

Pinardi, N. & Coppini, G., 2010. Operational oceanography in the Mediterranean Sea: the second stage of development.

Pollard, R.T., 1970. On the generation by winds of inertial waves in the ocean. In *Deep Sea Research and Oceanographic Abstracts*. pagg. 795–812.

Poulain, P.M., 2001. Adriatic Sea surface circulation as derived from drifter data between 1990 and 1999. *Journal of Marine Systems*, 29(1-4), 3–32.

Poulain, P.M. et al., 2010. Surface circulation in the Liguro-Provençal basin as measured by satellite-tracked drifters (2007-2009). *Journal of Marine Systems*.

Poulain, P.M. & Niiler, P.P., 1989. Statistical analysis of the surface circulation in the California Current System using satellite-tracked drifters. *Journal of Physical Oceanography*, 19(10), 1588–1603.

Poulain, P.M. & Zambianchi, E., 2007. Surface circulation in the central Mediterranean Sea as deduced from Lagrangian drifters in the 1990s. *Continental Shelf Research*, 27(7), 981–1001.

Price, J.F., Weller, R.A. & Schudlich, R.R., 1987. Wind-driven ocean currents and Ekman transport. *Science*, 238(4833), 1534.

Price, J.M. et al., 2006. Preliminary assessment of an oil-spill trajectory model using satellite-tracked, oil-spill-simulating drifters. *Environmental Modelling & Software*, 21(2), 258–270.

Reed, M., Aamo, O.M. & Daling, P.S., 1995. Quantitative analysis of alternate oil spill response strategies using OSCAR. *Spill Science & Technology Bulletin*, 2(1), 67-74.

Reed, M. et al., 1999. Oil Spill Modeling towards the Close of the 20th Century: Overview of the State of the Art. *Spill Science & Technology Bulletin*, 5(1), 3-16.

Reed, M., Turner, C. & Odulo, A., 1994. The role of wind and emulsification in modelling oil spill and surface drifter trajectories. *Spill Science & Technology Bulletin*, 1(2), 143-157.

Rinaldi, E. et al., 2010. Lagrangian and Eulerian observations of the surface circulation in the Tyrrhenian Sea. *Journal of Geophysical Research*, 115(C4), C04024.

Risken, H., 1989. *The Fokker-Planck equation*, Springer.

Rupolo, V., 2007. Observing turbulence regimes and Lagrangian dispersal properties in the oceans. *Lagrangian analysis and prediction of coastal and ocean dynamics*, 231–274.

Shen, H.T., Yapa, P.D. & Petroski, M.E., 1987. A Simulation Model for Oil Slick Transport in Lakes. *Water Resources Research*, 23(10), PP. 1949-1957.

Sibert, J.R. et al., 1999. An advection-diffusion-reaction model for the estimation of fish

movement parameters from tagging data, with application to skipjack tuna (Katsuwonus pelamis). *Canadian Journal of Fisheries and Aquatic Sciences*, 56(6), 925–938.

Smagorinsky, J., 1963. General circulation experiments with the primitive equations. *Monthly weather review*, 91(3), 99–164.

Sotillo, M. et al., 2008. Towards an operational system for oil-spill forecast over Spanish waters: Initial developments and implementation test. *Marine Pollution Bulletin*, 56(4), 686-703.

Taylor, G.I., 1922. Diffusion by Continuous Movements. *Proceedings of the London Mathematical Society*, s2-20(1), 196-212.

Thomson, D.J., 1987. Criteria for the selection of stochastic models of particle trajectories in turbulent flows. *Journal of Fluid Mechanics*, 180, 529–556.

Tompson, A.F.B. & Gelhar, L.W., 1990. Numerical Simulation of Solute Transport in Three-Dimensional, Randomly Heterogeneous Porous Media. *Water Resources Research*, 26(10), PP. 2541-2562.

Tonani, M. et al., 2008. A high-resolution free-surface model of the Mediterranean Sea. *Ocean Science*, 4(1), 1–14.

Torgrimson, G.M., 1980. The on-scene spill model: A user's guide. Tech. Rep., *Hazardous Materials Response Branch*, Natl. Oceanic & Atmos. Admin., Seattle, Wash.

Wang, J.H., & Shen, Y.M. 2010. Development of an integrated model system to simulate transport and fate of oil spills in seas. *Science China technological sciences*, 53(9), 2423-2434.

Wang, S.D., Shen, Y.M., Guo, Y.K., & Tang, J. 2008. Three-dimensional numerical simulation for transport of oil spills in seas. *Ocean engineering*, 35(5-6), 503-510.

Woods, J., 2002. Primitive equation modelling of plankton ecosystems. , Ocean Forecasting, Conceptual Basis and Applications. N. Pinardi and J. Woods (eds.). Springer-Verlag Berlin Heidelberg.

Wunsch, C., 1998. The work done by the wind on the oceanic general circulation. *Journal of Physical Oceanography*, 28, 2332–2340.

Ursella, L., Poulain, P.M. & Signell, R.P., 2006. Surface drifter derived circulation in the northern and middle Adriatic Sea: Response to wind regime and season. *Journal of Geophysical Research*, 111(C3), C03S04.

Zavatarelli, M. & Pinardi, N., 2003. The Adriatic Sea modelling system: a nested

approach. In *Annales Geophysicae*. pagg. 345–364.

Zavatarelli, M. et al., 2002. Diagnostic and prognostic model studies of the Adriatic Sea general circulation: Seasonal variability. *Journal of Geophysical Research*, 107(C1), 3004.

Zhang, H.M., Prater, M.D. & Rossby, T., 2001. Isopycnal Lagrangian statistics from the North Atlantic Current RAFOS float observations. *Journal of Geophysical Research*, 106(C7), 13817.